แนวทางไฮบริดในการสร้างแบบจำลองสามมิติจากภาพเอกซเรย์คอมพิวเตอร์ตรวจลำไส้ใหญ่
ที่มีการเตรียมลำไส้ใหญ่โดยการกลืนสารทึบรังสี

นางสาวภัทราพร พรหมคำตัน

A HYBRID APPROACH FOR RECONSTRUCTING 3D MODEL FROM

ORAL CONTRAST-ENHANCED CT COLONOGRAPHY IMAGES

Miss Pataraporn Promkumtan

A Dissertation Submitted in Partial Fulfillment of the Requirements

for the Degree of Doctor of Philosophy Program in Computer Science

Department of Mathematics and Computer Science

Faculty of Science

Chulalongkorn University

Academic Year 2011

Thesis Title	A HYBRID APPROACH FOR RECONSTRUCTING 3D MODEL FROM ORAL CONTRAST-ENHANCED CT COLONOGRAPHY IMAGES
By	Miss Pataraporn Promkumtan
Field of Study	Computer Science
Thesis Advisor	Assistant Professor Nagul Cooharojananone, Ph.D.
Thesis Co-advisor	Assistant Professor Rajalida Lipikorn, Ph.D.

Accepted by the Faculty of Science, Chulalongkorn University in Partial Fulfillment of the Requirements for the Doctoral Degree

…………………………………………….. Dean of the Faculty of Science

(Professor Supot Hannongbua, Dr.rer.nat.)

THESIS COMMITTEE

…………………………………………….. Chairman

(Professor Chidchanok Lursinsap, Ph.D.)

……………………………………….……. Thesis Advisor

(Assistant Professor Nagul Cooharojananone, Ph.D.)

…………………………………………….. Thesis Co-advisor

(Assistant Professor Rajalida Lipikorn, Ph.D.)

…………………………………………….. Examiner

(Suphakant Phimoltares, Ph.D.)

…………………………………………….. Examiner

(Associate Professor Laddawan Vajragupta, M.D.)

…………………………………………….. External Examiner

(Assistant Professor Panjai Tantasanawong, Ph.D.)

ภัทราพร พรหมคำตัน : แนวทางไฮบริดในการสร้างแบบจำลองสามมิติจากภาพเอกซเรย์คอมพิวเตอร์ตรวจลำไส้ใหญ่ที่มีการเตรียมลำไส้ใหญ่โดยการกลืนสารทึบรังสี. (A HYBRID APPROACH FOR RECONSTRUCTING 3D MODEL FROM ORAL CONTRAST-ENHANCED CT COLONOGRAPHY IMAGES) อ. ที่ปรึกษาวิทยานิพนธ์หลัก : ผศ.ดร.นกุล คูหะโรจนานนท์, อ. ที่ปรึกษาวิทยานิพนธ์ร่วม : ผศ.ดร.รัชลิดา ลิปิกรณ์, 107 หน้า.

วิทยานิพนธ์นี้เสนอกรอบการทำงานแบบไฮบริดในการสร้างแบบจำลองสามมิติจากภาพเอกซเรย์คอมพิวเตอร์ตรวจลำไส้ใหญ่ที่มีการเตรียมลำไส้ใหญ่โดยการกลืนสารทึบรังสี กรอบการทำงานนี้ประกอบด้วยสามส่วนหลัก ได้แก่ การล้างลำไส้ใหญ่ การตรวจจับผนังลำไส้ใหญ่ การคัดแยกลำไส้ใหญ่และการสร้างแบบจำลองสามมิติ ส่วนแรกคือ การล้างลำไส้ใหญ่ด้วยวิธีเคมีนคลัสเตอร์ริงและการดำเนินการมอร์โฟโลจี ค่าเฉลี่ยตัวกรองเกาส์เซียนแบบความถี่ต่ำผ่านสองขนาดต่างกัน ถูกนำมาใช้ร่วมกับตัวกรองแบบมัธยฐาน เพื่อสร้างผนังลำไส้ใหญ่ให้เหมือนจริงเท่าที่เป็นไปได้ การทดสอบกระทำกับข้อมูลจำนวนสี่ชุด การประเมินผลโดยรังสีแพทย์ที่มีความชำนาญแสดงให้เห็นว่าความแม่นยำในการล้างลำไส้ใหญ่เป็นที่น่าพึงพอใจ ส่วนที่สองคือ การตรวจจับผนังลำไส้ใหญ่ ที่ประยุกต์ใช้การเพิ่มความเข้มการไหลของเวกเตอร์เกรเดียนต์และขอบภาพแบบไฮบริด เพื่อช่วยในการตรวจจับผนังลำไส้ใหญ่ การทดสอบกระทำกับข้อมูลจำนวนแปดชุดและทำการเปรียบเทียบกับวิธีการที่มีอยู่ จากการประเมินผลโดยรังสีแพทย์สองท่านที่มีความชำนาญ พบว่าวิธีการที่นำเสนอให้ผลลัพธ์ดีกว่าแม้ว่าเป็นกรณียาก หลังจากนั้นการคัดแยกลำไส้ใหญ่ที่อาศัยโครงสร้างทางกายวิภาคและการวิเคราะห์ความจุได้นำมาประยุกต์ใช้กับภาพที่ได้จากส่วนก่อนหน้า ท้ายที่สุดแบบจำลองสามมิติได้สร้างขึ้นจากข้อมูลยี่สิบชุด

ภาควิชา คณิตศาสตร์และวิทยาการคอมพิวเตอร์ ลายมือชื่อนิสิต _____

สาขาวิชา วิทยาการคอมพิวเตอร์ _____ ลายมือชื่อ อ.ที่ปรึกษาวิทยานิพนธ์หลัก _____

ปีการศึกษา 2554 _____ ลายมือชื่อ อ.ที่ปรึกษาวิทยานิพนธ์ร่วม _____

5073859223 : MAJOR   COMPUTER SCIENCE

KEYWORDS :   CT COLONOSCOPY / IMAGE PROCESSING / SEGMENTATION / CLASSIFICATION / DEFORMABLE MODEL

PATARAPORN PROMKUMTAN : A HYBRID APPROACH FOR RECONSTRUCTING 3D MODEL FROM ORAL CONTRAST-ENHANCED CT COLONOGRAPHY IMAGES. ADVISOR : ASST.PROF. NAGUL COOHAROJANANONE, Ph.D., CO-ADVISOR : ASST.PROF. RAJALIDA LIPIKORN, Ph.D., 107 pp.

This dissertation proposes a hybrid framework for 3D model reconstruction from oral contrast-enhanced CT colonography images. The framework is composed of three main parts which are colon cleansing, colon wall detection, and colon segmentation and 3D model reconstruction. The first part is colon cleansing which is performed by applying K-means clustering and morphological operations. The average Gaussian low pass filter of two different sizes combined with median filter are employed to reconstruct colon wall to be as realistic as possible. The examination was performed on four datasets. The results evaluated by an expert radiologist revealed that the accuracy on colon cleansing is satisfactory. The second part is colon wall segmentation which applies enhanced gradient vector flow and hybrid edge to assist colon wall detection. The examination was performed on eight datasets and compared with the existing techniques. The results evaluated by two expert radiologists revealed that the proposed method gives better results even in difficult cases. Afterward, colon segmentation based on anatomical structures and volume analysis, is applied to images obtained from the previous parts. Finally, 3D models are reconstructed from twenty datasets.

Department : Mathematics and Computer Science   Student's Signature _____

Field of Study : Computer Science _____   Advisor's Signature _____

Academic Year : 2011 _____   Co-advisor's Signature _____

ACKNOWLEDGEMENTS

CONTENTS

List of Tables

List of Figures

CHAPTER I

INTRODUCTION

1.1 Introduction and Problem Review

One of the most leading causes of risk to death from cancer if the pathological symptoms are lately diagnose in both men and women, is colorectal cancer [1]. Most colorectal cancers can be successfully treated if the suspect of pre-cancer cells called polyps are detected and diagnosed at an initial stage. Optical colonoscopy is presently utilized for examining colorectal cancer. This technique is operated by inserting an endoscope through the anus and transmits an image of the entire colon to a video monitor [2, 3]. The process on inserting and moving an endoscope to examine the entire colon takes approximately one hour to perform and often causes more invasive and uncomfortable to the patient. Furthermore, another disadvantage of this examining method is that the endoscope camera may not cover the entire colon wall and there is also a small risk of the endoscope puncturing through the patient's colon wall, in this case the critical surgery is required. Prior to this inspection technique, the patients undergo a physical bowel cleansing preparation which comprise either cleansing colon with a large volume of liquids or taking medication to clear colon in order to enable the camera to see as much of the colon wall as possible, and undergo enemas to induce bowel movements. This physical bowel preparation is always more unfriendly and discomfort than the examining stage. Particularly most of the patients are generally old and weak. Consequently they are incapable of drinking the full designate amount of laxative and there are some feces remain inside the colon [2].

Virtual colonoscopy, known as computed tomographic (CT) colonography, is another colorectal cancer screening which is performed by scanning the patient's abdomen starting from the rectum up to diaphragm to include the entire colon and then producing a series of cross sectional CT images in two and three dimensions for viewing inside of the colon [4], [5], [6]. This procedure can assist the doctors to diagnose pathological symptom in colon and bowel such as polyps and cancer. Furthermore, the examination of CT scanning does not require the insertion of a long tube through the colon as the optical colonoscopy does. This colon examining method uses gentle colon cleansing and air inflation into the colon. On a day prior to obtaining virtual colonoscopy, the patients undergo bowel preparation of mild

laxatives and a low residue diet. The purpose of bowel preparation is to produce the optimal results of virtual colonoscopy. Since the retained feces in the colon lumen can be ambiguous polyps and also impede visualization of the colon. The removing bulk of feces and liquefy the fecal as stream is necessary to make colon wall has high contrast interface.

For virtual colonoscopy, the patients do not require physical cleansing of the colon, instead they take oral contrast enhancement materials (CEF) in hours before the examination to provide the remained residue fluid radio-opaque. Then the remained stool and residue fluid is enhanced so that they can be easily distinguished from other tissues [7]. The carbon dioxide gas or room air is slowly inflated into the colon through the small rectal tube to make any retained material homogeneous and distend the colon not to collapse during the CT screening. After carbon dioxide gas or room air inflation, the colon is basically filled with gas or room air and the remained residue materials are then homogenized with contrast enhanced fluid.

However, in cases where the colon is not sufficiently insufflation the colon structure is fragmented [8]. Afterward, the CT scanning by a spiral CT scanner is performed and all of CT images are acquired in a single breath hold to reduce motion artifacts. Consequently, the CT colonoscopy technique performs faster, less invasive and also more comfortable for the patients than the other common colorectal cancer screening methods. An additional advantage is that the radiologist can also see the abdominal structures in the CT scan images, which is more helpful for doctors in identifying other health problems when examining the images.

The problems of the current virtual colonosopy can be separated into four main categories. The first problem is colon cleansing technique for eliminating any retained material of contrast-enhanced fluid (CEF) inside the colon lumen. The second problem is the partial volume effect (PVE). The third problem is colon segmentation and the last problem is colon wall detection. The details of these problems are more described as follows.

1.1.1   Problem 1: Colon Cleansing

The first problem is colon cleansing technique for eliminating any retained material of contrast-enhanced fluid inside the colon lumen. The precision of diagnosis by CT colonography depends on a cleaning view of the colon lumen. The residual material inside the colon such as stool and fluid are often problematic. If the residual materials remain, they can be misinterpreted as a part of colon and cause some polyps unable to be detected.

Since the current colonoscopy techniques require a clarifying colon lumen for making precision on polyps detection [6], [7]. The eliminating of retained feces inside the colon is also important to produce the cleaning view of colon in CT colonography. However, the physical bowel cleansing preparation is often more unfriendly and uncomfortable to the patients. In the case that patients fail to drink the full quantity of laxative, the feces remains stick to the colon wall, which encumber the visualization of colon and have the chance that some polyps might remain undetected.
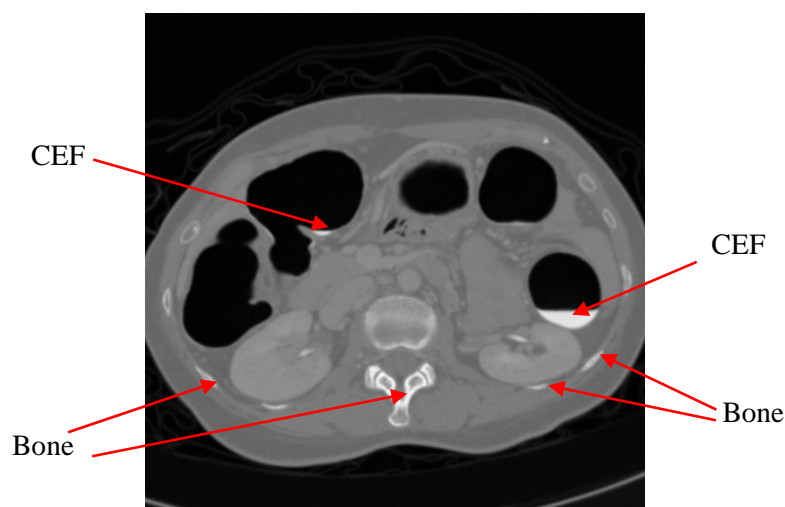
Figure 1.1 Contrast-enhanced fluid (CEF) and bone

In order to make the CT colonoscopy friendly to the patients, the residual materials are removed from CT images by computed cleansing instead of the physical bowel cleansing method. Therefore, the patients undergo the standard bowel preparation of low residue diet and take a colonic lavage to liquefy the remained feces. The contrast-enhanced agent is given to the patients to provide the remained fluid radio-opaque as shown in Figure 1.1. This bowel preparation also assists in segmenting and removing of residual materials inside colon lumen. Nevertheless, the retained materials of contrast enhanced fluid (CEF) appearing in the CT image also have high intensities similar to bone as shown in Figure 1.1 and they cause the segmentation of residual materials to be more complicated. The accuracy of colon cleansing is necessary for removing the enhanced residuals without the effect on the colon wall or polyps.

Moreover, the remaining enhanced materials inside the colon making the colon detection is difficult and also prevents a continuous on colon segmentation as shown as Figure 1.2 [8].

(a) (b)

Figure 1.2 Connect regions of (a) air inside colon are separated by residual materials (b) air plus residual materials in colon (From: [8])

1.1.2   Problem 2: Partial Volume Effect

The second problem is the partial volume effect (PVE). Even if the intensities of the residual materials have been enhanced with the contrast-enhanced agent, they also do not show an explicit boundary due to the partial volume effect. The partial volume effect voxels appear at the boundaries locating between two different intensity regions whose intensity do not match with either of the two regions.
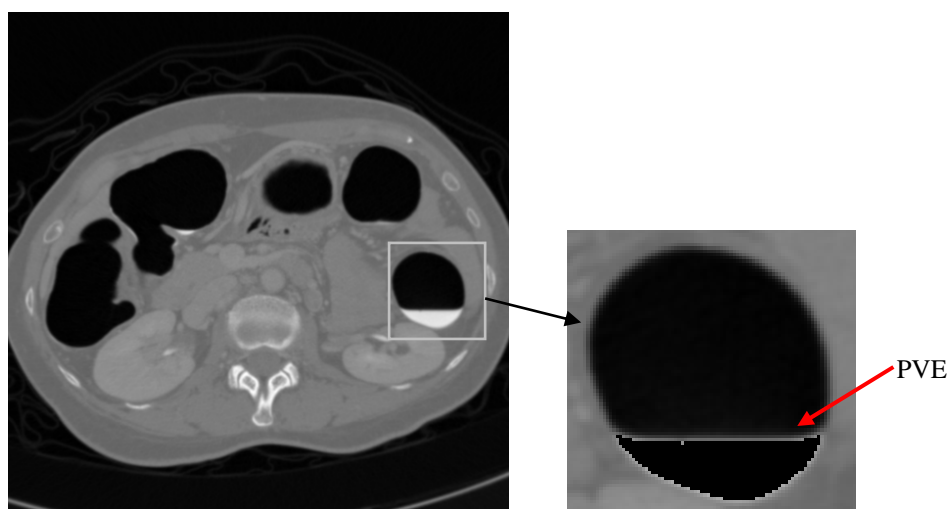
Figure 1.3 Partial volume effect (PVE)

The simple threshold subtraction of the residual materials inside colon gives the fastest result for cleansing colon. However, it cannot eliminate the partial volume effect

voxels between the boundaries of two different intensity regions such as the thin voxels lying between the residual fluids and air. Since the partial volume effect voxels have the same intensity range as soft-tissue and are identified as soft-tissue voxels, they cannot be successfully eliminated. Moreover, the simple threshold subtraction also increases aliasing effects at the inner colon boundary after cleansing colon as illustrated in Figure 1.3. It is instantaneously apparent when taking a closer look at the surface of colon wall boundary. The intensity values at the colon lumen transits rapidly from soft tissue to air region. The rapidly transition intensity boundary also indicates the missing of thin soft tissue layer or colonic mucosa that presented at the surface of colon wall boundary.

Many techniques on colon cleansing and partial volume effect removing have been reported. Principal component analysis cooperated with learning vector quantization are applied for image classification and colon cleansing [9], [10]. Vertical filter and gradient-magnitude-based region growing is utilized for removing the partial volume effect boundary [11]. However, these techniques did not mention the effect of the sharpen intensity at the mucosa layer after colon cleansing. Segmentation rays are operated to define the profile pattern for detecting the intersection boundary and the reconstruction graph is employed for removing the residuals [12], [13]. Non-linear transfer function and a morphological dilation operation are manipulated to find the intensity profile of enhanced material [14]. Similarly, threshold function combined with triangular intensity transformation is presented for colon cleansing method [15]. Nevertheless, this method requires cautious selection of intensity characteristics for assigning the classification tasks. A half-sized data is applied for generating the local and global histograms of contrast-enhanced materials for making a binary mask and then applied the morphological dilation operation to obtain seeding for region growing [16]. This method also has to carefully set an optimal threshold and has a limitation with the inhomogeneous enhanced materials.

1.1.3   Problem 3: Colon segmentation

Because colon is not the only air filled organ appear inside the abdomen, the other connected organs such as the lower portion of lung, the small bowel or intestine and stomach, are possible partially filled with air and sometimes are presented in CT images [17]. These air filled organs can be misunderstood and interpreted as apart of colon. The example of the lung appearing in CT image is shown in Figure 1.4.
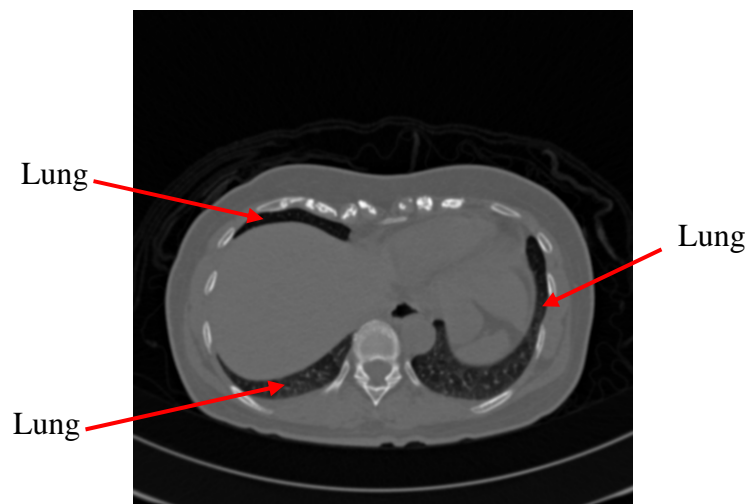
Figure 1.4 Lung appearing in CT image

Especially, the intestine, which is the organ that connects to colon at the cecum, is always connected and interpreted as apart of to colon after performing colon segmentation.

(a)   (b)
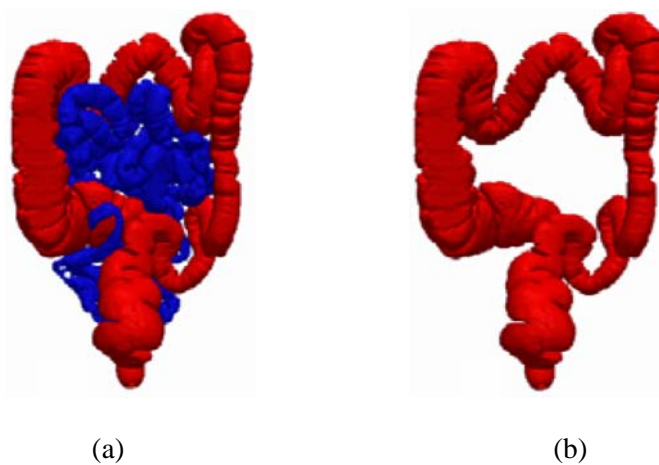
Figure 1.5 Connected regions of (a) colon and contiguous intestine
(b) colon segmentation (From: [16])

During examining process, the colon is distended by gas inflation to make any retain fluid homogeneous and make the colon bigger than intestine. Consequently, the small-size intestine is implicitly separated and cannot be segmented as a part of colon. However, in the case that small intestine which contiguous to colon is inflated by air, it is segmented as a part of colon. The example of the connected regions of intestine and colon are shown in Figure 1.5 [16].

1.1.4   Problem 4: Colon wall detection

Moreover on the last problem, the artifact such as the blurring surface and contrast diminution at locations where the colon lumen interface with air as shown in Figure 1.6, can reduce the capability of colon wall segmentation.
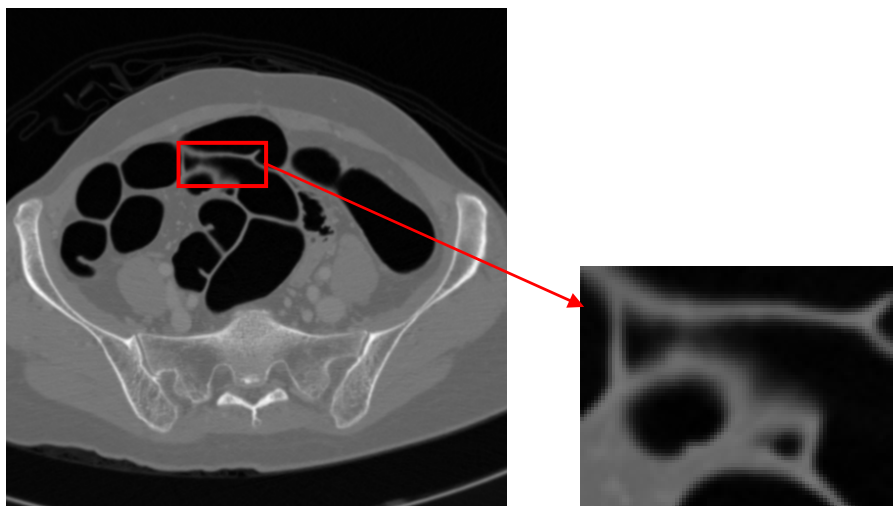
Figure 1.6 Blurring surface and diminution of contrast
where the colon lumen interface with air

Many automatic algorithms for colon wall segmentation have been developed. The basic techniques of colon wall segmentation usually apply region growing [8], [11], [16]–[18]. These methods have a limit on the optimal threshold setting and require the refinement of colon border.

Another approach is operated on the immersion based watershed algorithm to compute the border of colon lumen using gradient map [14], [15], [19], [20]. Nevertheless, these methods also have a restriction on the complication of colon border.

The deformable model based level set methods [21]–[24] are presented for colon lumen segmentation, however, the identification on the descend intensity shaded voxels appearing on the border of colon lumen and soft tissue are problematic.

Many researches on medical images applied deformable model or snake in image segmentation. The traditional deformable model is described as a curve that moves in an image domain with the control of internal forces derived from its curve and the external

forces computed from an image. Thus, the internal forces are assigned to keep the deformable model smooth when curve is deformed. The external forces are assigned to drive the deformable model move to a desired object in an image. However, the traditional deformable model has limitation on a small capture range and also difficulties in driving into the concave boundary regions [25]–[26].

Consequently, a gradient vector flow (GVF) deformable model is designed as an extension model whose external energy is defined as a gradient vector diffusion deriving from the edge map [25]–[29]. The gradient vector field has a more capture range and can force the deformable model into concave regions. The gradient vector flow deformable model has been utilized in medical images for segmentation such as lung, liver, kidney, chest, and brain due to its good performance [30]–[33]. However, the blurring area or the low intensity shaded on the border of colon wall makes the gradient vector flow deformable model difficult to detect and locate the edges.

1.2 Proposed Method

In this dissertation, a framework for reconstructing 3D colon model from oral contranst-enhanced CT colonography images is proposed. The framework is composed of three main parts which are developed for solving the previously described problems. The first part is colon cleansing and the second part is colon wall detection. Then, the colon segmentation and 3D model reconstruction are performed. The details of multistage process in proposed framework are described as follows:

The first part of proposed framework is colon cleansing process which uses the K-means clustering algorithm to detect and eliminate any retained materials of contrast-enhanced fluid (CEF) inside the colon lumen and applies the morphological operations to remove the undesirable partial volume effect between two distinct intensity regions of air and contrast-enhanced materials. The proposed segmentation method employs the K-means clustering algorithm because the number of clusters for partitioning particular regions is known and it converges to the optimal solution faster when compared with the other pixel-based methods [34], [35]. Unlike supervised classification or classification through Neural Network such as Learning Vector Quantization (LVQ) [9], [10] and Self-Organizing Maps (SOM) [36], K-means clustering does not require any analyst specified training data and can also reduce the complexity of computation when the examination of a large number of unknown data is applied.

Moreover, the proposed cleansing method can also improve the rapid transition in intensities at the mucosa layer after undergoing colon cleansing and performs reconstruction of colon wall to be realistic and similar to natural colon lumen by applying average Gaussian low pass filter of two different sizes combined with median filter. Additional, the reconstructing edge is constructed only the areas of cleansing with out effect on the other areas which are not contain contrast enhanced material.

The second part of proposed framework is colon wall detection process. In this process, we propose the enhanced gradient vector flow (EGVF) for assisting on detection and localization of colon lumen. The proposed algorithm for enhanced gradient vector flow is composed of two stages.

The fist stage is the calculation of hybrid edge detector which combines the edge from two detectors, the Canny edge detector [37], [38] and the Laplacian of Gaussian (LoG) detector [33]. The scale of threshold values which is applied on Canny edge detectors is automatically set by applying the Otsu's method [40], [41] with gradient magnitude and the threshold of Laplacian of Gaussian detector is mechanically setting by the mean absolute value of Laplacian of Gaussian [39]. Despite that the Canny edge detection algorithm can produce good edges on the strong edges, the smoothly shaded objects and blurred boundary such as the protrusion layers of colon wall are sometimes miss locating. Moreover, the Canny edge detector identifies any pixel as edge if its magnitude is more than its neighbors without examining the deviations between this pixel and its neighbors, and also slightly more sensitive to weak edges [42]. While the Laplacian of Gaussian detector defines the locations of edges by examination wider area nearby pixel, although it is sensitive to noise [43], [44]. Hence, the Laplacian of Gaussian detector is additionally combined with Canny edge detector to assist in capturing the protrusion layer of colon lumen. Therefore, the hybrid edge detector from both detectors can assist and operate better than performing either the Canny edge detector or the Laplacian of Gaussian detector alone in edge localization and noise reduction.

On the second stage, the hybrid edge from the hybrid detector is then used as an edge mask to locate the enhanced edge and construct an enhanced edge map. The enhanced edge map produces the enhanced gradient vector field and also contribute the enhanced gradient vector flow deformable model in better performance on detection the colon wall.

The third part is colon segmentation and 3D model reconstruction. The proposed colon segmentation method bases on the anatomical structures of colon and volume analysis is applied to the images obtained from the previous part. Then, the proposed colon

segmentation is performed for separation of colon from other organs in abdominal such as stomach and intestine. Finally, the identification colon structure is acquired for rendering the 3D colon model.

1.3 Research objectives

1. To develop colon cleansing method for oral contrast-enhanced CT colonography images.

2. To develop colon segmentation method for oral contrast-enhanced CT colonography images.

3. To reconstruct 3D colon model from oral contrast-enhanced CT colonography images.

1.4 Scopes of the Study

In this dissertation, the scope of work is as follows:

1. The proposed algorithm is performed on the oral contrast-enhanced CT Colonography images with low noise of sizes 512×512 pixels, resulting in 500–700 slices for each dataset and containing both supine and prone position.

2. All CT Colonography images are acquired by a spiral CT scan from the Department of Radiology, Chulalongkorn University.

3. The proposed algorithm focuses on
   Colon cleansing method
   - Detect and remove partial volume effect and contrast-enhanced materials
   - Reconstruct colon wall from unnatural rapid intensities transition
   Colon segmenting method
   - Eliminate other organs which locate adjacent to the colon such as small intestine
   Reconstructing of 3D colon model
   - Internal surface and external surface

4. The experimental results are evaluated by the expert radiologists.

1.5 Expected Outcome

1. Colon cleansing method for oral contrast-enhanced CT colonography images.

2. Colon segmentation method for oral contrast-enhanced CT colonography images.

3. 3D colon model from oral contrast-enhanced CT colonography images.

1.6 Research Plans

1. Study techniques on colon screening.

2. Study related papers and documents of previous work.

3. Prepare the equipment and data for performing research such as

   - Computer for programming and storage data
   - CT Colonography images.

4. Design colon cleansing technique for oral contrast-enhanced CT Colonography images.

5. Design a technique for colon wall detection and a method for colon segmentation to be used in reconstructing of 3D colon model.

6. Analyze experimental results and conclude the outcomes.

7. Write the dissertation.

1.7 Ethical consideration

Due to the National Health Act 2007, the using of patient's radiology images in this research should acquire the acceptation from patients. However, the researchers cannot provide the acceptation from patient because the researcher is not directly connected to the patients. Moreover, the data which are used in this research are the intensity level of the radiology images applying only numeric code with nameless. Consequently, the information of the owner of radiology images cannot be acquired. Nevertheless, the ethical consideration for this research had already been approved by the Ethics Committee of Faculty of Medicine, Chulalongkorn University.

1.8 Organization of the Dissertation

This dissertation is organized as follows. Chapter 1 reviews the introduction and problems of the dissertation. Chapter 2 describes the basic theories and literature reviews of related works. In chapter 3, the proposed framework for reconstructing 3D colon model from oral contrast-enhanced CT colonography images is displayed. The results of the proposed techniques and evaluation assessment are shown in chapter 4. Finally, in chapter 5, it describes summary of conclusion.

CHAPTER II

BASIC THEORIES AND LITERATURE REVIEW

In this chapter, the principles and theories related to the study are described. Virtual colonoscopy and the optical colonoscopy are described in the fist section. Next section, edge detection methods; canny edge detector, and Laplacian of Gaussian (LoG) detector which is the fundamental edge detector in image segmentation are expressed. K-means clustering which is used for classification and Otsu's method which is employed in image threshold are mentioned respectively. The concept of the traditional gradient vector flow (GVF) deformable model, watershed segmentation and level set method are described. The last section, the related work in colon cleansing and colon wall detection is reviewed and discussed.

2.1 Virtual Colonoscopy and Optical Colonoscopy

Virtual colonoscopy or computed tomographic (CT) colonography is a new method for screening colorectal cancer which employs a computed tomography and computers to produce two-dimensional cross-sections of the colon and a computer program combines all images together to produce a three-dimensional image [45], [46] as illustrated in Figure 2.1 [47]. This technique has assisted a radiologist for evaluating the results of virtual colonoscopy and identify abnormalities.

The patients who are operated with the computed tomography colonography should take a clear liquid diet for a day or two days before the test and then take strong laxatives or enemas the night before or morning before the examination to clear residual or stool. Additionally, the patients will drink a contrast solution before the examination to enhance any remaining stool in the colon or rectum. On the scanning process, the patients will be examined in supine position on the computed tomography scanner table. A thin lubricated tube will be inserted gently placed into the rectum and the colon will be slowly inflated with carbon dioxide through the rectal tube. After that, the computed tomography scanner table moves through the scanner to produce the images. The patients will be asked to hold their breath during the scan about ten to fifteen seconds to abstain from distortion on the images and will be repositioned in prone position for a second set of images. After the examination,

the tube is removed. The whole procedure generally takes about ten minutes and does not require sedatives.

The advantages of virtual colonoscopy are that it is not invasive tests such as the optical colonoscopy. It performs essentially faster, more comfortable for patients and does not require sedation. The patients can return to normal activities immediately after examination and safe for patients who take anticoagulation medication. However, the doctor cannot take tissue biopsy during virtual colonoscopy if abnormalities are found. Virtual colonoscopy does not show details such as polyps smaller than five millimeters in diameter as a conventional colonoscopy. Patients may feel bloated or have cramps, but these symptoms should go away when the air passes through the body.

Figure 2.1 CT Colonography (From: [47])

Optic colonoscopy is the basic tool for colorectal cancer examination. A doctor can see the entire colon and looks for any abnormalities such as cancer, inflammation and polyps from a display monitor. If any abnormalities are found, the doctor can take tissue biopsy [48] as illustrated in Figure 2.2 [49].

A patient who requires the optical colonoscopy should drink only clear liquids for at least a day before the examination and avoids red or purple food color, which could be mistaken for blood in the colon. Moreover, he needs to take laxatives the day before the test

and possibly an enema that morning. The patient should not eat or drink anything after midnight of the night before the test. The entire procedure usually takes about 30 minutes and patient will be given a sedating medicine before this procedure. The patient will lie on the left side with knees flexed and a drape will cover during the procedure. The breathing rate, heart rate and blood pressure will be measure during and after the examination. The doctor performs a digital rectal examination before inserting a colonoscopy tube. A colonoscopy tube with one end connected to a camera and the other ends connected to a display monitor is used for examination. A colonoscopy tube is inserted into an anus and passes it through the rectum and colon. [50]. When a colonoscopy tube is inserted or pushed further into the colon, patient may feel an urge and discomfort. The colonoscopy tube will deliver air into the colon and suction will be used to remove any blood or liquid stools to make it easier for the doctor see the lining of the colon. If a small polyp is found the doctor may clip the polyp from the wall of the colon by passing a wire loop through the colonoscopy. For a bigger size of polyp or tumor or other abnormal organs, a biopsy may be done.

Figure 2.2 Optical colonoscopy (From: [49])

The advantage of optical colonoscopy is that the doctor will look at the inner walls of the colon. If any abnormalities are found, the doctor will perform tissue biopsy. However, the patient may feel bloated or have cramps for a while after examination [50]. If any bleeding occurs in the colon, the doctor can pass a heater probe, electrical probe, laser or special medicines through the scope to stop the bleeding site [48]. Moreover, some patients may have low blood pressure or change in heart rhythms due to the sedation during the test [50].

2.2 Edge Detection

Edge detection has an important role in various areas of image analysis and computer vision. It is always applied as a part of segmentation and is used to identify the regions within an image. Edge detection is the process for determining and locating sharp discontinuous intensities of an image. The discontinuous of intensities are sudden changes in pixel intensity that occur between the boundaries of objects in an image. The purpose of performing edge detection is to provide a significant description of object boundaries. If the edges in an image are precisely identified, all of objects which derived from edge detection can be located and fundamental properties such as area, perimeter, compactness, and shape can be determined [51]. Consequently, edge detection is an essential tool for identification and classification of objects in an image.

An edge is the boundary between objects and background which indicates the boundary of an object. It usually represents a important local alteration in image intensities, and always based on discontinuity in either the image intensities or the first derivative of the image intensities. Discontinuities of image intensities can be either step discontinuities where the image intensity sudden alternates from one value on one side of the discontinuity to a distinct value on the different side, or line discontinuities where the intensity values sudden alternates and gives to the beginning value of short distance. However, step and line edges are not regular in real images such as ultrasound images, magnetic resonance images and noisy images. The discontinuity of intensity value is not immediately changed, but gradually occurs over a finite area in real images. For this reason, line edges come to be roof edges and step edges come to be ramp edges [52]. Illustrations of one-dimensional intensity level of edge profiles are shown in Figure 2.3.

(a)　　　　　　　　　　　(b)

(c)　　　　　　　　　　　(d)
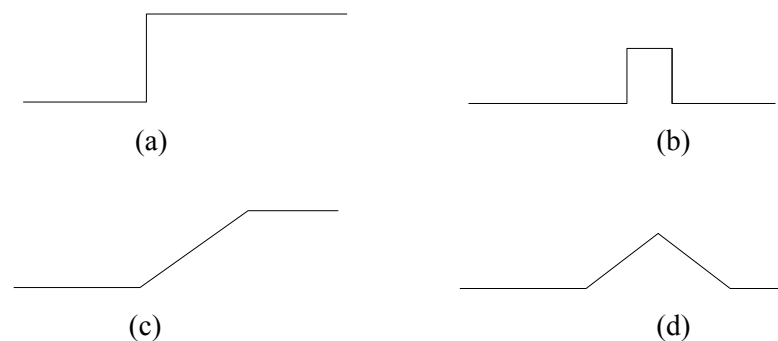
Figure 2.3 (a) Step edge (b) Line edge (c) Ramp edge (d) Roof edge

The process of edge detection usually has three steps. The first step is started by image filtering which is ordinarily used to improve the performance of an edge detector with respect to noise. However, the potential of edge detection is diminished by the number of times filtering is applied. The second step is image enhancement which assists on accentuate pixels where there is an important alteration in local intensity values and is normally performed by calculating the gradient magnitude of the image. The last step is edge detection which applied for identifying edge pixels which are strong edges in an image. There are many techniques for edge detection. However, most of them are based on two categories [51]. The first category is the gradient method which finds edges by determining the maximum and the minimum in the first derivatives of an image. The second category is the Laplacian method which applies the second derivative of an image to identify edges.
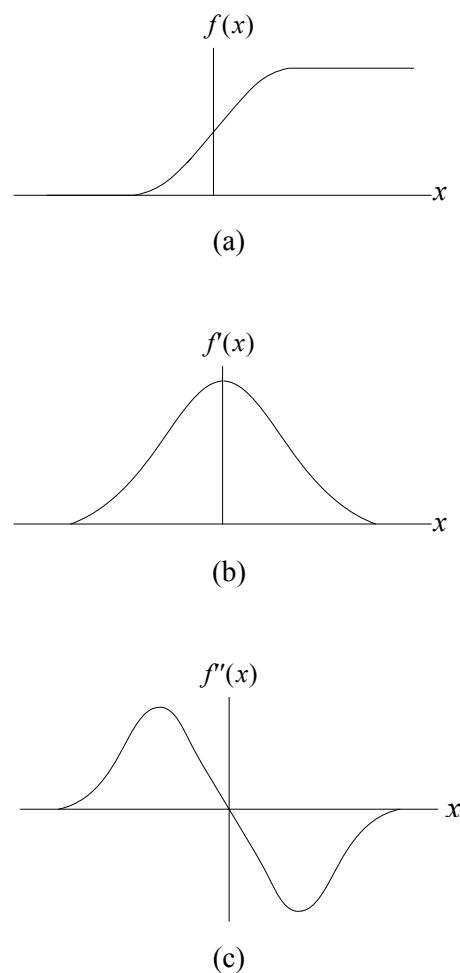
Figure 2.4 (a) Gray level profile, (b) The first derivative of gray scale profile,

(c) The second derivative of gray scale profile

The example for intensity level of image where the discontinuity appears as shape of a ramp is displayed in Figure 2.4 (a). The first derivative of an image and the second derivative of an image are shown in Figure 2.4 (b) and Figure 2.4 (c), respectively.

The basic characteristic of edge is that it has higher intensity values than its surrounding. The first derivative shows the maximum value placed at the centre of the edge in the intensity profiles. A pixel is identified as location of an edge if the gradient magnitude value exceeds the threshold value. The gradient magnitude value is compared to the threshold value and the edge is detected at the location where the gradient exceeds the threshold. On the other hand, when the first derivative is achieved at the maximum, the second derivative becomes zero. Hence, another different method to find the place of an edge is to locate the zeros in the second derivative.

2.2.1 Gradient

The gradient is defined as a vector operation. It is used to measure the changes of intensities value on continuous intensities area in an image. Significant changes in the gray values in an image can be detected by using a discrete approximation for the gradient. The gradient magnitude of an image is calculated by applying the first derivative operator [41], [51]. The gradient of an image $f(x,y)$ at the location x and y is given by

$$\nabla f = \begin{bmatrix} G_x \\ G_y \end{bmatrix} = \begin{bmatrix} \dfrac{\partial f}{\partial x} \\ \dfrac{\partial f}{\partial y} \end{bmatrix} \tag{1}$$

where ∇ is gradient operator of an image which defined as a vector points in the direction of maximum rate of intensity change.

The fist derivative in x direction is expressed by $\partial/\partial x$ and the fist derivative in y direction is expressed by $\partial/\partial y$. The gradient in x direction is denoted as G_x and the gradient in y direction is denoted as G_y. These gradient in both direction can be combined together to calculate the gradient magnitude of each point and identify the orientation of that gradient.

The gradient magnitude of an image, denoted by $mag(\nabla f)$ or $|G|$, is calculated by

$$mag(\nabla f) = |G| = \sqrt{G_x^2 + G_y^2} \tag{2}$$

The direction of the gradient, denoted by θ, is given by

$$\theta = \tan^{-1}\left(\frac{G_x}{G_y}\right) \tag{3}$$

Since, the calculation of the gradient magnitude of an image is based on gaining the partial derivatives $\partial/\partial x$ and $\partial/\partial y$ of the intensity value at every pixel location. The simplest approximation of the first order derivative of image $f(x,y)$ at the location x and y is given by

$$\frac{\partial f}{\partial x} \cong f(x+1,y) - f(x,y) \tag{4}$$

$$\frac{\partial f}{\partial y} \cong f(x,y) - f(x,y+1) \tag{5}$$

On the other hand, the derivatives are performed on an entire image by using different masks such as Roberts operator, Sobel operator, and Prewitt operator.

The Roberts operator is one of the simplest operators which fast undergoes to compute 2-D spatial gradient estimation on an image [41], [51]–[53]. Pixel value at each point in an output image represents the absolute value of gradient magnitude of the input image at that point. The simple approximation of gradient magnitude in both direction G_x and G_y which provided by the Roberts operator can be implemented using the convolution masks are displayed in Figure 2.5.

1	0
0	-1

G_x

0	1
-1	0

G_y

Figure 2.5 Convolution masks of Roberts operator

The Sobel operator consists of 3×3 convolution masks. These masks are designed to respond maximally to edges on vertical and horizontal relative pixels. The gradient magnitude of G_x and G_y of Sobel operator employ the convolution masks as Figure 2.6.

-1	0	1
-2	0	2
-1	0	1

G_x

1	2	1
0	0	0
-1	-2	-1

G_y

Figure 2.6 Convolution masks of Sobel

The Prewitt operator is similar to the Sobel operator and is used for detecting vertical and horizontal edges in images [41], [51]–[53]. It can be implemented using convolution masks as given in Figure 2.7.

-1	0	1
-1	0	1
-1	0	1

G_x

1	1	1
0	0	0
-1	-1	-1

G_y

Figure 2.7 Convolution masks of Prewitt's

2.2.2 Laplacian

The second derivative of a smoothed step edge is a function that crosses zero at the location of the edge [41], [54]–[56]. The formula of Laplacian is defined as

$$\nabla^2 f = \frac{\partial^2 f}{\partial x^2} + \frac{\partial^2 f}{\partial y^2}$$

(6)

where ∇^2 is the Laplacian operator or the second derivative operator.

The Laplacian along the *x* direction and *y* direction are approximated using difference equation as given

$$\frac{\partial^2 f}{\partial x^2} = f(x+1,y) - 2f(x,y) + f(x-1,y) \tag{7}$$

$$\frac{\partial^2 f}{\partial y^2} = f(x,y+1) - 2f(x,y) + f(x,y-1) \tag{8}$$

Since an input image is expressed by value of discrete pixels, the computation of a discrete convolution masks can be employed by approximating the second derivatives in definition of Laplacian. The commonly used of Laplacian masks are shown in Figure 2.8

0	1	0
1	-4	1
0	1	0

1	1	1
1	-8	1
1	1	1

-1	2	-1
2	-1	2
-1	2	-1

Figure 2.8 Convolution masks of Laplacian filter

2.2.3 Canny Edge Detector

The Canny edge detector is considered as the optimal edge detector which is applied for step edges disturbed by white Gaussian noise [51]. It is designed to satisfy three main concepts [43]. The first concept is to diminish the determination of ascertaining false edges and misplaced actual edges. The second concept is the distance between the detected edges as found by the detector and actual edges are to be at the minimum. The last concept is to decrease multiple responses of false edge to guarantee there is only one response to consider as an actual edge point. Consequently, the Canny edge detector can identify the actual edge occurring at minimum and do not response to non-edge. The implementation of the Canny edge detector algorithm must be as followed [41], [52]–[54].

The first step, any noise in the original image is filtered out before locating and detecting any edges. The image $I(x, y)$ is convolved with a Gaussian filter.

$$F(x, y) = |G(x, y) * I(x, y)| \tag{9}$$

where x, y is the coordination of a pixel in the image, * is convolution and $G(x,y)$ is a Gaussian filter that is given by

$$G(x,y) = \frac{1}{\sqrt{2\pi}\sigma} e^{-\left(\frac{x^2+y^2}{2\sigma^2}\right)} \tag{10}$$

where σ is the standard deviation that controls the degree of smoothing.

The Gaussian filter is used to reduce any noise in the original image before trying to locate and detect any edges. A convolution mask is regularly much smaller size than the input image. Consequently, the convolution mask is moved over an image and operating as a square of pixels. If the value of σ is bigger, the size of the Gaussian filter should be larger. This makes more blurring, but essential for noisy images. However, the larger width of Gaussian mask makes less accurate in locating edge and the lower width of Gaussian mask makes detector sensitivity to noises. The result from convolving is an array of smoothed data.

The second step is to estimate the edge strength by computing the gradient operator or the first derivative operator to emphasis the edge region of an image. The gradient magnitude and gradient direction are calculated according to the following equation

$$F(x,y) = \nabla(G(x,y)*I(x,y)) \tag{11}$$

where ∇ is the gradient operator that can be given by

$$\nabla F(x,y) = \left[\frac{\partial F}{\partial x}, \frac{\partial F}{\partial y}\right] \tag{12}$$

Due to the rule on linearity of the operator, the first derivative of convolution Gaussian operator to an image is as same as the first derivative of Gaussian operator convolution with an image as follows.

$$F(x,y) = (\nabla G(x,y))*I(x,y) \tag{13}$$

For this reason, the first derivative of Gaussian operator can be calculated in advance so only one convolution needs to be performed at run-time on the image.

The third step is computing the edge direction and cooperating the edges with a orientation that can be traced in an image. Four probable directions are analyzed when expressing the surrounding pixels. The first orientation is 0 degree in the horizontal direction. The second orientation is 45 degree along the positive diagonal. The third orientation is 90

degree in the vertical direction and the last orientation is 135 degree along the negative diagonal. The orientation can be described by taking a half of circle and partitioning it into five regions, the region of five sectors is show as Figure 2.9. Hence, the edge orientation is determined into one of these four orientation depending on which orientation it is closest.
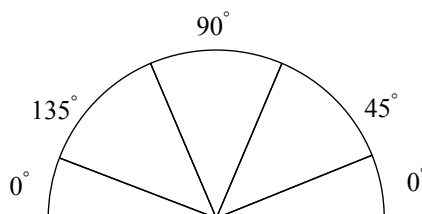
Figure 2.9 Possible directions of the surrounding pixels

The forth step is non-maxima suppression which is used to detect along the edge in the edge orientation and suppress any pixel value that is not estimated to be an edge. This will contribute a thin line along the edge region in the output image. The non-maximal suppression is implemented by quantizing the angle of the gradient to one of the four sectors such as 0 degree in the horizontal direction, 45 degree along the positive diagonal, 90 degree in the vertical direction and 135 degree along the negative diagonal.

The final step, the hysteresis is performed for eliminating any streaking edge. Streaking edge is defined as the discontinuous of edge contours caused by the gradient oscillates more and less the threshold. If a single threshold value is employed to an image, an average strength of edge that are equal or more than the threshold value will be analyze. Therefore, the noise region where the edge drops below the threshold is eliminated. However, it will also make the region which above the threshold receiving an edge appear as a streak or dashed line. To avoid this effect, the hysteresis is implied by using two thresholds, a high threshold, T_{high}, and a low threshold, T_{low}. Any pixel in an image that has a value greater than T_{high} is identified as an edge pixel. Otherwise, any pixels that are contiguous to this edge pixel and that have a value more than T_{low} are defined as edge pixels.

2.2.4 Laplacian of Gaussian (LoG) Detector

The Laplacian operator is defined as the second derivative of a smoothed step edge. It is defined as a function which crosses zero at the position of the edge. The edge points are ascertained by estimating the zero crossing of the second derivative of an image [55]-[57].

Since an input image is expressed as a set of discrete pixels, a discrete convolution mask of Laplacian operator can be found by approximating the second derivatives of Laplacian. The Laplacian operator which is approximated as a second derivative measurement on an image is sensitive to noise. Consequently, it is necessary to eliminate the noise prior to edge enhancement. This process is called the Laplacian of Gaussian (LoG) operation. Thus, an image is smoothed with Gaussian smoothing filter before applying the Laplacian filter in order to reduce high frequency components of noise before performing the differentiation.

An output of the LoG operator, $H(x, y)$, of an image, $I(x, y)$, is obtained by

$$H(x,y) = \nabla^2 (G(x,y) * I(x,y)) \tag{14}$$

where ∇^2 is the second derivative or Laplacian operator, $G(x,y)$ is the Gaussian filter and $*$ is convolution.

The second derivative of Gaussian operator or the Laplacian of Gaussian operator with standard deviation σ is calculated by

$$\nabla^2 G(x, y) = (\frac{x^2 + y^2 - \sigma^2}{\sigma^4}) e^{-\left(\frac{x^2+y^2}{2\sigma^2}\right)} \tag{15}$$

where σ is standard deviation that controls the degree of smoothing.

Because the convolution operation is associative. In the first stage, the Gaussian smoothing filter is convolved with the Laplacian filter and then the result from that convolved filters is convolved with an image to acquire the required result. Since both masks, the Gaussian masks and the Laplacian masks, are normally much smaller size than an image, this operation regularly applies less arithmetic computations.

As previously described on the linearity of the Laplacian of Gaussian operator, the Laplacian of Gaussian operator is able to be computed beforehand in order to only one convolution requires to be undergone on an image. Consequently, an output of the LoG operator can be rewritten in order to decrease the computational time as follows

$$H(x,y) = (\nabla^2 G(x,y)) * I(x,y) \tag{16}$$

2.3 K-means clustering

Image segmentation is a significant stage in medical image classification and analysis for assisting in radiological diagnosis and evaluation. Fundamentally, the methods of image segmentation can be divided into three types: edge-based methods, region-based methods, and pixel-based methods [34], [35].

K-means clustering is one of pixel-based methods. K-mean clustering algorithm is simple, effective, less computational time complexity and can quickly converge to the approximate optimal solution when assessed with other method such as region-based or edge-based methods. Moreover, the method is more practicable and suitable for medical image segmentation since the number of clusters is normally known from the discriminative regions of human anatomy.

K-means clustering classifies data by iteratively computing a mean value for each cluster and adding an observed data into a cluster whose mean value is closest to its data. The algorithm of K-means clustering is started by initiating the centroid of each cluster. These centroids should be selected in an appropriate way because different locations cause different results. Thus, the better way is to set them as further away from each other as possible. The next step, each data belonging to a given data set and associate to it, is taken to the nearest centroid. Consequently, each data is assigned to a cluster whose centroid is the nearest or the Euclidean distance is minimum.

Then after, the centroid of each cluster is recalculated for minimizing an objective function, such as a squared error function.

The objective function is calculated as follows

$$J = \sum_{j=1}^{k} \sum_{i=1}^{n} \left\| x_{i,j} - c_j \right\|^2 \tag{17}$$

where $x_{i,j}$ is data x_i which is in cluster j, c_j is the centroid of cluster j, k is the total number of cluster and n is the number of data.

Consequently, the centroids vary their value step by step until no more alters or that is to say the centroids do not alter any more.

2.4 Otsu's method

Otsu's method is a technique which is employed to mechanically undergo histogram shape-based image threshold to find the optimum threshold value that minimizes the intra-class variance and to separate image components as foreground or background. The adequate threshold value is calculated for separating the two classes of pixels so that the summation of foreground and background can spread at the minimum of intra-class variance [40], [41].

The intra-class variance is defined as a weighted sum of variances of the two classes and calculated by

$$\sigma_w^2 = w_1\sigma_1^2 + w_2\sigma_2^2 \tag{18}$$

where σ_1^2 is the variance of pixels in the background which have intensities below the threshold t and σ_2^2 is the variance of pixels in the foreground which have intensities above the threshold t. While w_1 and w_2 are the probabilities distributions of the two classes which are separated by the threshold t.

The variances of both classes in foreground and background are given by

$$\sigma_1^2 = \sum_{i=0}^{t-1}(i-\mu_1)^2 \, p_i / w_1 \tag{19}$$

$$\sigma_2^2 = \sum_{i=t}^{L-1}(i-\mu_2)^2 \, p_i / w_2 \tag{20}$$

where μ_1 and μ_2 are the mean intensities of pixels in foreground and background, respectively. The probabilities distributions of the two classes are denoted by w_1 and w_2 respectively. The probabilities of pixels that have intensity value i is denoted by p_i, where the range of intensity value i is from 0 to L-1 and L is the maximum level of intensities.

The values of mean intensities of pixels in the two classes in foreground and background, μ_1 and μ_2, are calculated as follows.

$$\mu_1 = \sum_{i=0}^{t-1} i p_i / w_1 \tag{21}$$

$$\mu_2 = \sum_{i=t}^{L-1} ip_i / w_2 \tag{22}$$

The total mean of gray levels in all pixels, denoted by μ_T, is given by

$$\mu_T = \sum_{i=0}^{L-1} ip_i \tag{23}$$

The probabilities distributions of the two classes, w_1 and w_2, in foreground and background are given as follows.

$$w_1 = \sum_{i=0}^{t-1} p_i \tag{24}$$

$$w_2 = \sum_{i=t}^{L-1} p_i \tag{25}$$

The probabilities of pixels that have intensity value i, denoted by p_i, are obtained by

$$p_i = ni / N \tag{26}$$

where n_i is the number of pixels at level i and N is the number of total pixels, with the condition $p_i \geq 0$ and

$$\sum_{i=0}^{L-1} p_i = 1 \tag{27}$$

Because the exhaustive search to find the threshold value that minimizes the intra-class variance has a lot of computations, Otsu express that minimizing the intra-class variance is equal to maximize the inter-class variance or the between-class variances, σ_b^2, as given.

$$\sigma_b^2 = \sigma_T^2 - \sigma_w^2 \tag{28}$$

$$\sigma_b^2 = w_1 (\mu_1 - \mu_T)^2 + w_2 (\mu_2 - \mu_T)^2 \tag{29}$$

where σ_w^2 is intra-class variance and σ_T^2 is the total variances or the combine variance.

From equation (23), on the other hand, the value of total mean intensity of all pixels, μ_T, can also be computed by

$$\mu_T = w_1\mu_1 + w_2\mu_2 \tag{30}$$

where

$$w_1+w_2=1 \tag{31}$$

Then, the between-class variances can easily be rewritten to

$$\sigma_b^2 = w_1 w_2 (\mu_1 - \mu_2)^2 \tag{32}$$

The optimal threshold value which corresponding to this condition is then used for separating the foreground and the background of an image.

While, the total variance of gray levels or the combine variance of gray levels, σ_T^2, is calculated by

$$\sigma_T^2 = \sigma_w^2 + \sigma_b^2 \tag{33}$$

2.5 Morphological Operation

Morphological operations process an image based on shape structuring. Morphological operations employ a structuring element to an input image to generate an output image. The fundamental operations in mathematical morphology are erosion and dilation.

2.5.1 Dilation

Morphological dilation uses vector addition to combine two sets of elements. The dilation $X \oplus B$ is the point set of all possible vector additions of pair elements from sets X and B. Morphological dilation is mathematically defined as follows [56].

$$X \oplus B = \{p \mid p=x+b, \, x \in X \text{ and } b \in B\} \tag{34}$$

The example in mathematic is as given.

$X=\{(0,3), (0,4), (1,0), (1,1), (1,2), (2,2)\}$

$B=\{(0,0), (1,0)\}$

$X \oplus B =\{(0,3), (0,4), (1,0), (1,1), (1,2), (2,2), (1,3), (1,4), (2,0), (2,1), (2,2), (3,2)\}$

For image processing, morphological dilation is an operation that grows or thickens objects in a binary image. The definite manner of this growing or thickening is depended on a shape structuring element [41].

The example of morphological dilation is illustrated in Figure 2.10.

```
0 0 0 0 0 0 0 0 0 0 0 0 0 0 0 0 0 0
0 0 0 0 0 0 0 0 0 0 0 0 0 0 0 0 0 0
0 0 0 0 0 0 0 0 0 0 0 0 0 0 0 0 0 0
0 0 0 0 0 1 1 1 1 1 1 1 0 0 0 0 0
0 0 0 0 0 1 1 1 1 1 1 1 0 0 0 0 0
0 0 0 0 0 1 1 1 1 1 1 1 0 0 0 0 0
0 0 0 0 0 0 0 0 0 0 0 0 0 0 0 0 0 0
0 0 0 0 0 0 0 0 0 0 0 0 0 0 0 0 0 0
0 0 0 0 0 0 0 0 0 0 0 0 0 0 0 0 0 0
```

(a)

```
      1
     1
    1
   1
  1
```

(b)

```
0 0 0 0 0 0 0 0 0 0 0 0 0 0 0 0 0 0
0 0 0 0 0 0 0 1 1 1 1 1 1 1 0 0 0
0 0 0 0 0 0 1 1 1 1 1 1 1 0 0 0
0 0 0 0 0 1 1 1 1 1 1 1 1 0 0 0
0 0 0 0 1 1 1 1 1 1 1 1 0 0 0 0
0 0 0 1 1 1 1 1 1 1 1 0 0 0 0 0
0 0 0 1 1 1 1 1 1 1 0 0 0 0 0 0
0 0 0 1 1 1 1 1 1 1 0 0 0 0 0 0 0
0 0 0 0 0 0 0 0 0 0 0 0 0 0 0 0 0 0
```

(c)

Figure 2.10 (a) Original image (b) Structuring element

(c) Output from morphological dilation

2.5.2 Erosion

The morphological erosion uses vector subtraction to combine two sets of elements. Neither erosion nor dilation is an invertible transformation. The morphological erosion is mathematically defined as $X\ominus B$ and calculated as follows [56].

$$X\ominus B = \{p|\ p=x+b \in X \text{ for every } b \in B\} \tag{35}$$

The example in mathematics is shown as given.

$X=\{(0,3), (1,0), (1,1), (1,2), (1,3), (1,4), (2,3), (3,3)\}$

$B=\{(0,0), (1,0)\}$

$X\ominus B =\{(0,3), (1,3), (2,3)\}$

For image processing, the morphological erosion is an operation that shrinks or thins objects in a binary image. The definite manner of shrinking is depended on a shape structuring element [41]. The example the morphological erosion is illustrated in Figure 2.11.

```
0 0 0 0 0 0 0 0 0 0 0 0 0 0 0 0 0 0
0 0 0 0 0 0 0 0 0 0 0 0 0 0 0 0 0 0
0 0 0 0 0 1 1 1 1 1 1 1 0 0 0 0 0 0
0 0 0 0 0 1 1 1 1 1 1 1 0 0 0 0 0 0
0 0 0 0 0 1 1 1 1 1 1 1 0 0 0 0 0 0
0 0 0 0 0 0 0 0 0 0 0 0 0 0 0 0 0 0
0 0 0 0 0 0 0 0 0 0 0 0 0 0 0 0 0 0
```

(a)

```
1
1
1
```

(b)

```
0 0 0 0 0 0 0 0 0 0 0 0 0 0 0 0 0 0
0 0 0 0 0 0 0 0 0 0 0 0 0 0 0 0 0 0
0 0 0 0 0 0 0 0 0 0 0 0 0 0 0 0 0 0
0 0 0 0 0 1 1 1 1 1 1 1 0 0 0 0 0 0
0 0 0 0 0 0 0 0 0 0 0 0 0 0 0 0 0 0
0 0 0 0 0 0 0 0 0 0 0 0 0 0 0 0 0 0
0 0 0 0 0 0 0 0 0 0 0 0 0 0 0 0 0 0
```

(c)

Figure 2.11 (a) Original image (b) Structuring element

(c) Output from morphological erosion

2.6 Traditional Deformable Model

The deformable model has been used in the domain of image processing to find the contour of an object in an image [25]–[29]. In additional, it is always used in image processing and computer vision to detect objects, and to determine their shapes such as edge detection, shape modeling, image segmentation, image recognition and image understanding. The deformable model performs a segmentation task without knowing or predetermining the shape. Therefore, this property makes them very useful in variety of applications.

The application of deformable model begins with the setting of initial contour on the object boundary. The initial contour is used as an input to start algorithm of deformable model. The algorithm proceeds and the deformable model starts deforming to minimize its energy function at every step. In the process, the contour of deformable model is driven to the object boundary in an image and stops when it acquires the minimum energy function at the point where the contour covers around the object of interest. However, the deformable model has limitation on a less capture range and also difficulties in driving into the boundary of concave regions.

The traditional deformable model, also known as snakes model, is defined as a curve that moves within an image domain with the control of internal forces derived from the curve itself and the external forces derived from an image. The internal forces are assigned to keep the deformable model smooth while deformation is undergone. The external forces are assigned to drive the deformable model forward to a desired object in an image.

The traditional deformable model is used for representing the boundary of interesting object using a parametric curve $C(s) = (x(s), y(s))$, $s \in [0,1]$, that moves through the domain of an image to minimize the energy function,

$$E = \int_0^1 \frac{1}{2} \left[\alpha \, | \, C'(s) \, |^2 + \beta \, | \, C''(s) \, |^2 \right] + E_{ext}(C(s)) ds \tag{36}$$

where $C'(s)$ and $C''(s)$ denote the first and the second derivatives of $C(s)$ with respect to s. The first two terms are the internal forces which are calculated from the curve itself and the third term E_{ext} is the external energy function acquired from an image. The parameter α and β are weighting parameters, which control the tension and the rigidity of curve.

The external energy function, E_{ext}, which is assigned to move a deformable contour toward to edges, is given as follows:

$$E_{ext}(x,y) = -\left|\nabla(G_\sigma(x,y) * I(x,y))\right|^2 \tag{37}$$

where $I(x,y)$ is a gray intensity image, ∇ is the gradient operator and $G_\sigma(x,y)$ is a two dimensional Gaussian function with standard deviation σ.

A parametric curve that minimizes E, must satisfy the Euler – Lagrange equation which is given by

$$\alpha C''(s,t) - \beta C''''(s,t) - \nabla E_{ext} = 0 \tag{38}$$

In order to resolve a solution of equation (38), the parametric deformable model is made dynamic by treating C as a function of time t as $C(s,t)$. Then, partial derivative of C with respect to t is as follows.

$$C(s,t) = \alpha C''(s,t) - \beta C''''(s,t) - \nabla E_{ext} \tag{39}$$

2.7 Gradient Vector Flow Deformable Model

The gradient vector flow (GVF) deformable model is designed as an extension model which the external energy is estimated as a diffusion of gradient vector deriving from the edge. The advantages of the gradient vector flow deformable model over a traditional deformable model is that its resultant field has a more capture range and can forces the deformable model into boundary concavities [26]–[29], [58]–[62]. The example of comparison of traditional deformable model and gradient vector flow deformable model are shown as Figure 2.12 [28].

2.7.1 Gradient Vector Flow

The gradient vector flow deformable model starts by computing a field of forces, called the gradient vector flow force, over the image domain. The gradient vector flow forces are estimated by employing generalized diffusion equation to components of the gradient of the image edge map, and are used to drive the snake toward the boundaries of the object. In the gradient vector flow deformable model, the external force term $-\nabla E_{ext}$ in equation (39) is replaced with the gradient vector flow field, $\tilde{v}$, as follows.

$$C(s,t) = \alpha C''(s,t) - \beta C''''(s,t) + \tilde{v} \tag{40}$$

The parametric curve that solves the above equation is called gradient vector flow deformable model.

(a)   (b)

(c)   (d)
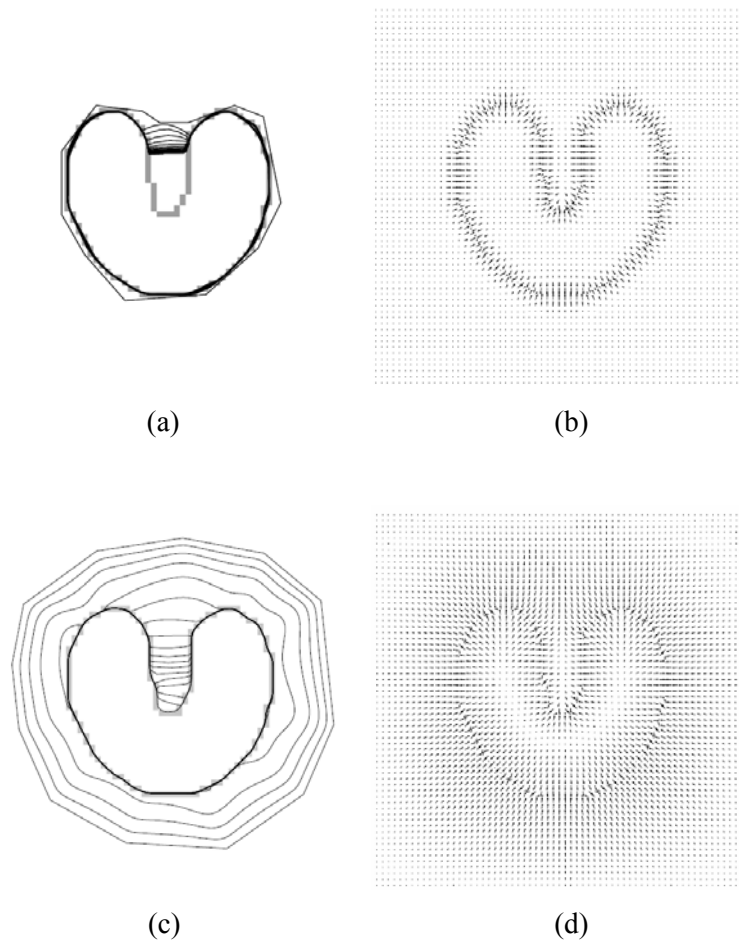
Figure 2.12 (a) Convergence of traditional forces (b) Traditional forces
(c) Convergence of gradient vector flow (d) Gradient vector flow forces (From: [28])

The gradient vector flow field which is identified as a vector field, $\tilde{v}(x,y)$, can be found by treating a vector field as a function of time t, and solving the following vector diffusion equation.

$$v_t = g(|\nabla f|)\nabla^2 v - h(|\nabla f|)(v - \nabla f) \qquad (41)$$

$$v(s,0) = \nabla f \qquad (42)$$

where v_t is the partial derivative of $v(s,t)$ with respect to t. and v defined as vector field. The term $g(|\nabla f|)$ and $h(|\nabla f|)$ are weighting parameters that are dependened on the gradient of the

edge map. The notation ∇ is the gradient operator, ∇^2 is the Laplacian operator which is applied to each spatial component of v separately and f is the edge map that has large magnitudes at locations near the edges.

Since $g(|\nabla f|)$ and $h(|\nabla f|)$ should be monotonically non-increasing and non-decreasing functions of $|\nabla f|$. The weighting parameters are defined as follows.

$$g(|\nabla f|) = \mu \tag{43}$$

$$h(|\nabla f|) = |\nabla f|^2 \tag{44}$$

where μ is the coefficient of gradient vector flow.

Since $g(|\nabla f|)$ is a constant, the smoothing occurs everywhere and $h(|\nabla f|)$ grows larger near strong edges. Thus, the gradient vector flow is computed using these weighting functions to converge to edge location.

Consequently, the gradient vector flow field can be found by.

$$v_t = \mu \nabla^2 v - (v - \nabla f)|\nabla f|^2 \tag{45}$$

where v_t is the partial derivative of vector field $v(x, y, t)$ with respect to t at x and y coordinations. The coefficient μ is denoted as regularization parameter to control the trade off between the first term and the second term of equation. The example of gradient vector field is shown in Figure 2.12 (d) [28].

2.7.2 Edge Map

Edge map $f(x,y)$ is derived from grey scale input image, $I(x,y)$, with the function of continuous position variables (x,y), using first derivative operator. This method gives both the magnitude and direction of the gradient information for every edge pixel found in an image.

The algorithm starts by smoothing an image by Gaussian convolution. Then after, a simple 2-D spatial first derivative operator is employed to the smoothed image to emphasis regions of the image with first derivatives, as the following equations.

$$f = \left| \nabla (G(x,y) * I(x,y)) \right| \tag{46}$$

$$G(x,y) = \frac{1}{\sqrt{2\pi}\sigma} e^{-\left(\frac{x^2+y^2}{2\sigma^2}\right)} \tag{47}$$

where $G(x,y)$ is a two-dimensional Gaussian function with standard deviation σ and ∇ is the gradient operator.

Then the edge map f is applied to compute the gradient of edge map, ∇f, of gradient vector flow. The gradient of edge map has vectors pointing toward the edges and have large magnitudes near the edges. Thus, a deformable model will move and converge to a stable configuration near the edge.

2.7.3 Gradient Vector Flow Deformable Model

From the discrete approximations for low-order continuous derivatives in one and two dimensions [59], the first order partial derivatives, the second order derivatives and the forth order derivatives can be approximated as follows.

$$C_t = \frac{\partial C}{\partial t} \tag{48}$$

$$C_t \approx \frac{C_s^{t+\delta t} - C_s^t}{\delta t} \tag{49}$$

$$C'' = \frac{\partial^2 C}{\partial s^2} \tag{50}$$

$$C'' \approx \frac{C_{s+\delta s}^{t+\delta t} + C_{s-\delta s}^{t+\delta t} - 2C_s^{t+\delta t}}{\delta s^2} \tag{51}$$

$$C'''' = \frac{\partial^4 C}{\partial s^4} \tag{52}$$

$$C'''' \approx \frac{C_{s+2\delta s}^{t+\delta t} - 4C_{s+\delta s}^{t+\delta t} + 6C_s^{t+\delta t} - 4C_{s-\delta s}^{t+\delta t} + C_{s-2\delta s}^{t+\delta t}}{\delta s^4} \tag{53}$$

where t represents the number of iterations, δt is the time step, and δs is the space step. The second and the fourth derivatives are estimated though as at the next time step.

The discrete approximations in equations (48)–(53) are substituted into equation (39) and give the following equation.

$$\frac{C_s^{t+\delta t}-C_s^t}{\delta t}=\alpha\left(\frac{C_{s+1}^{t+\delta t}+C_{s-1}^{t+\delta t}-2C_s^{t+\delta t}}{\delta s^2}\right)$$

$$-\beta\left(\frac{C_{s+2}^{t+\delta t}-4C_{s+1}^{t+\delta t}+6C_s^{t+\delta t}-4C_{s-1}^{t+\delta t}-C_{s-2}^{t+\delta t}}{\delta s^4}\right)-\nabla E_{ext} \tag{54}$$

Then, the term δt is moved to the right side.

$$C_s^{t+\delta t}-C_s^t=\alpha\frac{\delta t}{\delta s^2}\left(C_{s+1}^{t+\delta t}+C_{s-1}^{t+\delta t}-2C_s^{t+\delta t}\right)$$

$$-\beta\frac{\delta t}{\delta s^4}\left(C_{s+2}^{t+\delta t}-4C_{s+1}^{t+\delta t}+6C_s^{t+\delta t}-4C_{s-1}^{t+\delta t}+C_{s-2}^{t+\delta t}\right)-\delta t\nabla E_{ext} \tag{55}$$

The coefficients of the same variable term are combined together and equation (55) is rewritten as follows.

$$C_s^t+\delta t\nabla E_{ext}=\left(\beta\frac{\delta t}{\delta s^2}\right)C_{s+2}^{t+\delta t}-\left\{\left(\alpha\frac{\delta t}{\delta s^2}\right)+4\left(\beta\frac{\delta t}{\delta s^4}\right)\right\}C_{s+1}^{t+\delta t}$$

$$+\left\{1+2\left(\alpha\frac{\delta t}{\delta s^2}\right)+6\left(\beta\frac{\delta t}{\delta s^4}\right)\right\}C_s^{t+\delta t}$$

$$-\left\{\left(\alpha\frac{\delta t}{\delta s^2}\right)+4\left(\beta\frac{\delta t}{\delta s}\right)\right\}C_{s-1}^{t+\delta t}+\left(\beta\frac{\delta t}{\delta s^4}\right)C_{s-2}^{t+\delta t} \tag{56}$$

For easy understanding, the term in equation (56) is rewritten by applying the following definition.

$$a=\left(\alpha\frac{\delta t}{\delta s^2}\right)$$

$$b=\left(\beta\frac{\delta t}{\delta s^4}\right) \tag{57}$$

Then, equation (56) can simply be represented as

$$C_s^t - \delta t \nabla E_{ext} = b\, C_{s+2}^{t+\delta t} - \{a+4b\} C_{s+1}^{t+\delta t} + \{1+2a+6b\} C_s^{t+\delta t}$$

$$- \{a+4b\} C_{s-1}^{t+\delta t} + b\, C_{s-2}^{t+\delta t} \tag{58}$$

Similarly, when defining the term $p = b$, $q = -a - 4b$ and $r = 1 + 2a + 6b$, equation (58) can easily be written as

$$C_s^t - \delta t \nabla E_{ext} = p\, C_{s+2}^{t+\delta t} + q\, C_{s+1}^{t+\delta t} + r\, C_s^{t+\delta t} + q\, C_{s-1}^{t+\delta t} + p\, C_{s-2}^{t+\delta t} \tag{59}$$

Then, the terms on the right side are denoted by $\widetilde{C}_s^{t+\delta t}$.

$$\widetilde{C}_s^{t+\delta t} = p\, C_{s+2}^{t+\delta t} + q\, C_{s+1}^{t+\delta t} + r\, C_s^{t+\delta t} + q\, C_{s-1}^{t+\delta t} + p\, C_{s-2}^{t+\delta t} \tag{60}$$

Equation (59) can be rewritten as follows.

$$C_s^t - \delta t \nabla E_{ext} = \widetilde{C}_s^{t+\delta t} \tag{61}$$

From equation (60), the deformable model gives a set of N simultaneous linear equations for the x and y co-ordinates. When $C_0 = C_N$, the deformable model forms a closed loop with $C_0^{t+\delta t} = C_N^{t+\delta t}$.

Then equation (60) can be written as follows.

$$\begin{bmatrix} r & q & p & & & p & q \\ q & r & q & p & & & p \\ p & q & r & q & p & & \\ & \ddots & \ddots & \ddots & \ddots & \ddots & \\ & & p & q & r & q & p \\ p & & & p & q & r & q \\ q & p & & & p & q & r \end{bmatrix} \begin{bmatrix} C_0^{t+\delta t} \\ C_1^{t+\delta t} \\ C_2^{t+\delta t} \\ \vdots \\ C_{N-3}^{t+\delta t} \\ C_{N-2}^{t+\delta t} \\ C_{N-1}^{t+\delta t} \end{bmatrix} = \begin{bmatrix} \widetilde{C}_0^{t+\delta t} \\ \widetilde{C}_1^{t+\delta t} \\ \widetilde{C}_2^{t+\delta t} \\ \vdots \\ \widetilde{C}_{N-3}^{t+\delta t} \\ \widetilde{C}_{N-2}^{t+\delta t} \\ \widetilde{C}_{N-1}^{t+\delta t} \end{bmatrix} \tag{62}$$

Each row of the matrix can be represented as a convolution mask for evaluating the derivatives. The constant values of the matrix are as follows.

$$p = \beta \frac{\delta t}{\delta s^2} \tag{63}$$

$$q = -\alpha \frac{\delta t}{\delta s^2} - 4\beta \frac{\delta t}{\delta s^4} \tag{64}$$

$$r = 1 + 2\alpha \frac{\delta t}{\delta s^2} + 6\beta \frac{\delta t}{\delta s^4} \tag{65}$$

When matrix **M** represents a circulant marix in equation (62), then equation (62) can be simply rewritten as follows.

$$\mathbf{M}C^{t+\delta t} = \widetilde{\mathbf{C}}_s^{t+\delta t} \tag{66}$$

The term on the right side of equation (66) is substituted with $\widetilde{C}_s^{t+\delta t} = C_s^t - \nabla E_{ext}$ from equation (61).

$$\mathbf{M}\mathbf{C}^{t+\delta t} = \mathbf{C}_s^t + \delta t \nabla \mathbf{E}_{ext} \tag{67}$$

After that, multiply equation (67) by inverse matrix of matrix **M** is performed, then equation (67) can be written as follws.

$$\mathbf{C}^{t+\delta t} = \mathbf{M}^{-1}(\mathbf{C}_s^t - \delta t \nabla \mathbf{E}_{ext}) \tag{68}$$

Due to the gradient vector flow deformable model, the external forces are defined as a diffusion vector field of gradient vector flow of edge map. Then, the term $-\nabla \mathbf{E}_{ext}$ is expressed with the gradient vector flow, v_t.

$$\mathbf{C}^{t+\delta t} = \mathbf{M}^{-1}(\mathbf{C}_s^t + \delta t v_t) \tag{69}$$

Since the gradient vector flow deformable model is identified with the x and y coordinates, the terms v_t in equation (69) can be rewritten for the x and y direction as given.

$$x^{t+\delta t} = \mathbf{M}^{-1}(x^t + \delta t v_t) \tag{70}$$

$$x^{t+\delta t} = \mathbf{M}^{-1}(y^t + \delta t v_t) \tag{71}$$

2.8 Watershed Segmentation

The concept of watershed is based on viewing the height of the area as proportional to gray intensity level of an image. The bright areas have high altitude and the dark areas have low altitude, then they might look like the geography surface [63], [64] as shown in Figure 2.13.

(a)	(b)
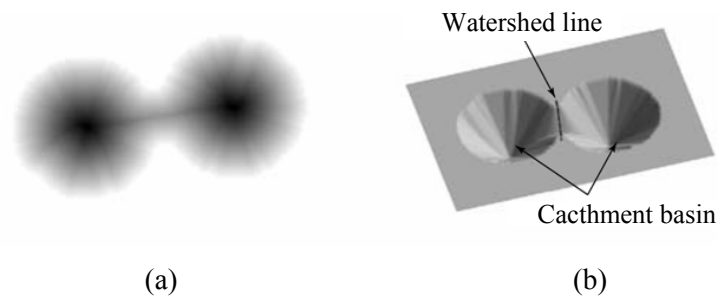
Figure 2.13 (a) Gray intensity level of an image (b) Geography surface of an image.

In the geographic interpretation, there are three types of points for consideration

1) The points form regional minimum of the surface.

2) The points where a pond of water fall with certainty to a single minimum or the points at which construct a gradient interior region are called catchment basin or watershed of that minimum.

3) The points where a pond of water fall with certainty to more than one minimum and form crest lines dividing different catchment basins, they are termed by partition lines or watershed lines.

The objective of watershed segmentation is to find all of the watershed lines. Suppose that a hole is punched into each regional minimum and the entire geography is flooded by letting water leak at a uniform rate through the hole at the bottom of catchment basin as Figure 2.14 (a). If the water of neighboring catchment basins is likely to merge, a dam is created to avoid the water spilling from one basin into the other as shown in Figure 2.14 (b). A dam is built all the way to the highest surface altitude or to the maximum gray intensity value. Consequently only the top of the dams represent the water line. These dam boundaries are the divide lines of the watersheds. Therefore, the extracted edges of all dams form the watershed segmentation [64].
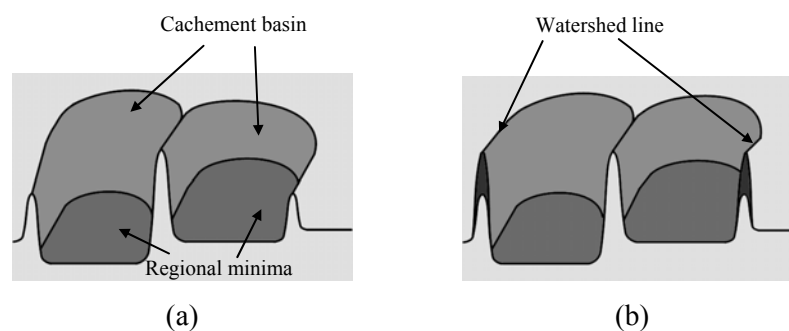
Figure 2.14 (a) Two regional minima (in dark)

(b) Dams built to prevent merging of rising water between different catchment basins

Binary morphological dilation is applied for constructing dam. The steps of the watershed algorithm to find the edge image is performed as follow. Initially, the set of pixels with the minimum gray level are 1, others are 0. In each subsequent step, the water is flooded in the topography surface from the bottom. The pixels that cover with flooding water are 1 and others are 0. The dam must be built to keep water from spilling across the basins [41].

Assumed that there are two connected components at flooding step $n-1$. Afterward, assumed that there is only one connected component at flooding step n. This means that the flooding water from those two catchment basins has combined together at flooding step n.

Let q denotes a single connected component. The dilation of a connected component in each step is performed by the structuring element with two conditions

Condition 1: The dilation has to be constrained *to q*. It means that the center of the structuring element can be located only at the points inside q during dilation.

Condition 2: The dilation cannot be performed on the set of points that may cause the sets being dilated to merge

When satisfaction by two conditions, the dam is built by the points where the dilation would make the two catchment basins going to merge. Then, the connected path of one-pixel thick is build as separating dam at the nth stage of flooding.

Since, direct employing of the watershed segmentation algorithm sometimes may produces over segmentation of an image due to peculiarities of the gradient and noise [10], [41], [65], [66], the solution is to confine the number of acceptable regions by applying the preprocessing with knowledge of the interesting object to segmentation method. A marker is

defined as a connected component belonging to an image. Selection of markers consists of two principal stages, preprocessing and determination of criterion to satisfy the area and location of markers. There are two types of markers, the first type is an internal marker which is related with the interesting objects and another type is an external marker which is related with the background. The internal markers normally define the region surrounded by the higher altitude points or every region should be a connected component or every point in the region should have the same gray level value. Internal markers are applied to confine the number of acceptable regions by identifying the objects of interest. The external markers are pixels which are assured as belonging parts of the background. External markers can be some regions of particular background color. Marker selection can be found by simple procedures based on gray intensity to more complex descriptions involving size, shape, location, relative distances, and texture content.

2.9 Level Set Method

In level set, formulation of deformable contour denoted by C, is expressed by the zero level set $C(t) = \{(x, y) \mid \phi(t, x, y) = 0\}$ of a level set function $\phi(t, x, y)$. The evolution equation of the traditional level set function ϕ can be defined in the general form of level set equation as given [67]–[69].

$$\frac{\partial \phi}{\partial t} + F|\nabla \phi| = 0 \qquad (72)$$

Function F is called the speed function which depends on an image data and the level set function, ϕ.

Since traditional level set has problems with incorrectly moved [69], the variation level set formulation is defined as follows

$$\varepsilon(\varphi) = \mu P(\phi) + \varepsilon_m(\phi) \qquad (74)$$

where $\mu>0$ is a parameter controlling the effect of penalizing the deviation of ϕ from a signed distance function, and $\varepsilon_m(\phi)$ is external energy that would drive the motion of the zero level curve of ϕ. The energy term of $P(\phi)$ is called internal energy of the function ϕ and defined as follows

$$P(\phi) = \int \frac{1}{2}(|\nabla \phi - 1|)^2 dxdy \tag{73}$$

In order to create deformable models which are dynamic curves that move toward the object boundaries, the edge indicator function g of an image I, is defined as follows

$$g = \frac{1}{1 + |\nabla G_\sigma * I|^2} \tag{75}$$

where G_σ is the Gaussian function with standard deviation σ.

The external energy that can move the zero level curve towards the object boundaries is defined by,

$$\varepsilon_{g,\lambda,v}(\phi) = \lambda L_g(\phi) + vA_g(\phi) \tag{76}$$

where λ is the coefficient of weight length term that is greater than 0 and v is the coefficient of weight area term which that is greater than 0 when the initial contour is outside an object and less than 0 when initial contour is inside an object.

The terms $L_g(\phi)$ is weight length term and $A_g(\phi)$ is weight area term, are given by

$$L_g(\phi) = \int_\Omega g\delta(\phi)|\nabla \phi| dxdy \tag{77}$$

$$A_g(\phi) = \int_\Omega gH(-\phi)dxdy \tag{78}$$

where δ is the Dirac function, g is the edge indicator function, and H is the Heaviside function. Then the total energy function is rewritten as follows,

$$\varepsilon(\varphi) = \mu P(\phi) + \varepsilon_{g,\lambda,v}(\phi) \tag{79}$$

Then, the external energy term, $\varepsilon_{g,\lambda,v}(\phi)$, drives the zero level set toward the object boundaries, while the internal energy term, $\mu P(\phi))$, controls the deviation of ϕ from a signed distance function during its evolution.

2.10 Literature Review

Chen et al. [9] applied a multistage process that employed a modification of self-adaptive vector quantization to compute a low-level classification of image and utilized a region-growing method to extract high-level features. Statistical analysis on intensity vectors of voxels cooperate with nearby voxels are use to make low-level classification. The residual fluid, stool, and air voxels inside colon are extracted and bone voxels are eliminated in high-level processing. The method had good ability on reproducing and repeating consrtuction colon model and had some problem due to partial volume effect.

Lakare et al. [10] presented an automatic and robust tagged-residue detection technique using vector quantization based classification. The multistep techniques were employed to reduce intensity variation among the residual materials. First, the unsupervised and self-adapting vector quantization algorithm was manipulated for classification. Afterwards the resultant classes were sorted by the average intensities. The groups of classes were computed their average intensity and applied a conservative threshold to help in discriminating soft tissue from tagged material. However, their technique did not mention the effect of the sharpen intensity at the mucosa layer after colon cleansing.

Sato et al. [11] described an automatic colon segmentation method with patient-friendly bowel preparation which was more appropriate for digitally removing undesirable remain materials in the colon. The vertical filter was applied to eliminate the partial volume effect voxels based on its intensities features. For detecting colon wall, the gradient-magnitude-based region growing algorithm was performed to improve the accuracy of the boundary. The results were illustrated with both extracted 2D images and a reconstructed 3D colon model. Nevertheless, this technique did not mention the effect of the sharpen intensity at the mucosa layer after colon cleansing.

Lakare et al. [12–13] presented a technique for segmentation and digital colon cleansing. This method used the characteristics analysis on the intersection between two distinct intensity regions. To find each intersection between two distinct intensity regions, the cast rays or segmentation rays was performed through the volume. The proposed methods also associated reconstruction and classification task to examine each intersection using detecting ray. Furthermore, the volumetric contrast enhancement technique was utilized to reconstruct colon wall that missing by segmentation, which aided to improve quality on colon model rendering. However, this method required cautiously selecting the intersection characteristics for assigning classification and reconstruction tasks.

Skalki et al. [14–15] applied non-linear transfer function and a morphological dilation operation to find the intensity profile of contrast-enhanced material. Moreover, the threshold function combined with triangular intensity transformation is presented for colon cleansing method. Notwithstanding, this method requires the cautiously selecting the characteristics for assigning the classification tasks.

Bidgoli et al. [16] applied in half-sized of volume data for image segmentation in order to reduce the memory usage and processing time. The process utilized global and local histograms of contrast-enhanced fluids to construct adaptive thresholds for determination the tissue regions and applied them to automatically initiate seeding and region growing. Their method could applied to all part of colon lumen and can be extracted any parts of it, even they might be covered by enhancement fluid. The subjective and objective evaluations described that the error leakage of non colon organ was minimized. Even so, this method also had a limit on imported setting of an optimal threshold.

Bevilacqua et al. [17] described a complete image processing framework for virtual colonscopy. The developed algorithms covered the entire process that allows a virtual navigation inside the colon lumen, starting from a dataset of axial CT slices. The contrast-enhanced fluids were removed by transfer function. The abdominal organs such as lung, intestine and colon segmentation were acquired by region growing.

Sadleir et al. [18] proposed a multistage algorithm to find the centerline of colon. The process began with identifying voxels that represent the colon lumen using a simple 3D region growing algorithm with threshold selecting and then after topological thinning was applied to find the centerline of colon.

Lapeer et al. [19], [20] proposed a combined approach to 3D medical image segmentation using marker-based watersheds and active contours. The cooperation of two approaches was employed for solving the contour initialization problem in active contour model and non smoothing problem in marker-based watershed segmentation. Then, fast initial contour from the watershed algorithm and fine-tuning using active contours is performed. However, this technique requires the manually place maker on the original images.

Yuchong et al. [21] developed a fast, accurate, and patient-friendly computer-aided diagnosis (CAD) of CT Colonography and improved the robustness and accuracy of colon wall segmentation. The active contour model based level set method was assisted for colon lumen detection. Nevertheless, the paper did not mention about the contrast-enhanced

material. Datasets which used in examination were not performed colon cleansing, then segmented colon was included contrast-enhanced material.

Uitert et al. [22] developed a level set based method to roughly scan the location of colon tissue boundary. After determining the location, the algorithm segments the entire colon wall is performed. The results of colon wall were shown with the different thickness of outer colon wall and inner colon wall. However, the accuracy on colon wall detection should be improved.

Hamidpour et al. [23] proposed a two-stage based segmentation to extract the rough initial contours at first. Then, extracted boundaries were smoothed and fined using a modified geometric deformable model algorithm which improving the stopping terms of the level set algorithm. The proposed methods aimed at removing false contours which obtained during the first stage and performed smoothen in the second stage. The improvement of accuracy of the segmentation method was compared with region growing method. However, the datasets were not performed colon cleansing. Then, colons included with contrast-enhanced materials were segmented by level set method.

Chen et al. [24] used a simple threshold method and intensity equalization to remove contrast-enhanced materials. Then after, the adaptive level set technique is applied for colon segmentation. During iteration, the information in each region is considered by estimating the parameters of probability density function. However, the enhanced material still remained and the initial contour was done by manual seeding.

CHAPTER III

PROPOSED FRAMEWORK

This chapter describes the proposed framework for reconstructing 3D colon model from oral contrast-enhanced CT colonography images.
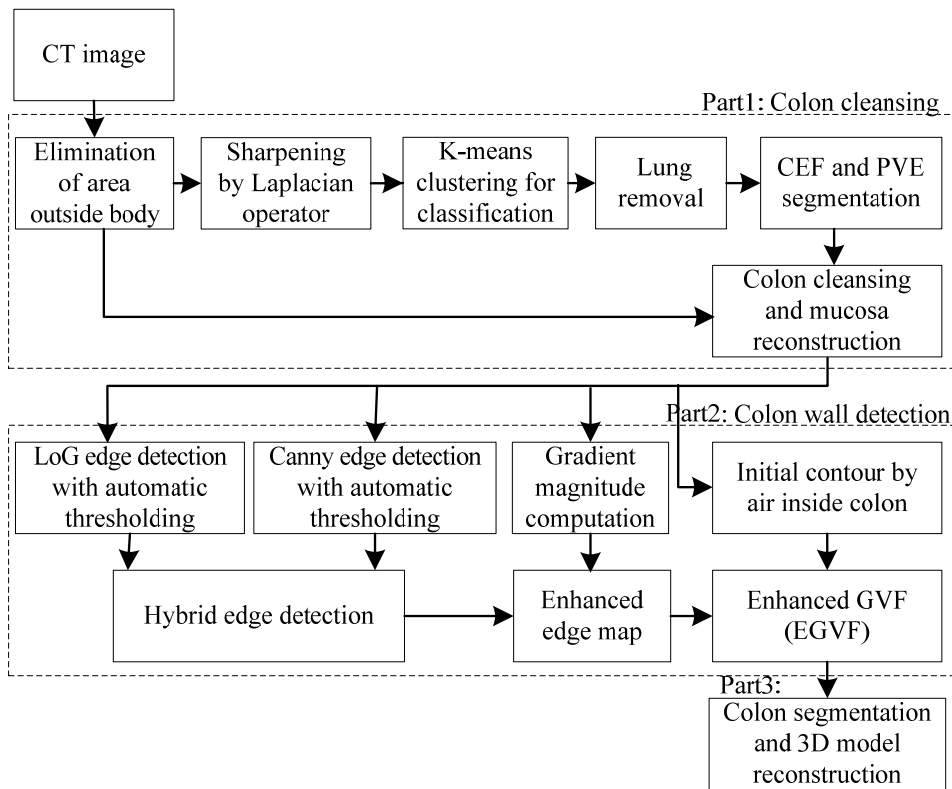
Figure 3.1 Framework of the proposed method

The proposed framework is composed of three main parts as shown in Figure 3.1. The first part is colon cleansing and the second part is colon wall detection. Then, the colon segmentation and 3D model reconstruction are performed. The details of multistage process in proposed framework are described as follows:

The first part of the proposed framework is colon cleansing process which uses the K-means clustering algorithm to detect and to eliminate any retained materials of contrast-enhanced fluid (CEF) inside the colon lumen and applies the morphological operations to

remove the undesirable partial volume effect between two distinct intensity regions of air and contrast-enhanced materials. Moreover, the proposed cleansing method can also improve the rapid transition in intensities at colon wall after colon cleansing and reconstruct mucosa layer of colon wall to be as realistic as possible by applying average Gaussian low pass filter of two different sizes combined with median filter. The second part of the proposed framework is colon wall detection. In this process, the enhanced gradient vector flow (EGVF) is used to assist on detection and localization of colon lumen. The enhanced gradient vector flow algorithm is composed of two stages. The first stage is the calculation of hybrid edge detector, which combines the edge from two detectors, the Canny edge detector and the Laplacian of Gaussian (LoG) edge detector. The scale of threshold values which is applied on Canny edge detector and Laplacian of Gaussian detector are automatically set. In the second stage, the hybrid edge acquired from the hybrid edge detector is used as an edge mask to locate the enhanced edge and to construct an enhanced edge map. The enhanced edge map produces the enhanced gradient vector field and contributes the enhanced gradient vector flow deformable model in better performance on detecting the colon wall.

Afterward, the segmentation method bases on anatomical structures of colon and volume analysis are employed. Eventually, colon segmentation is performed for separation of colon from other organs and identification of colon structure for rendering the 3D colon model.

3.1 Image Acquisition

Since the retained feces in bowel shaped regions of lumen can conceal polyps and the real shape of colon. Removing the retained feces with colonic lavage is essential to provide clarified view of colon wall and to produce the optimal CT colonoscopy results. For this reason, the patients undergo the standard bowel preparation of low residue diet and take colonic lavage to make the retained feces become liquidity. The contrast-enhanced agent is taken to provide the remained residue fluid radio-opaque and the colon lumen is inflated with carbon dioxide gas or room air through the small rectal tube to distend the colon for better viewing during the CT scanning and make the remained materials are homogenized. After bowel preparation, the CT colonoscopy scanning is performed in a single breath hold by a spiral CT scanner. Scanning parameters are applied with 120 kVp, 180–280 mA and field of view (FOV) in the range of 34–40 cm. are varied by the abdomen size. The acquired images are constructed at 1 mm. intervals with 512×512 voxels, resulting in 500–700 slices for each dataset and also are achieved in supine and prone positions.

An example of CT image is illustrated in Figure 3.2. The fundamental components in a CT image are composed of air, soft tissue, fat, muscle, bone, and fluid with enhanced material. Sometimes, other connected organs in abdomen such as the lower portion of lung, stomach, and small bowel or small intestine, may be partially filled with air and sometimes are presented in CT images.
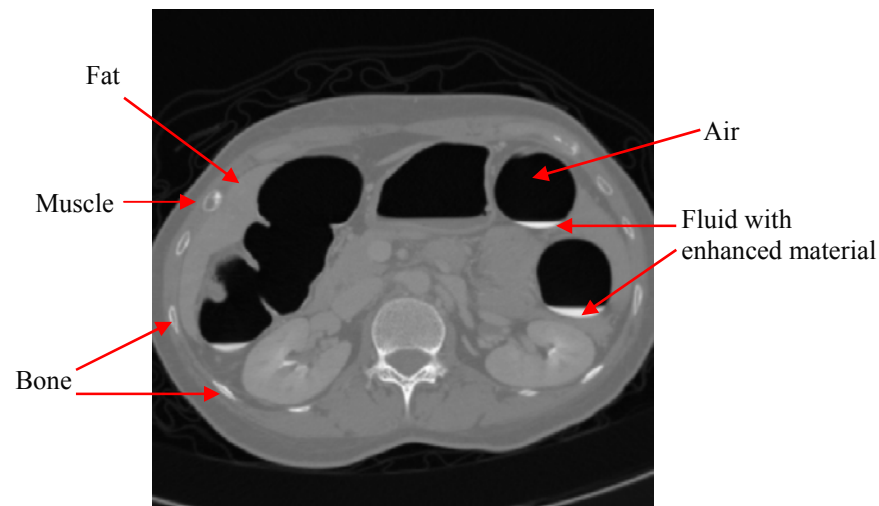
Figure 3.2 Example of CT image

From Figure 3.2, the areas where X-ray can easily pass, are represented in low intensity level or in dark color such as air is displayed as black, muscle is displayed as dark gray, soft tissue and fat are displayed as bright gray. In the opposite way, the areas where X-ray can partially pass or cannot pass are represented in high intensity or bright color such as bone is displayed as white, fluid and stool with enhancement material are displayed as white.

3.2 Segmentation and Elimination of Area Outside Body

Segmentation is an important stage for identifying the boundary inside colon lumen and distinguishing residual material retained inside the colon. In the first process, the voxels outside the body are automatically detected by thresholding with Otsu's method and are discarded from CT images in order to eliminate the extra computing time. The procedure begins with treating the normalized histogram as a discrete probability density function, then Otsu's method is applied to a shape-based histogram to determine the threshold that maximizes the between-class variance, which is used to separate a CT image into two classes as foreground and background.

The Otsu's method algorithm is as follows:

1. The histogram and probability of each intensity level i of an image are computed. The range of the intensity value i starts from 0 to L-1.

2. The probability distributions of the two classes of foreground and background ,assigned as w_1 and w_2 respectively, and the mean intensity values of the pixels in the two classes of foreground and background ,denoted as μ_1 and μ_2 respectively, are initiated.

3. The values of threshold t are step through all possible values of threshold $t = 0$, 1, 2, 3, …, L-1 and used for calculation .

- The probability distributions of the two classes w_1, w_2, which are separated by the threshold t and also the mean intensity value of pixels in the two classes μ_1, μ_2, and the total mean value of pixels, μ_T are updated iteratively and applied for computing.

- The between-class variance $\sigma_b^2(t)$ is computed.

4. The optimal threshold, which corresponds to the maximum, $\sigma_b^2(t)$, is desired.

(a)   (b)
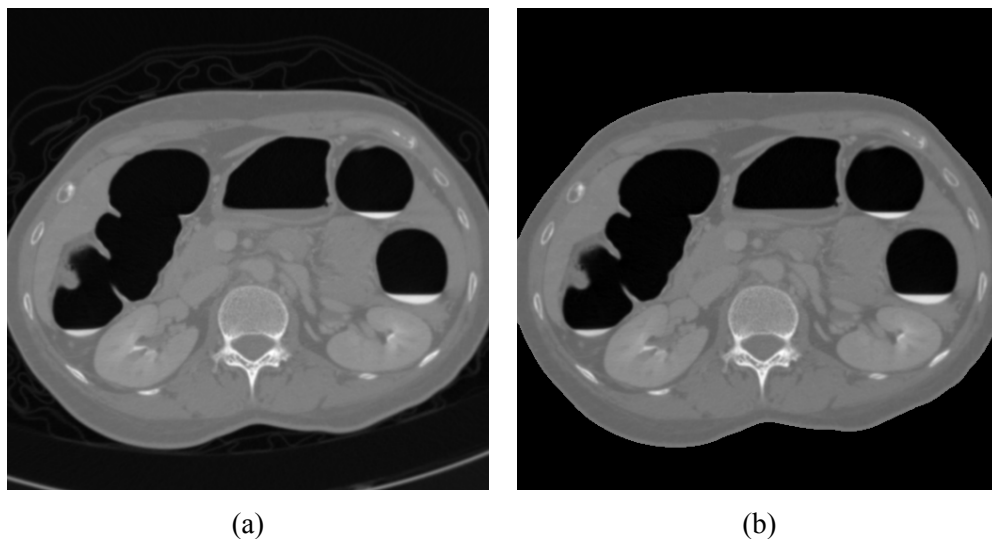
Figure 3.3 (a) Original CT image (b) After elimination of area outside abdomen

The optimal threshold value which corresponds to the condition that the between-class variance is maximum, is used for separating the foreground and the background of a CT image. Moreover, the platform of a CT scanner is sometimes scanned and included into a CT image. Consequently, the connected component analysis is applied to find the boundary of

each component and the largest connected component is then assumed to be abdomen. Finally the areas outside of the abdomen are discarded in the next process of classification task. The example result after eliminating area outside abdomen is shown in Figure 3.3.

3.3 Abdominal Classification by K-means Clustering

The CT image classification is an important stage in abdominal classification since it is used for identifying the bound inside colon lumen and distinguishing the residual material retained inside the colon. From the first process, the voxels outside the body are automatically detected and are discarded in order to reduce computational time. Afterward, all voxels inside the body contour are classified as either the colon lumen or the residual material retained inside the colon. The segmentation method applies K-means clustering algorithm because the number of clusters for partitioning particular region is known and it converges to the optimal solution faster when compared with other pixel-based methods. Furthermore, K-means clustering does not require analyst-specified training data and can reduce the complexity of computation when the examination of a large number of unknown pixels is applied.

3.3.1 Image Sharpening by Laplacian Operator

However, directly applying the intensity level of original image with K-means clustering cannot be precise when separating voxels which located between the two transition regions and also miss the small artifact of contrast-enhanced material. Consequently, image intensity is then sharpened by applying the Laplacian operator to highlight the discontinuity intensity levels and to unstress regions of slowly varying intensity levels. The sharpened image $I_{sh}(x,y)$ from the Laplacian operator is acquired by

$$I_{sh}(x,y) = I(x,y) - \nabla^2 I(x,y) \tag{80}$$

where ∇^2 is the Laplacian operator and $I(x,y)$ is an original image at coordinates x and y.

The Laplacian operator assists in enhancement on the locations of discontinuity gray-level while preserving background tone. Then, the voxels between the soft tissue layer and the contrast-enhanced material have higher contrast than the original image. Then, the intensities from the sharpened image are used as features for K-means clustering in the next process.
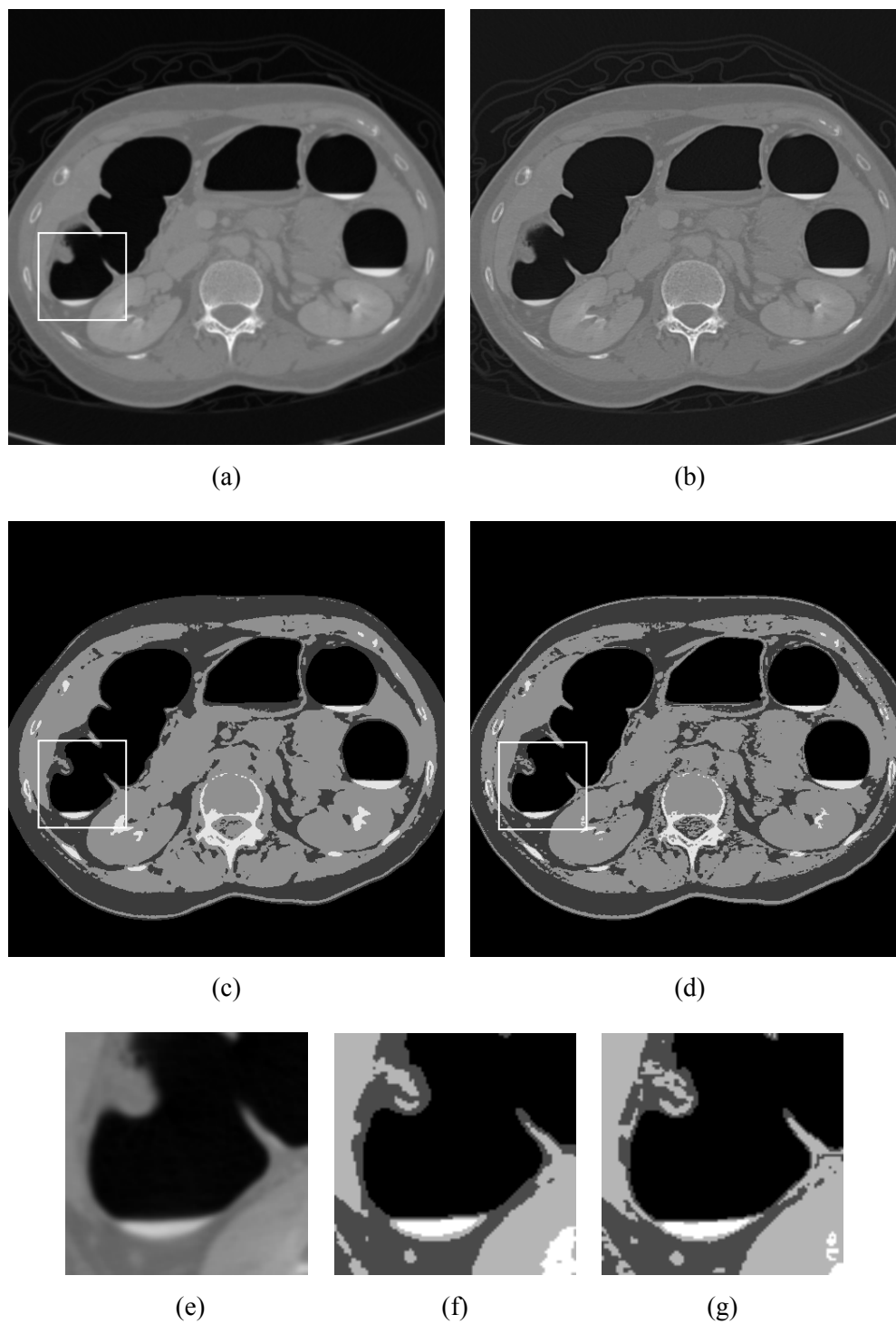
Figure 3.4 (a) Original CT image (b) Sharpened image by Laplacian operator, K-means clustering on (c) original image (d) sharpened image, Zoomed view of (e) original image (f) K-means clustering on original image (g) K-means clustering on sharpened image

Example result of employing K-means clustering with the original intensity level and the result of using K-means clustering with sharpened intensity level by Laplacian operator

are illustrated in Figure 3.4 (c) and (d), respectively. In order to show explicitly comparative results, the zoomed view of K-means clustering on the original image and K-means clustering on the sharpened intensity level by Laplacian operator image, at the places where the square boxes locates, are illustrated in Figure 3.4 (f) and (g), respectively. From the zoomed view, the result from K-means clustering on sharpened intensity level by Laplacian operator image gives more accurate on classification.

3.3.2 K-means clustering

The intensities from an image after sharpening by Laplacian operator are then used as features to classify all voxels inside the body contour into four main regions:

1. air
2. soft tissue and fat
3. muscle
4. contrast-enhanced materials and bone.

K-means clustering is applied for data classification by iteratively computing the mean intensity for each cluster and adding an observed voxel into a cluster whose mean intensity is closest to its intensity. Let feature vector X be the dataset of intensity levels of a CT image where x_i is an element of X. The objective of clustering is to obtain four main regions and to assign each cluster as C_1, C_2, C_3 and C_4 respectively. Thus, all voxels whose vectors belong to cluster C_j where $j = 1, 2, 3,$ and 4, are assigned to that cluster C_j.

The algorithm is as follows:

1. The cluster centroid of each cluster, z_1, z_2, z_3, and z_4 are randomly initiated from the range of data.

2. At the pth iterative step, feature vectors x_i are assigned to a cluster whose centroid is nearest to x_i or whose Euclidean distance is the minimum as expressed in the following relation:

$$x_i \in C_{j,p} \ \text{if} \ \left\| x_i - z_{j,p} \right\| < \left\| x_i - z_{k,p} \right\| \tag{81}$$

where $\|\cdot\|$ represents Euclidean distance fucntion, $C_{j,p}$ denotes a cluster j at p^{th} iteration whose centroid is $z_{j,p}$ and $k = 1, 2, 3, 4$ with the condition that $j \neq k$

3. The next step, the new centroid of each cluster, $z_{j,p+1}$, is recalculated in order to minimize the criterion function:

$$J = \sum_{i=1}^{N_j} \left| x_{i,j} - z_{j,p+1} \right| \tag{82}$$

where $x_{i,j}$ is in C_j. The value of $z_{j,p+1}$ that can minimize this criterion becomes the new centroid of a cluster and can be computed by:

$$z_{j,p+1} = \frac{1}{N_j} \sum_{i=1}^{N_j} x_i \tag{83}$$

where N_j is the number of voxels of cluster j with $p+1^{th}$ iteration.

4. The algorithm ends if $z_{j,p+1}$ is equal to $z_{j,p}$ or in other words the centroids are not changed anymore. Otherwise, it will return to the second step to recalculate the clusters. Then, the algorithm repeats clustering with a new set of cluster centroids.

An example result after performing K-means clustering algorithm to classify four clusters of CT image regions is shown in Figure 3.5.

(a)   (b)
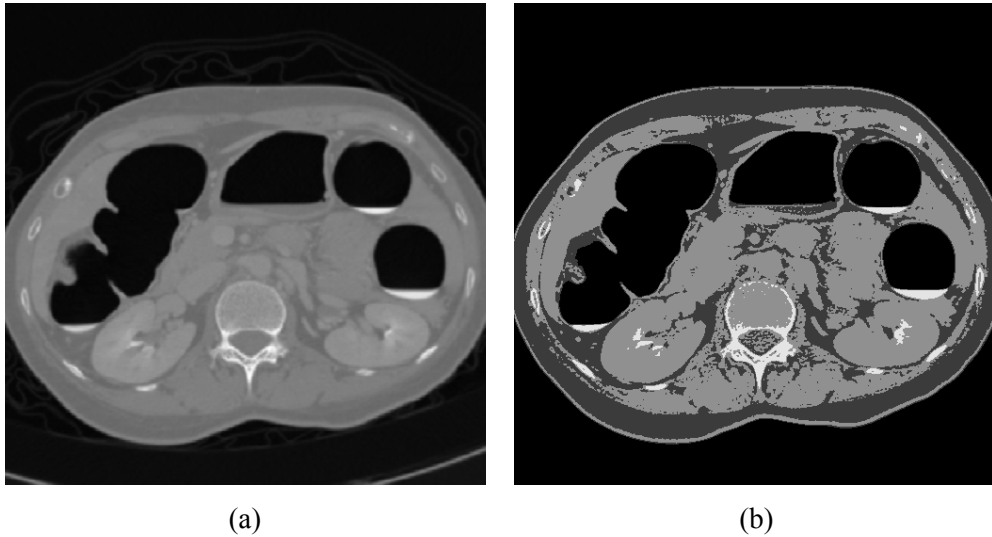
Figure 3.5 (a) Original CT image (b) Classification of CT image by K-means clustering
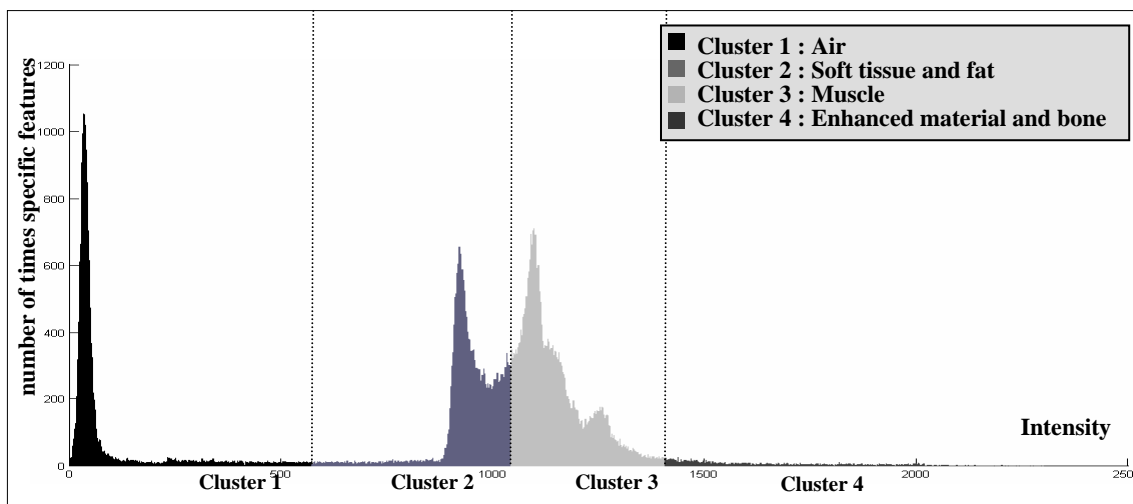
Figure 3.6 Intensity profile of each cluster

After accomplishing K-means clustering stage, the intensity levels of a CT image that belong to the four regions are shown in Figure 3.5 (b). The result shows that all voxels inside the body contour are classified into four regions, i.e., 1) air, 2) soft tissue or fat, 3) muscle, 4) contrast-enhanced materials and bone. While air regions are in black color, soft tissue or fat regions are in dark gray color, muscle regions are in bright gray color, and contrast-enhanced materials and bone regions are in white color. The histogram of intensity profile of each cluster is shown in Figure 3.6.

3.4 Lung Segmentation and Removal

Due to the fact that a CT image does not contain only colon, it sometimes includes air inside lung and bone. These organs increase the computational time when examining a suspected object in the cleansing method because bones are in the same cluster as contrasted-enhance material and sometimes they are contiguous to lung. If contiguous bone and lung occur, the algorithm of contrasted-enhance material segmentation determines bones as contrasted-enhance material and removes them if they are contiguous to air inside lung. Consequently, the removing of lung is employed to eliminate the extra time. In order to exterminate lung, the anatomical characteristic of lung, which is composed of many blood vessels, is considered for separating lung from colon. Preliminary, the air regions are constructed with a binary mask and labeled as $Mask_{Air}$. If the segment of $Mask_{Air}$ have holes insides, it means that these holes are blood vessel as in lung and this segment is ignored.

3.5 Automatic CEF Segmentation

In this process, the region of contrast-enhanced materials and bones are defined as $Mask_{CEF-Bone}$ as illustrated in Figure 3.7 (b). Similarly, the regions of soft tissues and muscles are both combined together and called $Mask_{Tissue}$ as shown in Figure 3.7 (c).

(a)

(b)

(c)

(d)
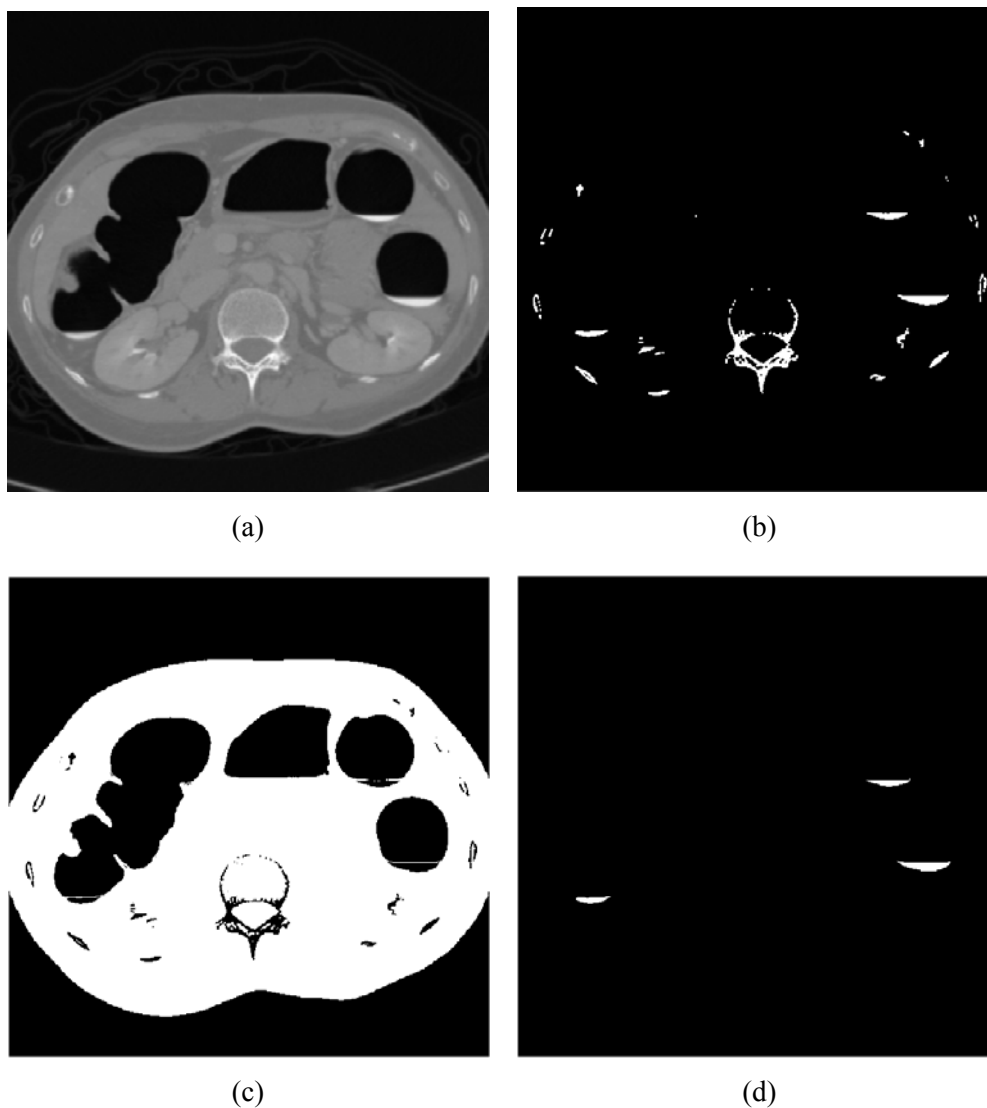
Figure 3.7 (a) Original CT image (b) $Mask_{CEF-Bone}$ (c) $Mask_{Tissue}$ (d) $Mask_{CEF}$

Because $Mask_{CEF-Bone}$ does not include only contrast-enhanced materials but also contains bone regions, the separation of both components is required. According to the nature of enhanced fluids, they are in spate at the lower part of colon lumen due to the nature of gravity and also appear at the location between colon wall and air region. Consequently, voxels that surround $Mask_{CEF-Bone}$ are then observed and examined for these restrictions to

distinguish the enhanced materials from bones. Then, the contrast-enhanced materials are separated and denoted as $Mask_{CEF}$ as Figure 3.7 (d).

After that, the areas which are interfaces between the contrast-enhanced materials and soft tissues are analyzed for improving boundary of $Mask_{CEF}$. If the gradient magnitude of any voxel which locates on the areas between $Mask_{CEF}$ and $Mask_{Tissue}$, is local maximum and its intensity is in range of $Mask_{CEF}$, this voxel is added to $Mask_{CEF}$, otherwise is discarded.

3.6 Automatic PVE Segmentation

Although the contrast-enhanced materials are detected, the partial volume effect between air and enhanced materials still remain and are classified as the region of $Mask_{Tissue}$. In order to determine the partial volume effect voxels, the morphological dilation is applied on each segment of $Mask_{CEF}$ and its contiguous $Mask_{Air}$ using the morphological disk-shaped structuring element. Then, the boundary that includes the interface layer of the partial volume effect voxels, assigned as $Mask_{merge}$, is calculated by merging the boundaries of both dilated masks of each segment of $Mask_{CEF}$ and its contiguous $Mask_{Air}$ with OR operation and then applying morphological erosion afterward as follows.

$$Mask_{merge} = ((Mask_{Air,i} \oplus s_e) \vee (Mask_{CEF,i} \oplus s_e)) \ominus s_e \qquad (84)$$

where the symbol $\oplus$ and $\ominus$ represent morphological dilation and erosion with the disk-shaped structuring element s_e that radius equals to one. $Mask_{CEF,i}$ is each segment of $Mask_{CEF}$, $Mask_{Air,i}$ is a segment of $Mask_{Air}$ which is contiguous to $Mask_{CEF,i}$ and i represents each colon segment that has contrast-enhanced material. The symbol $\vee$ represents OR operation that merges the dilated of $Mask_{CEF,i}$ and $Mask_{Air,i}$ which are the components in the same colon segment together.

The suspected partial volume effect voxels which are interface between air and contrast-enhanced material, called $Mask_{TestPVE.}$, are identified by the intersection of $Mask_{merge}$, $Mask_{Tissue}$ and the dilation of each $Mask_{CEF}$. Then, $Mask_{TestPVE.}$, are obtained by applying AND operation on $Mask_{merg}$, $Mask_{Tissue}$ and the dilation of each segment of $Mask_{CEF}$, as given.

$$Mask_{TestPVE} = Mask_{Merge} \wedge Mask_{Tissue} \wedge (Mask_{CEF,i} \oplus s_e) \qquad (85)$$

where the symbol $\wedge$ represents AND operation.

Since there are two possible types of each component of $Mask_{TestPVE}$; i.e., soft tissue or partial volume effect, the inspection is performed on each suspicious component with the assumptions that partial volume effect voxels are the interface layer appearing between air and enhanced material, otherwise they are defined as tissue.

Therefore, each segment of $Mask_{TestPVE}$ is examined by this fundamental constrain. Eventually, the constituent that includes partial volume effect regions is determined and then labeled as $Mask_{PVE}$, as illustrated in Figure 3.8.

(a)   (b)
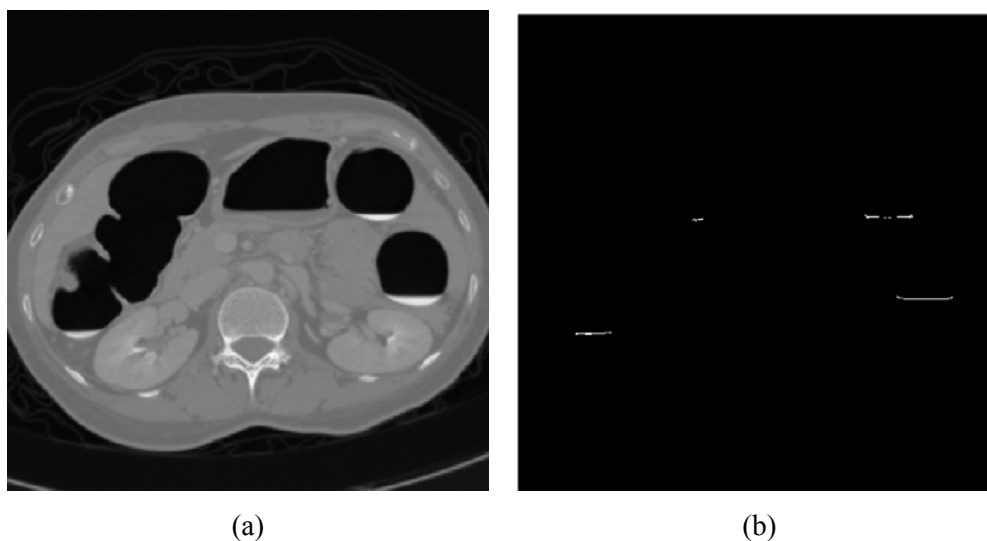
Figure 3.8 (a) Original CT image (b) $Mask_{PVE}$

3.7 Colon Cleansing and Mucosa Reconstruction

The boundary of $Mask_{Air}$, $Mask_{PVE}$ and $Mask_{CEF}$ are combined together to make the entire colon mask and denoted as $Mask_{Colon}$. Subsequently, $Mask_{PVE}$ is dilated to ensure that all partial volume effect voxels are detected and removed. The voxels of dilated $Mask_{PVE}$ that are inside the boundary of $Mask_{Colon}$ are added in to $Mask_{PVE}$.

Afterward, dilated $Mask_{PVE}$ and $Mask_{CEF}$ are added together and relabeled as $Mask_{Remove}$ and is subtracted from the original CT image. The boundaries of $Mask_{Remove}$ for subtracting contrast-enhanced material from original CT image are shown in Figure 3.9 (b), where white color boundaries represent dilated $Mask_{PVE}$ and gray color boundaries represent $Mask_{CEF}$.

(a)   (b)
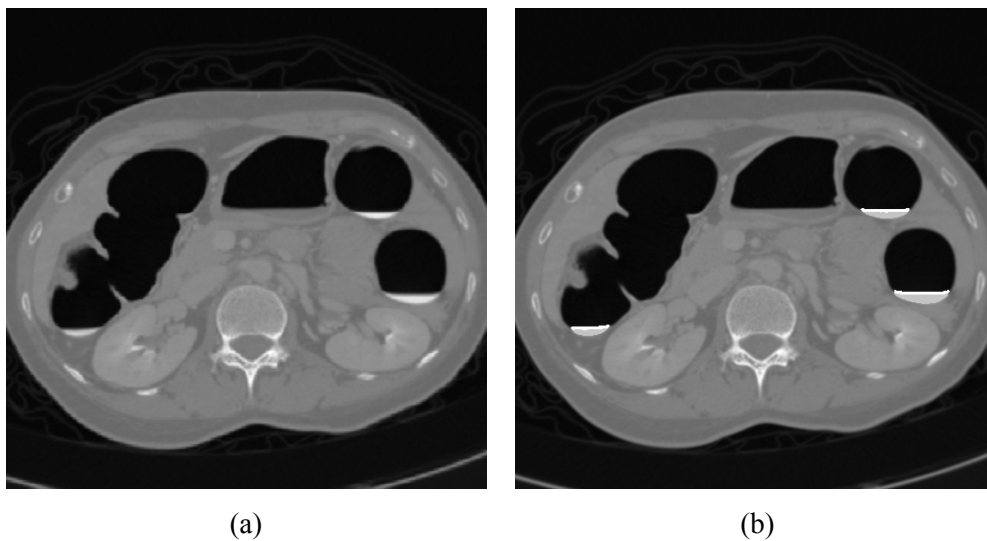
Figure 3.9 (a) Original CT image (b) $Mask_{Remove}$

The result after colon cleansing, when $Mask_{Remove}$ is subtracted from the original CT image, is shown in Figure 3.10 (a). Consequently, the effect of the contrast-enhanced fluids and the partial volume effect voxels are successfully eliminated.

(a)   (b)
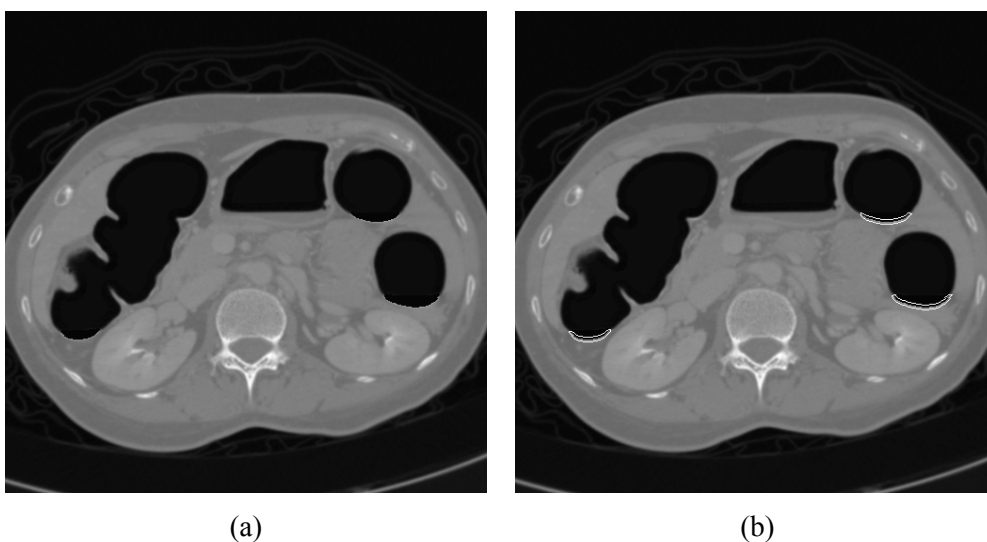
Figure 3.10 (a) Cleansing colon image (b) Area of reconstructed edge, $Edge_i$

However, after colon cleansing process there are still some sharp transitions of intensity along the colon lumen wall. Therefore, the reconstruction of the mucosa layer at the intersection of contrast-enhanced fluids and soft tissues is accomplished in the next step. In a

CT image, the mucosa layer of colon wall is represented by pixel layers, which extend from the soft tissue at inner border of colon lumen to air. In order to detect the inner border of colon wall, the AND operation is then performed between the edges of $Mask_{Colon}$, assigned as $Mask_{Colon,\text{edge}}$, and $Mask_{Remove}$ to extract the edge contour, and labeled as $Edge_{Remove}$.

$$Edge_{\text{Re}move} = Mask_{Colon,edge} \wedge Mask_{\text{Re}move} \tag{86}$$

Continually, the reconstructed edge of mucosa layer is contributed on the adjacent pixels of the $Edge_{Remove}$ and denoted as $Edge_i$, where i is the order of edge selection starting from two pixels inner layer along border of mucosa layer toward the $Edge_{Remove}$ and spread to three pixels outer layer next to $Edge_{Remove}$, toward the air, respectively. The example areas of reconstructed edges, $Edge_i$, of colon lumen are shown in Figure 3.10 (b) in the white contour around the areas of colon lumen that are subtracted contrast-enhanced fluids.

Then, the estimated intensity value of each voxel of the reconstructed $Edge_i$, is calculated by averaging the intensity values of the image after performing Gaussian low pass filter with two different mask sizes as follows

$$I_{Edge,i} = (I_{G5,i} + I_{GM3,i})/2 \tag{87}$$

where $I_{Edge,i}$ is the intensity value of each voxel of mucosa layer at the reconstructed $Edge_i$. The notation $I_{G5,i}$ is the intensity value at each voxel of $Edge_i$ after convolving the cleaned colon image by Gaussian low pass filter with mask size equal to five and $I_{GM3,i}$ is the intensity value at each voxel of $Edge_i$ after convolving the cleaned colon image by the Gaussian low pass filter with mask size equal to three and afterward performing median filtering.

Since the bigger mask size makes an image more blurred on transition shading at the colon wall and the smaller mask size cannot completely reduce the effect of rapid transition of intensity level. Moreover, the median filter is added after convolving with the Gaussian filter of size three to eliminate the inharmonious intensity due to small size of a filter.

Consequently, the average intensity of the convolving Gaussian low pass filter with two different window sizes is calculated and replaced on the reconstructed edge. Finally, the smoothed mucosa is then substituted into the subtracted image and the natural appearing of transition intensity on the mucosa layer is created as shown in Figure 3.11 (b) and (d).
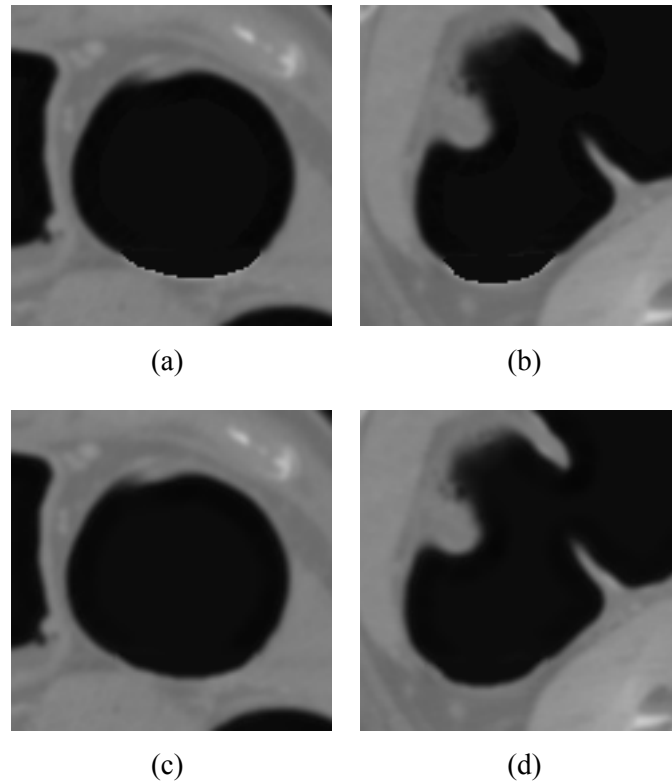
Figure 3.11 Zoomed view of (a) (b) Cleansing edge, (c) (d) Reconstructed edge

3.8 Hybrid Edge Detection

The proposed hybrid edge detection is a combination between Canny edge detection and Laplacian of Gaussian (LoG) edge detection to determine the edge. The hybrid edge detection from both detection can assist and operate better than performing either the Canny edge detection or the Laplacian of Gaussian edge detection alone in localization edge and minimizing noise. The hybrid edge detection algorithm composes of three stages, the first stage is Canny edge detection with automatic threshold, the second stage is Laplacian of Gaussian edge detection with automatic threshold, and final stage is hybrid edge constructing from Canny edge and Laplacian of Gaussian edge.

3.8.1 Canny Edge Detection with Automatic Thresholding

The first detector for applying in the hybrid edge detector is the Canny detector. The cleaned colon image is smoothen by Gaussian filter and the first derivative operator is applied on the smoothed image to calculate the gradient magnitude and its orientation. Then, the determining edges give rise as the ridges in the gradient magnitude image. Afterward non-maximum suppression is performed to track along the top of the ridges so that only the

gradient magnitudes at the points of the greatest local change are identified. Hysteresis is then applied for tracking edges and eliminating broken edges and streaks. Hysteresis depends on the setting scale of two thresholds T_1 and T_2 for detecting the edge location.

In the proposed method, the value of threshold T_1 in the Canny edge detection is automatically selected by utilizing the Otsu's method.

3.8.1.1 Gradient Magnitude Threshold Setting by Otsu's method

Normally, Otsu's method is used with the intensity values of original image. In the proposed procedure, the gradient magnitude of cleaned colon image is instead applied to the Otsu's method. The algorithm is as follows:

1. The gradient of an image denotes as a vector $\nabla f = [Gx, Gy]$ and the magnitude of an image are calculated from

$$mag(\nabla f) = |G| = \sqrt{G_x^2 + G_y^2} \tag{88}$$

where G_x and G_y are the gradient in x and y directions, respectively.

2. Next, the normalized histogram is computed as the discrete probability density function of each gradient magnitude value by

$$p_g = n_g / N, \ p_g \geq 0 \tag{89}$$

$$\sum_{g=0}^{g_{max}} p_g = 1 \tag{90}$$

where p_g is the probability of gradient magnitude value g. The range of the gradient magnitude value g starts from 0 to g_{max}. The notation n_g is the number of pixels at the gradient magnitude value g and N is the total number of all pixels.

3. Subsequently, the probability distributions of gradient magnitude value on foreground w_{g1} and background w_{g2}, are computed and updated iteratively by stepping through all possible threshold of gradient magnitude values t_g, starting from 0 to g_{max}.

$$w_{g1} = \sum_{g=0}^{t_g - 1} p_g \qquad (91)$$

$$w_{g2} = \sum_{g=t_g}^{g_{max}} p_g \qquad (92)$$

4. Similarly, the mean of gradient magnitude of the two classes of foreground and background, assigned as μ_{g1} and μ_{g2} respectively, and the total mean of gradient magnitude, assigned as μ_{gT}, are determined and updated iteratively through all possible t_g.

$$\mu_{g1} = \sum_{g=0}^{t_g - 1} g p_g / w_{g1} \qquad (93)$$

$$\mu_{g2} = \sum_{g=t_g}^{g_{max}} g p_g / w_{g2} \qquad (94)$$

$$\mu_{gT} = \sum_{g=0}^{g_{max}} g p_g \qquad (95)$$

5. According to the values of the possible threshold of gradient magnitude values t_g, the between-class variance is determined as follows.

$$\sigma_b^2 = w_{g1}[\mu_{g1} - \mu_{gT}]^2 + w_{g2}[\mu_{g2} - \mu_{gT}]^2 \qquad (96)$$

6. Eventually, the threshold of the gradient magnitude values, which corresponds to the maximum between-class variance, is defined, and called T_{Otsu}.

3.8.1.2 Automatic Threshold Setting for Canny Edge detection

The threshold T_1 for Hysteresis, is set to equal to T_{Otsu} and T_2 is calculated by

$$T_2 = k T_{Otsu} = k T_1 \qquad (97)$$

where k is a scaling factor which makes $T_2 < T_1$, in this case $k=0.4$ in order the weak edge to be detected. When the gradient magnitude is greater than threshold T_1, it is identified as a strong

edge. In the case that the gradient magnitude is between the two thresholds T_1 and T_2, it is identified as a weak edge, unless there is connected path from weak edge pixels to strong edge pixels, the edge linking is then performed.

Consequently, the result edges from Canny edge detection with automatic thresholding on hysteresis are acquired and labeled as f_C. Example result of Canny edge detection with automatic thresholding is shown in Figure 3.12 (b).

(a)   (b)
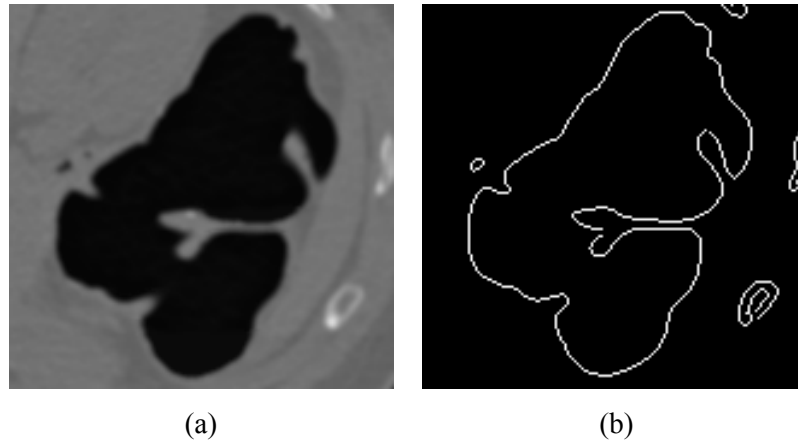
Figure 3.12 (a) Original CT image (b) Canny edge by automatically thresholding

3.8.2 LoG Detection with Automatic Thresholding

Another proposed detection in the hybrid edge detection is Laplacian of Gaussian edge detection. Initially, an image is smoothen by Gaussian filter and subsequently Laplacian of Gaussian is calculated as the second spatial derivative of the smoothed image. In order to estimate the edges location, the zero crossing detection is utilized on Laplacian of Gaussian image.

3.8.2.1 Automatic Threshold Setting for LoG Edge Detection

In the proposed method, the threshold value for the zero crossing operation, T_z, is automatically set by the mean of absolute value of Laplacian of Gaussian.

$$T_z = \frac{1}{mn}\sum_{x=1}^{m}\sum_{y=1}^{n}\left|LoG(x,y)\right| \tag{98}$$

where $LoG(x,y)$ is the intensity level estimating by the Laplacian of Gaussian image at coordinates x, y of an image whose size is $m{\times}n$. The result binary edge from the Laplacian of Gaussian edge detector is labeled as f_{LoG}. The example result of Laplacian of Gaussian edges by the proposed automatic thresholding are shown in Fig. 13 (b) in gray and white color.

3.8.2.2 Noisy Edge Removal

Due to there are many noisy edges from the Laplacian of Gaussian edges image caused by the texture of an image, the areas of estimating edges from the Laplacian of Gaussian edge detection are limited by applying the Otsu's threshold to the gradient magnitude image to eliminate noisy edges. Then, the Laplacian of Gaussian edges which are located at the positions that the gradient magnitude is more than the Otsu's threshold, are preserved, otherwise they are removed. Hence, the final Laplacian of Gaussian edges are acquired by

$$f_{LoG}(x,y) = \begin{cases} f_{LoG}(x,y) & \text{if } f_G(x,y) \geq T_{Otsu} \\ 0 & \text{if } f_G(x,y) < T_{Otsu} \end{cases} \tag{99}$$

where T_{Otsu} is the threshold of gradient magnitude image estimated by the Otsu's method and $f_G(x,y)$ is the gradient magnitude of an image at coordinates x, y.

(a)   (b)
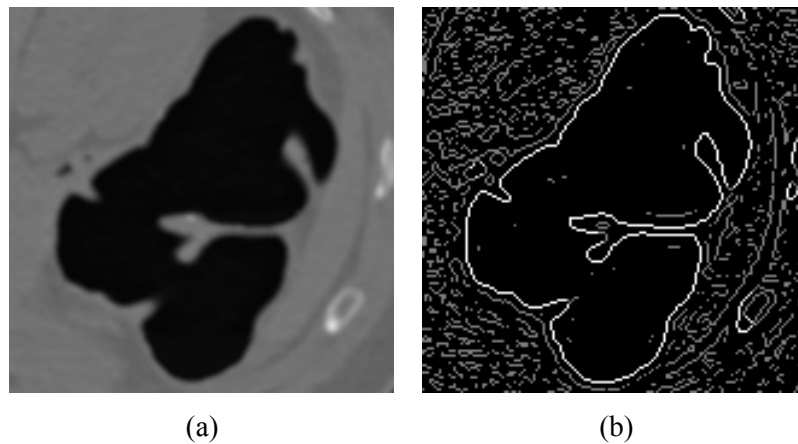
Figure 3.13 (a) Original CT image (b) LoG edge by automatically thresholding

The example result after eliminating noisy edges from the Laplacian of Gaussian edges by the proposed method is shown in Figure 3.13 (b) where Laplacian of Gaussian edges after removing noisy edges are in white color and discarding edges are gray color.

In order to eliminate extra edges, which are not relative to the colon border, the edges from both Canny edge and Laplacian of Gaussian edge detection which are contiguous to the air inside the colon, are conserved and the edges at other locations are eliminated.

3.8.3 Hybrid Edge

The proposed hybrid edge detection is acquired by combining the output from both Canny edge detection and Laplacian of Gaussian edge detection together. The algorithm is as follows.

1. If the edges detected by Canny edge detection are at the same location as those detected by Laplacian of Gaussian edge, they are preserved for hybrid edge map and assigned as f_{Hyb1}.

2. The remaining segments in Canny edge and Laplacian of Gaussian edge image which are not preserved, are called S_{Canny} and S_{LoG}, respectively. Each segment of S_{LoG} and each segment of S_{Canny}, which is contiguous to the S_{LoG}, are then analyzed by these functions.

$$E_{LoG} = \sum_{i=i_0}^{i_{n-1}} \sum_{j=j_0}^{j_{n-1}} \frac{I_{LoG}(i,j)}{n} \qquad (100)$$

$$E_{Canny} = \sum_{k=k_0}^{k_{m-1}} \sum_{l=l_0}^{l_{m-1}} \frac{I_{Canny}(k,l)}{m} \qquad (101)$$

where n, m are the numbers of pixels which represent each segment of S_{LoG} and S_{Canny}. The notation $I_{LoG}(i,j)$ is the intensity of each pixel of S_{LoG} which locates at coordinates $i=\{i_0, i_1, i_2,...., i_{n-1}\}$ and $j=\{j_0, j_1, j_2,...., j_{n-1}\}$. Similarly, $I_{Canny}(k,l)$ is the intensity of each pixel of S_{Canny} which is contiguous to S_{LoG} and locates at coordinates $k=\{k_0, k_1, k_2,...., k_{m-1}\}$ and $l=\{l_0, l_1, l_2,...., l_{m-1}\}$. In order to reduce computing time, any segment of S_{LoG} whose size less than 3 pixels are discarded.

3. Afterward, each segment of the remaining S_{LoG} and its contiguous S_{Canny}, which corresponds to the following function are gathered and assigned as hybrid edge, f_{Hyb}.

$$f_{Hyb}(a,b) = \begin{cases} S_{LoG}(i,j) \,|\, (a,b)=(i,j) & \text{if } E_{LoG} < E_{Canny} \\ & \text{or } (E_{LoG} > E_{Canny} \text{ and } 0 < n-m \leq k_s) \\ S_{Canny}(k,l) \,|\, (a,b)=(k,l) & \text{otherwise} \end{cases} \qquad (102)$$

where $S_{LoG} \notin f_c \cap f_{LoG}$, $S_{Canny} \notin f_c \cap f_{LoG}$, $S_{LoG}(i,j)$ is each segment of S_{LoG} which locates at coordinates $i=\{i_0, i_1, i_2,...., i_{n-1}\}$ and $j=\{j_0, j_1, j_2,...., j_{n-1}\}$, $S_{Canny}(k,l)$ is each segment of S_{Canny} which is contiguous to $S_{LoG}(i,j)$ and locates at coordinates $k=\{k_0, k_1, k_2,...., k_{m-1}\}$ and $l=\{l_0, l_1, l_2,...., l_{m-1}\}$, and k_s is the weight, in this case k_s is equal to three, to protect oversize of S_{LoG}.

4. Next, the remaining segments of S_{Canny} which are not contiguous to S_{LoG} and are not located at the position where $f_c \cap f_{LoG}=1$ are added to f_{Hyb}. Similarly, the preserved hybrid edges from step1, f_{Hyb1} are combined to f_{Hyb}. Finally, all of hybrid edges, f_{Hyb}, are acquired and are applied for calculating enhanced edge map in the next process. The example result of a combination of hybrid edges from two detectors is shown in Figure 3.14 (b).

(a)   (b)
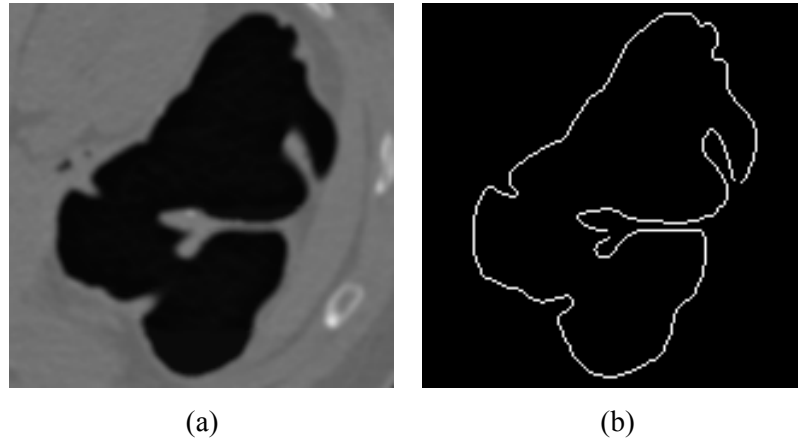
Figure 3.14 (a) Original CT image (b) Proposed hybrid edge

3.9 Enhanced Edge Map

To generate enhanced gradient vector flow field, the hybrid edges from previous stage are utilized as the edge mask to locate the enhancement edge. The gradient magnitudes at the location of hybrid edge mask, f_{Hyb}, are enhanced and the other locations, which do not correspond to the hybrid edge mask, are remained applying the original gradient magnitude. Then, the enhanced gradient magnitude, f_e, is obtained by

$$f_e(x,y) = \begin{cases} k_e \nabla(G(x,y) * I(x,y)) & x,y \in f_{Hyb} \text{ where } f_{Hyb}(x,y)=1 \\ \nabla(G(x,y) * I(x,y)) & \text{otherwise} \end{cases} \tag{103}$$

where k_e is the weight for enhancement the gradient magnitude, $G(x,y)$ is the Gaussian filter and the notation ∇ is the gradient operator performing on an image of cleaned colon $I(x,y)$ and

x, y are the coordinates of an image.

Consequently, the enhanced edge map, f_{eh}, can be calculated by

$$f_{eh}(x, y) = |f_e(x, y)|^2 \qquad (104)$$

The enhanced edge map can preserve gradient magnitude of real edges and relatively decrease gradient magnitude from noise. The example result of enhanced gradient magnitude is shown in Figure 3.15.

(a)   (b)
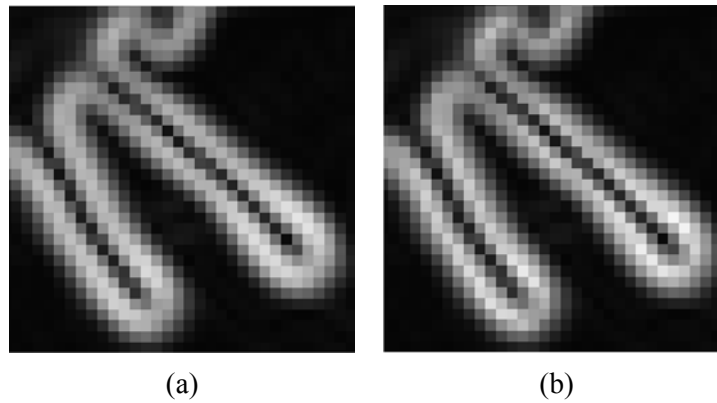
Figure 3.15 (a) Gradient magnitude (b) Enhanced gradient magnitude

3.10 Enhanced Gradient Vector Flow

Since the descending intensity shaded in lumen surface where colon lumen meet with air is a problem on detection colon wall. The proposed enhanced gradient vector flow (EGVF) applies enhanced gradient magnitude in previous stage to assist capturing ability. The processes to determine the enhanced gradient vector flow fields are described as follows.

3.10.1 Enhanced Gradient Vector Flow Field

The enhanced gradient vector flow field, $\widetilde{V}(x, y)$ is obtained by applying the partial differential equation in equation (41) with the enhanced gradient vector field V as function of time t and the traditional edge map, assigned as f in equation (41), is replaced by the enhanced edge map, f_{eh}.

$$V_t = \mu \nabla^2 V - \left(V - \nabla f_{eh}\right)\left|\nabla f_{eh}\right|^2 \tag{105}$$

where V_t is the partial derivative of V with respect to t, μ is denoted as regularization parameter, ∇ and ∇^2 are gradient operator and Laplacian operator which are applied to each spatial component of V separately.

3.10.2 Enhanced Gradient Vector Flow Deformable Model

The enhanced gradient vector flow deformable model is acquired by applying the enhanced gradient vector flow field in equation (105) on the x and y directions as follows.

$$u_t = \mu \nabla^2 u - \left(u - \nabla f_{eh}\right)\left|\nabla f_{eh}\right|^2 \tag{106}$$

$$w_t = \mu \nabla^2 w - \left(w - \nabla f_{eh}\right)\left|\nabla f_{eh}\right|^2 \tag{107}$$

where u and w are the enhanced gradient vector flow field on x and y directions, u_t is the partial derivative of u with respect to t and w_t is the partial derivative of w with respect to t.

Then, the enhanced gradient vector flow deformable model is identified by x and y co-ordinates as given.

$$x^{t+\delta t} = M^{-1}(x^t + \delta t u_t) \tag{108}$$

$$y^{t+\delta t} = M^{-1}(y^t + \delta t w_t) \tag{109}$$

where t represents the iteration time, δt is the time step and M is Circulant marix which represents the derivative equation of linear equation as follows.

$$M = \begin{bmatrix} r & q & p & & & p & q \\ q & r & q & p & & & p \\ p & q & r & q & p & & \\ & \ddots & \ddots & \ddots & \ddots & \ddots & \\ & & p & q & r & q & p \\ p & & & p & q & r & q \\ q & p & & & p & q & r \end{bmatrix} \tag{110}$$

when $p = \beta$, $q = -\alpha - 4\beta$ and $r = 1 + 2\alpha + 6\beta$.

3.11 Colon Segmentation and Reconstruction

The proposed colon segmentation is computed by utilizing the connected component in 3D space. The connected component, which is the largest volume, is assumed as colon, and the others such as the small intestine and stomach are eliminated. In the case that the small intestine is inflated and connected with colon volume, removal of small intestine is performed by considering the anatomical knowledge that the size of small intestine is smaller than colon and the position of small intestine is connected to colon at the end of colon called Cecum. The length of small intestine is longer than colon, approximately 7-10 meters long, and colon length is 1.5 meters long [17]. The colon anatomy is shorter and bigger than the small intestine. The separation of colon lumen and small intestine is accomplished by applying anatomical knowledge base.

The algorithm for colon segmentation is described as follows.

1. Firstly, the 3D connected component is analyzed with volume size calculation. The process of examining starts from the bottom of colon, called rectum. The connected component analysis is performed and the largest volume is assumed as colon candidates. This component called colon candidates because it sometimes has only colon and sometimes has small intestine contiguous with colon. The example result of contiguous small intestine and colon is shown in Figure 3.16 (a). The volume of colon candidates is identified as, V_{all}.

2. Secondly, the first part in the volume of colon candidates, called V_{colon1}, is examined for finding the started part of colon.

$$V_{colon1} = \frac{1}{p}V_{all}$$

(111)

where p is the scale factor to define the first part of colon candidates volume, in this case sets $p=6$ to protect the small intestine from being included into the first part of the volume if small intestine is inflated. Then, the largest connected component started from the bottom of colon, called rectum, and its volume, V_{colon1}, is defined as the start part of colon.

3. Next, the remaining connected components which are in the colon volume, V_{all}, and nearby the start part of colon, V_{colon1}, are examined for small intestine by anatomical characteristic of small intestine which size is longer and curl between the colon lumen. Hence, the connected component, which its length is more than L_{lim} and its center is lower than C_{lim} is defined as small intestine, and is removed.

$$L_{lim} = \frac{1}{3} L_{colon1} + k_L \qquad (113)$$

$$C_{lim} = L_0 + \frac{1}{2} L_{colon1} \qquad (114)$$

where L_{colon1} is defined as length of V_{colon1}, k_L is the weight adjustable for L_{colon1}, and L_0 is denoted as start location of V_{colon1}.

4. Then, the remaining connected components nearby the start part of colon, V_{colon1}, are combined with the remaining part in the colon volume, V_{all}. The connected component is analyzed starting from the rectum and the largest volume is assumed as colon. Any connected components, which are contiguous to the previously removed small intestine are implicitly separated from colon. The example result is shown in Figure 3.16 (b).

5. Finally, if any parts of small intestine remains, the morphological open operation is utilized and the contiguous area where small intestine connects to colon at cecum, is separated and the small intestine is successfully eliminated. The example results are shown in Figure 3.16 (c).

The reconstructing 3D model of colon is acquired by applying the Marching Cubes algorithm by Lorensen and Cline [70]. The surface rendering is performed by generating triangular meshes to create connected surface of colon and constructing 3D model.

(a)   (b)   (c)
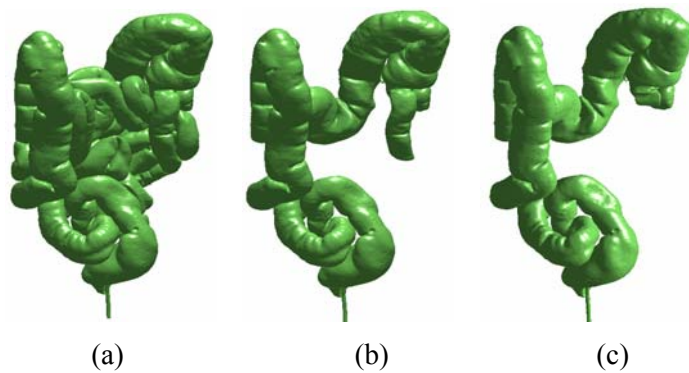
Figure 3.16 (a) Contiguous small intestine and colon
(b) Removed small intestine (c) Final stage

CHAPTER IV

RESULTS AND EVALUATION

The proposed framework for reconstructing 3D colon model from oral contrast-enhanced CT colonography images was examined and evaluated with two parts, the first part is colon cleansing and the second part is colon wall detection. Finally, the 3D model of colon is constructed. The details of evaluation are described as follows

4.1 Colon Cleansing

The pilot datasets used for colon cleansing experimentations were preprocessed with the same bowel preparation. The dataset contains 500-700 slices of CT images of size 512×512 voxels. The accuracy of the cleansing was satisfied, all partial volume effect voxels and the enhanced materials were successfully removed and the intensity profile along the layer between air and soft tissue after cleansing was smoothly reconstructed. The colon cleansing method was examined by the radiologist base on the capability of the cleansing method and the confidence on accuracy. The assessment criteria for evaluation on colon cleansing was achieved by the guidance of the expert radiologist, and are described as follows. The first assessment evaluated the capability on eliminating contrast-enhanced materials in each position inside colon in CT images. The scores are the percentage of cleansing that ranged from 1 to 5 as illustrated in Table 4.1.

Table 4.1 The percentage of cleansing

Scores	The percentage of cleansing
1	0-25%
2	26-50%
3	51-75%
4	75-99%
5	100%

The second assessment evaluated the accuracy of region cleansing effect on the colon lumen. The evaluated scores are ranged from 1 to 4 as shown in Table 4.2.

Table 4.2 The accuracy on the cleansing

Scores	The accuracy on the cleansing
1	uninteptable due to the artifact from fecal tagging
2	obvious wall irregularity
3	equivocal wall irregularity
4	no wall irregularity

The third assessment evaluated the confidence on the accuracy of colon cleansing technique. The evaluated scores are ranged from 1 to 3 as shown in Table 4.3.

Table 4.3 The confidence on the accuracy

Scores	The confidence on the accuracy
1	low confidence
2	moderate confidence
3	high confidence

The results of mean scores of each dataset which was evaluated on three criteria of assessments are shown in Table 4.4.

Table 4.4 The results of cleansing assessment.

	Percentage of cleansing (1 to 5)	Accuracy on the cleansing (1 to 4)	Confidence on accuracy (1 to 3)
Dataset 1	4.18	3.37	2.79
Dataset 2	4.80	3.57	2.91
Dataset 3	4.56	2.92	2.88
Dataset 4	4.82	3.29	2.90

From Table 4.4 on the first assessment on percentage of colon cleansing, the results show that most datasets have high percentages of cleansing, only one dataset has percentage of cleansing less than others due to the problem with small tiny spot artifact. The accuracy of colon cleansing was satisfied. Most of contrast-enhanced materials and partial volume effect voxels were successfully removed. Even the artifacts of inhomogeneous contrast-enhanced materials were also eliminated.

The example results of proposed colon cleansing method in CT images are illustrated in Figure 4.1. The results show that the proposed method can eliminate contrast-enhanced materials regardless of their sizes and forms.

(a) (c)

(b) (d)
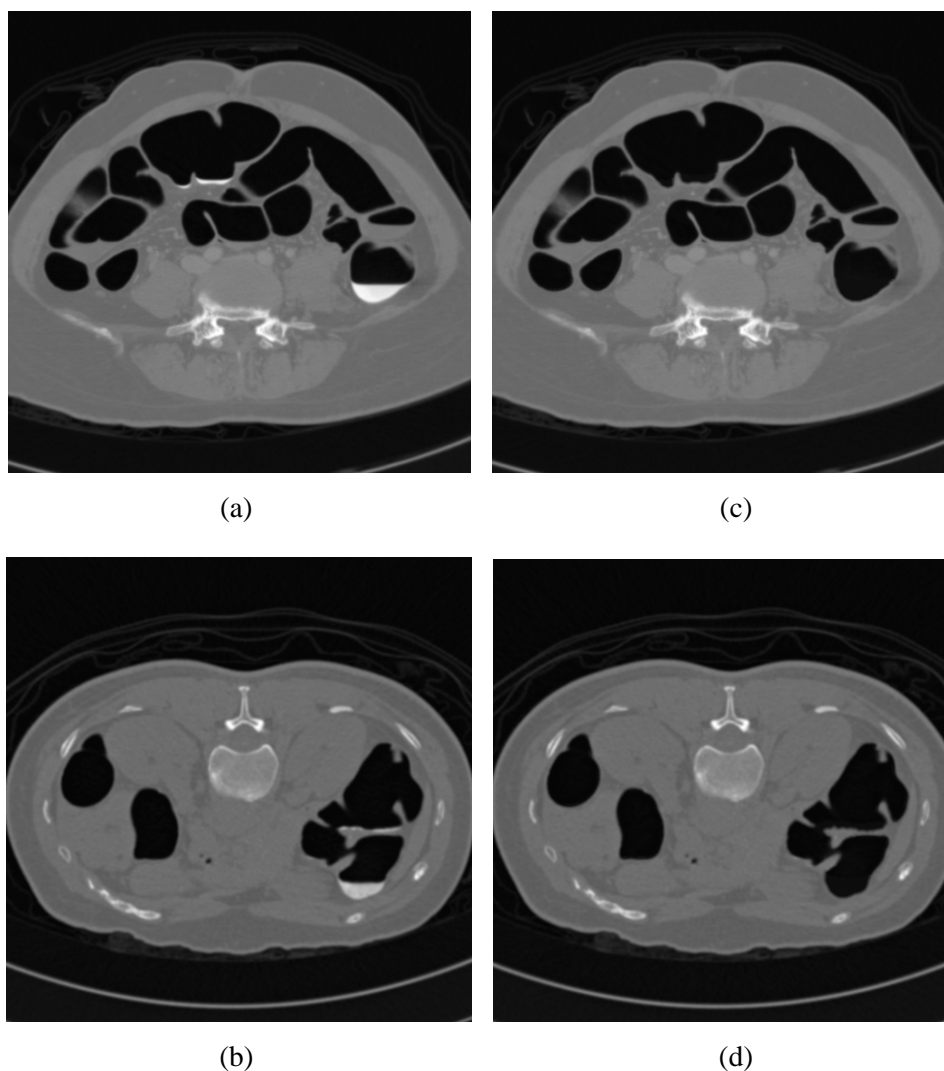
Figure 4.1 (a) (b) Original CT image

(c) (d) CT images after subtraction of CEF and mucosa layer reconstruction

The example results on zoomed view are illustrated in Figure 4.2 and Figure 4.3. The contrast-enhanced materials were successfully eliminated. The partial volume effect voxels were also removed and the reconstructed mucosa layer of colon lumen after subtraction of contrast-enhanced material, were satisfied. The results show that the proposed method can be used in different locations, and also has capability of eliminating variety forms of contrast-enhanced material.
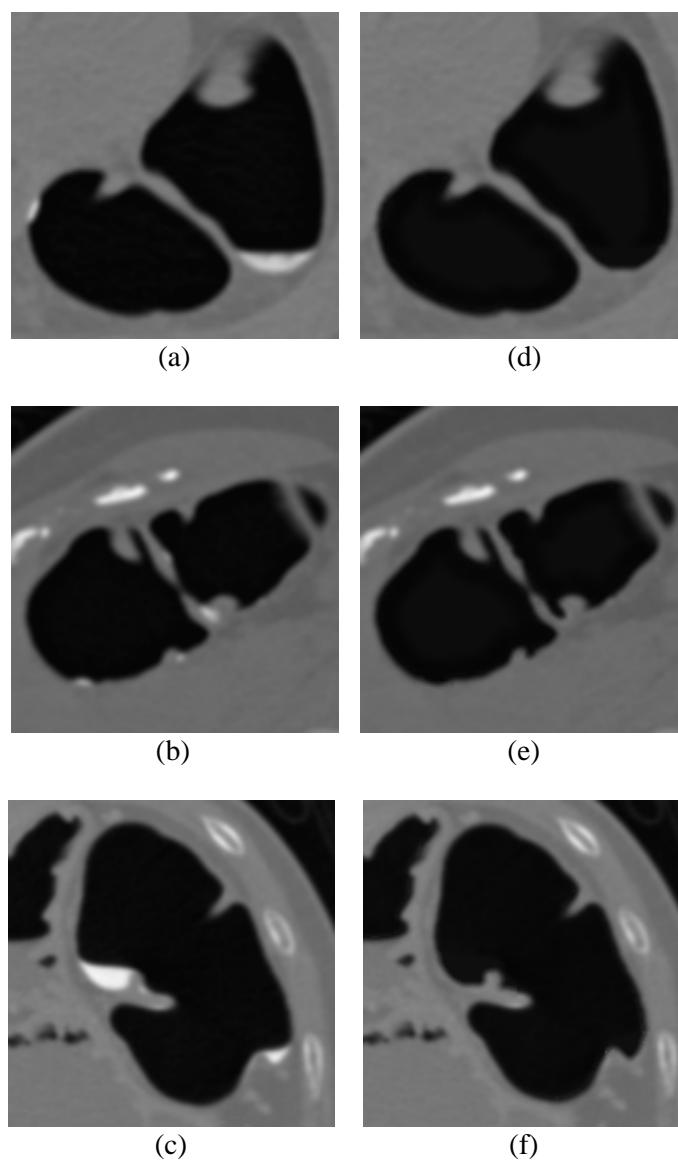
Figure 4.2 Zoomed view of (a)–(c) original CT image
(d)–(f) CT images after subtraction of CEF and mucosa layer reconstruction
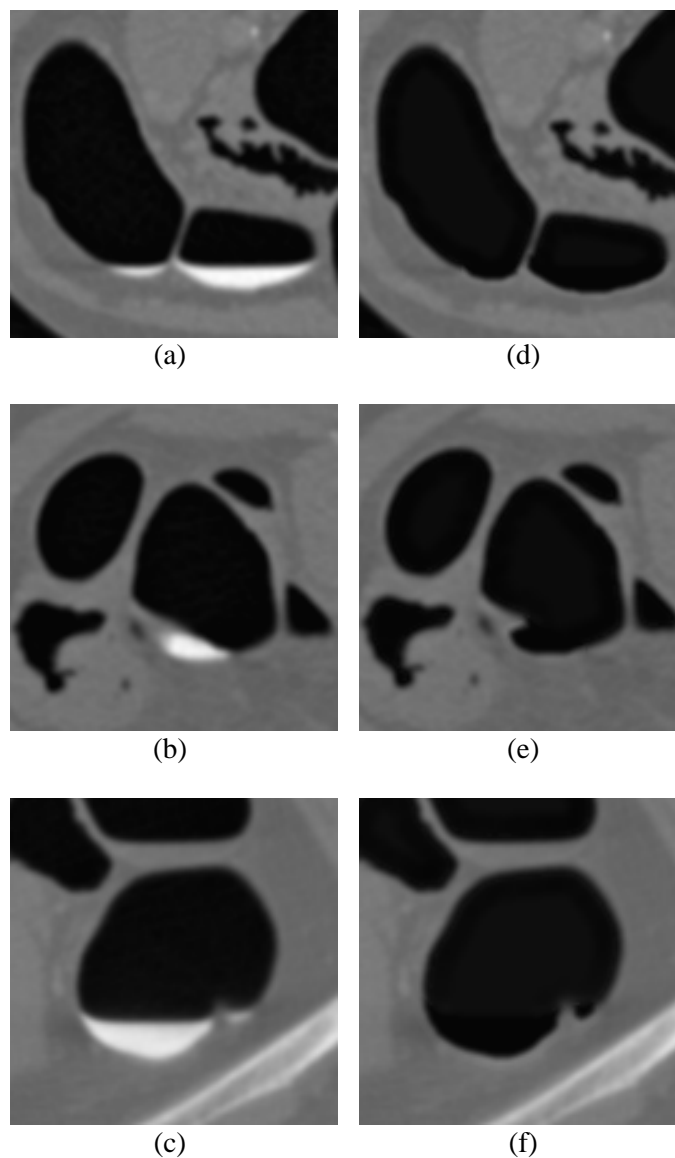
Figure 4.3 Zoomed view of (a)–(c) original CT image
(d)–(f) CT images after subtraction of CEF and mucosa layer reconstruction

From Table 4.4 on the second assessment, the scores of accuracy on the cleansing show that most datasets have satisfactory scores, only one dataset has scores less than the others due to the problem with the presence of beam hardening artifact. The results revealed that the proposed method could perform colon cleansing and the reconstructed mucosa layer of colon lumen at the area after subtraction of contrast-enhanced material were satisfied.

In order to represent the improvement of the proposed mucosa layer reconstruction method, the intensity profile along the reconstructed colon lumen before and after mucosa layer reconstruction are shown in Figure 4.4. The intensity profiles show that the mucosa layer

reconstruction assists in improvement of unnatural rapid transitions in the intensity level at the colon lumen after colon cleansing.

(a)

(b)
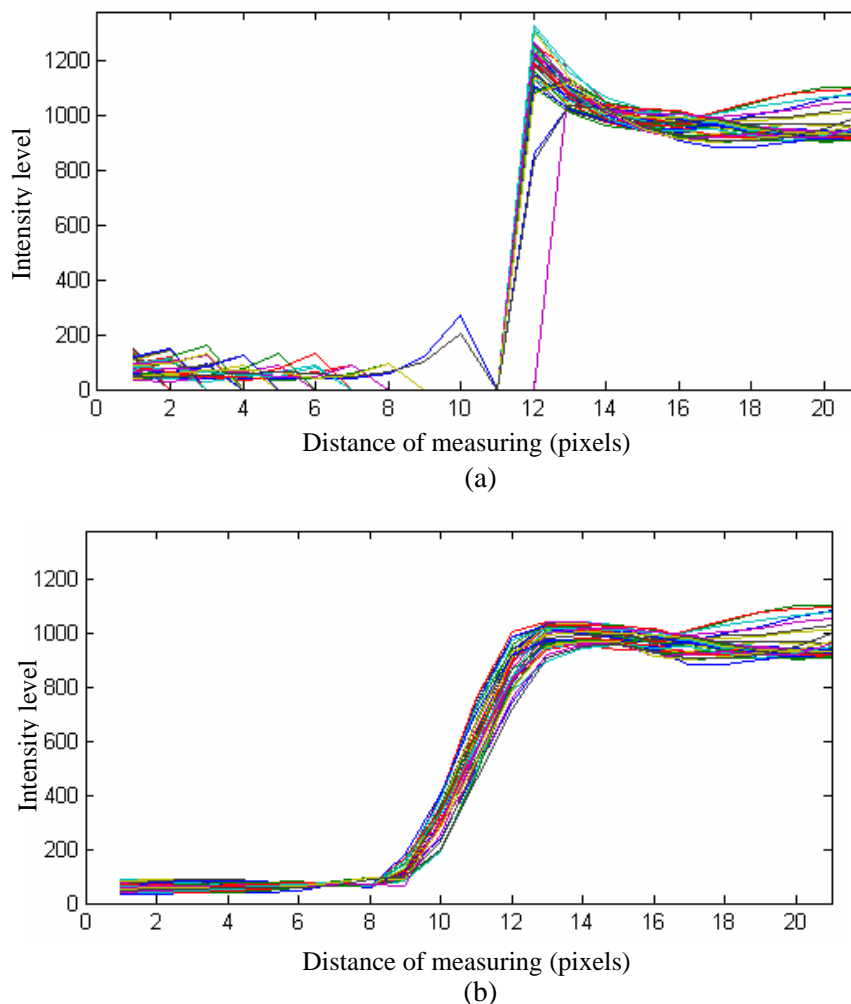
Figure 4.4 Intensity profile at colon wall (a) after subtraction of CEF

(b) after mucosa layer reconstruction

From Table 4.4 on the last assessment, the confidence on accuracy shows that the proposed method is satisfactory and sufficient to assist radiologists in diagnosing the colorectal cancer and can be used in 3D colon reconstruction.

However, in the case that patients did not follow the diet instruction prior to the bowel preparation, datasets may contain tiny spot of artifacts which sometimes could not be completely removed as shown in Figure 4.5. Moreover, when the presence of beam hardening artifact that made the residual materials not completely enhanced to occur, the colon wall was jagged as shown in Figure 4.6.
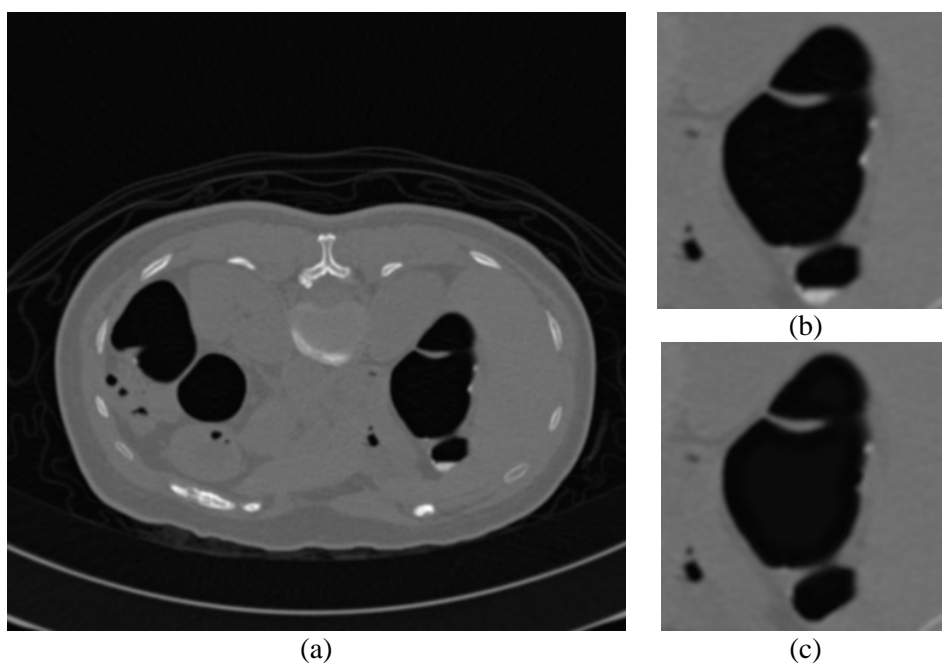
Figure 4.5 (a) Original CT image, zoomed view of
(b) original CT image (c) after colon cleansing with tiny spot artifact
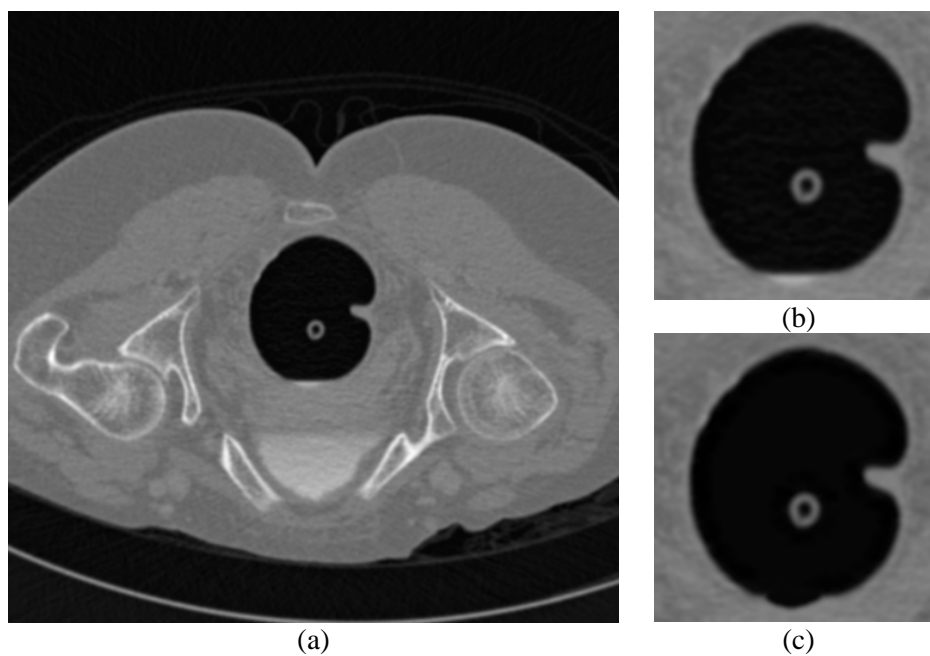
Figure 4.6 (a) Original CT image, zoomed view of
(b) original CT image (c) after colon cleansing with jagged colon wall

4.2 Colon Wall Detection

The proposed enhanced gradient vector flow (EGVF) is developed for assisting the traditional gradient vector flow (GVF) on colon wall detection. The results reveal that the enhanced gradient vector flow can assist in capturing and detecting the boundary of colon wall. The example of comparison results are shown in Figure 4.7.

(a) (d) (g)

(b) (e) (h)

(c) (f) (i)
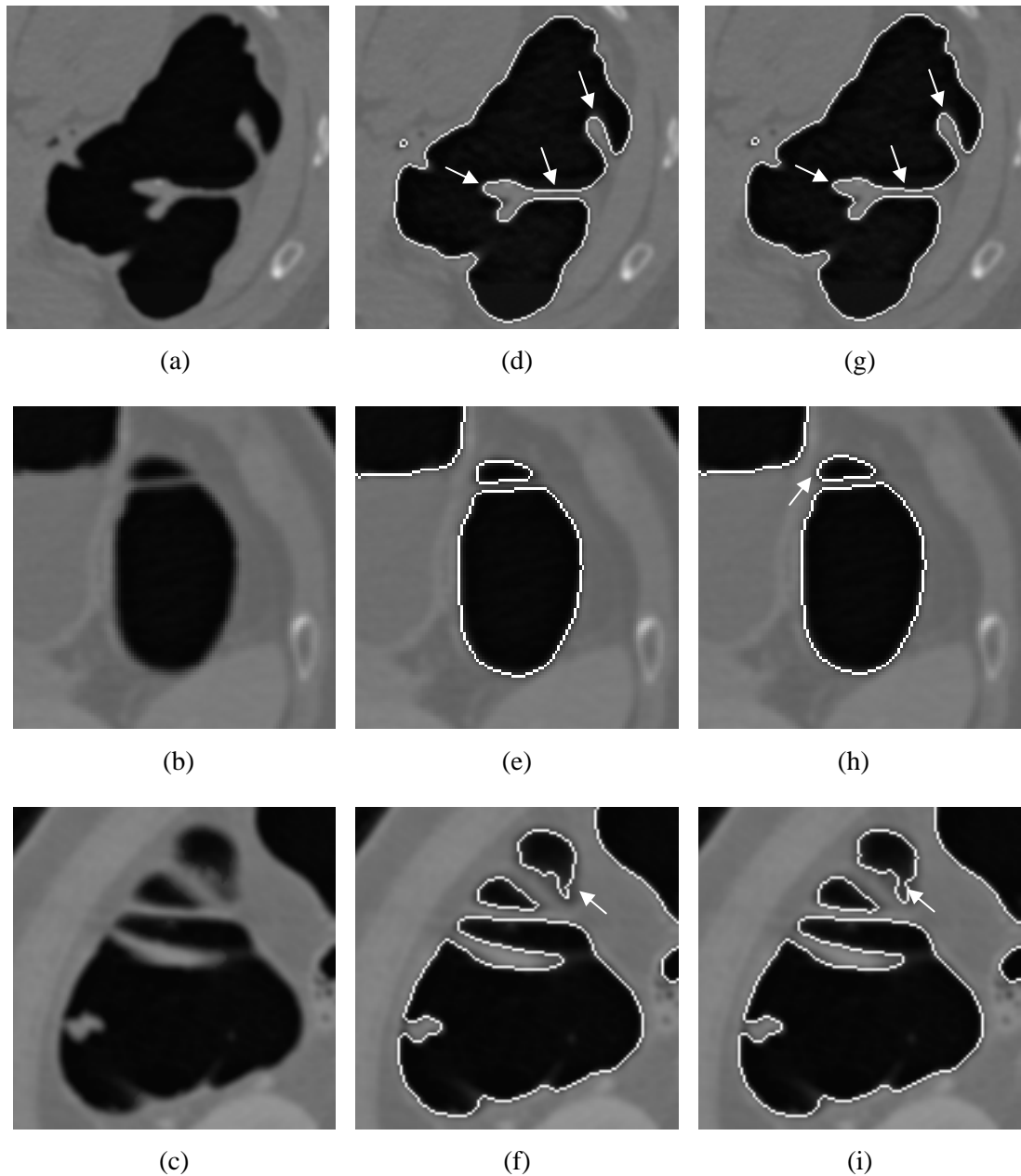
Figure 4.7 (a)–(c) Original CT image (d)–(f) Traditional GVF
(g)–(i) Proposed EGVF

From Figure 4.7 (a), (d), and (g) which are in the first row, the results show that the proposed method can assist on detection of colon wall with curly shape and almost like the can segment colon shape from original image than traditional gradient vector flow. Similarly, the results illustrated in Figure 4.7 (b), (e) and (h) which are in the second row, show that the proposed method can detect colon wall with the shape similar to the shape from original image. In the same way, the results in Figure 4.7 (c), (f) and (i) which are in the third row, show that the proposed method can assist on capturing boundary of colon with diminishing shaded intensity.

Moreover, the performance of proposed method on colon wall detection was compared with the existing method on colon wall segmentation, which are watershed algorithm and level set method. The assessment was operated by comparing the results from all techniques and evaluated the quality on accuracy of colon wall detection.

The quality on accuracy of colon wall detection was evaluated by two expert radiologists. The evaluation was also blinded assessment, so that the radiologists did not know any information about the techniques which were applied to each data. The evaluation was determined by the assessment scores from radiologists to consider on quality of colon wall detection of each dataset for all techniques. The assessment scores on quality of colon wall detection were ranged from 1 to 10, where 1=poor quality and 10=best quality. The visual inspection was performed by scrolling the image of marked colon wall detection from all techniques compare them with the original images.

In order to make the comparison reasonable, the initial contours of all techniques were automatically set in the same place by air inside colon. The gradient magnitude and the standard deviation were used in the same range. The weight parameters of all techniques were adjusted by step of 0.01 increments, and were selected from the best experimental results and employed to all datasets. For the proposed method that applied enhanced gradient vector flow, the weight parameters are μ=0.01, α= 0.03, β=0.01, and k_e=0.15. The algorithm of enhanced gradient vector flow deformable model was performed and the algorithm stopped if the area inside the deformable model in the last ten iterations has no progress. This stopping condition was also applied to the level set method. Moreover, four more datasets were added for more examination on different shapes of colons.

The comparative assessment scores on quality of colon wall detection on each dataset from both radiologists' evaluation for all techniques are shown in Table 4.5

Table 4.5 Assessment scores comparison on quality of colon wall detection

		Radiologist 1			Radiologist 2		
		Watershed	Level set	Proposed	Watershed	Level set	Proposed
Dataset 1	Mean	9.77	9.74	9.88	9.94	9.95	9.99
(1,352 segments)	S.D.	0.79	0.66	0.45	0.45	0.28	0.13
Dataset 2	Mean	9.90	9.91	9.97	9.89	9.88	9.98
(1,637 segments)	S.D.	0.49	0.39	0.19	0.57	0.43	0.20
Dataset 3	Mean	9.76	9.87	9.92	9.78	9.89	9.94
(9,45 segments)	S.D.	0.89	0.49	0.35	0.93	0.45	0.32
Dataset 4	Mean	9.82	9.91	9.93	9.88	9.97	9.99
(1,201 segments)	S.D.	0.96	0.44	0.37	0.89	0.23	0.10
Dataset 5	Mean	9.66	9.80	9.89	9.87	9.94	9.98
(1,854 segments)	S.D.	1.31	0.72	0.51	0.80	0.35	0.28
Dataset 6	Mean	9.79	9.93	9.95	9.86	9.95	9.98
(1,702 segments)	S.D.	1.02	0.38	0.30	0.89	0.33	0.22
Dataset 7	Mean	9.90	9.91	9.95	9.96	9.95	9.99
(1,729 segments)	S.D.	0.59	0.49	0.40	0.25	0.22	0.05
Dataset 8	Mean	9.85	9.89	9.92	9.92	9.96	9.99
(1,661 segments)	S.D.	0.68	0.38	0.32	0.57	0.24	0.12
Total mean		9.81	9.87	9.93	9.90	9.94	9.98

From Table 4.5, the assessment scores on quality of colon wall detection from both radiologists' evaluation on the proposed method, show that it gives better results on detection of colon wall than the other two techniques when comparing in each dataset. While some datasets, the assessment scores on quality of colon wall detection from both radiologists' evaluation on watershed algorithm is better than level set method. Similarly, some assessment scores on quality of colon wall detection from both radiologists' evaluation on level set method is better than watershed algorithm.

For simple comparison, the assessment scores on quality of colon wall detection of each datasets from both radiologists are represented by line graphs in Figure 4.8 and Figure 4.9, respectively. The scores reveal that the proposed colon wall detection method achieves better results than the others in each dataset evaluation.
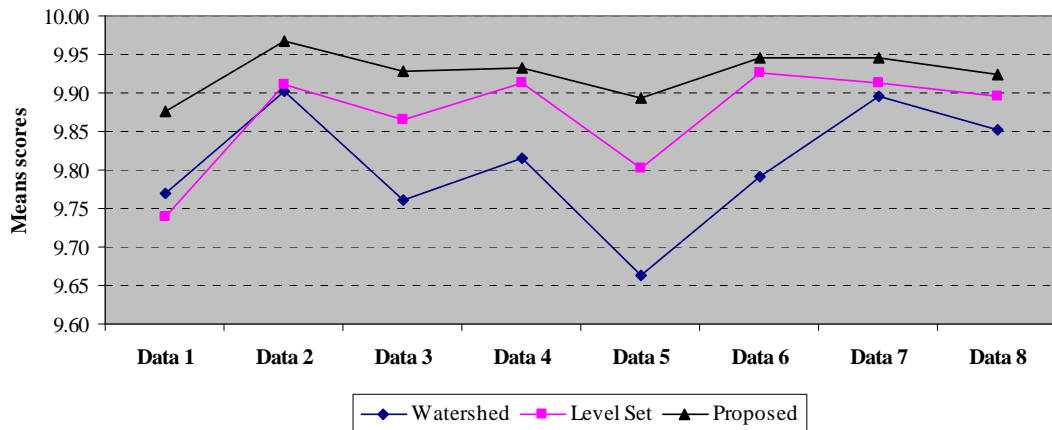
Figure 4.8 Assessment scores on quality of colon wall detection from radiologist1
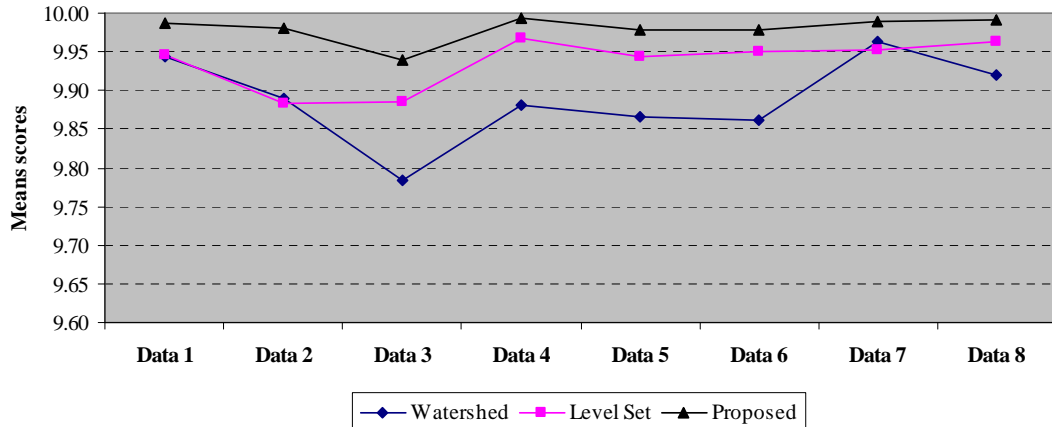
Figure 4.9 Assessment scores on quality of colon wall detection from radiologist2

From Table 4.5, the total mean of assessment scores on quality of colon wall detection of all datasets from both radiologists' evaluation on the proposed method are 9.93 and 9.98, respectively. While, the total mean of assessment scores on quality of colon wall detection of all datasets from both radiologists' evaluation on watershed algorithm are 9.81 and 9.90, respectively. The total mean of assessment scores on quality of colon wall detection of all datasets from both radiologists' evaluation on level set method are 9.87 and

9.94, respectively. Consequently, the results revealed that the proposed method gives better results on colon wall detection of all datasets than other existing methods such as watershed algorithm and level set method.

However, The total mean of assessment scores on quality of colon wall detection of all datasets from both radiologists evaluated to each technique, are not much different due to the number of segments of colon was many segments. In normal cases, all techniques could undergo similar way on the best performance of colon wall segmentation. Nevertheless, in the special cases which colon lumen has small thin layer or more descending shaded intensity on the border of colon lumen, each technique gives the results in special different ways.

The example results of the special cases from both radiologists are shown in Figure 4.10 and Figure 4.11.

(a)	(d)	(g)	(j)
(b)	(e)	(h)	(k)
(c)	(f)	(i)	(l)
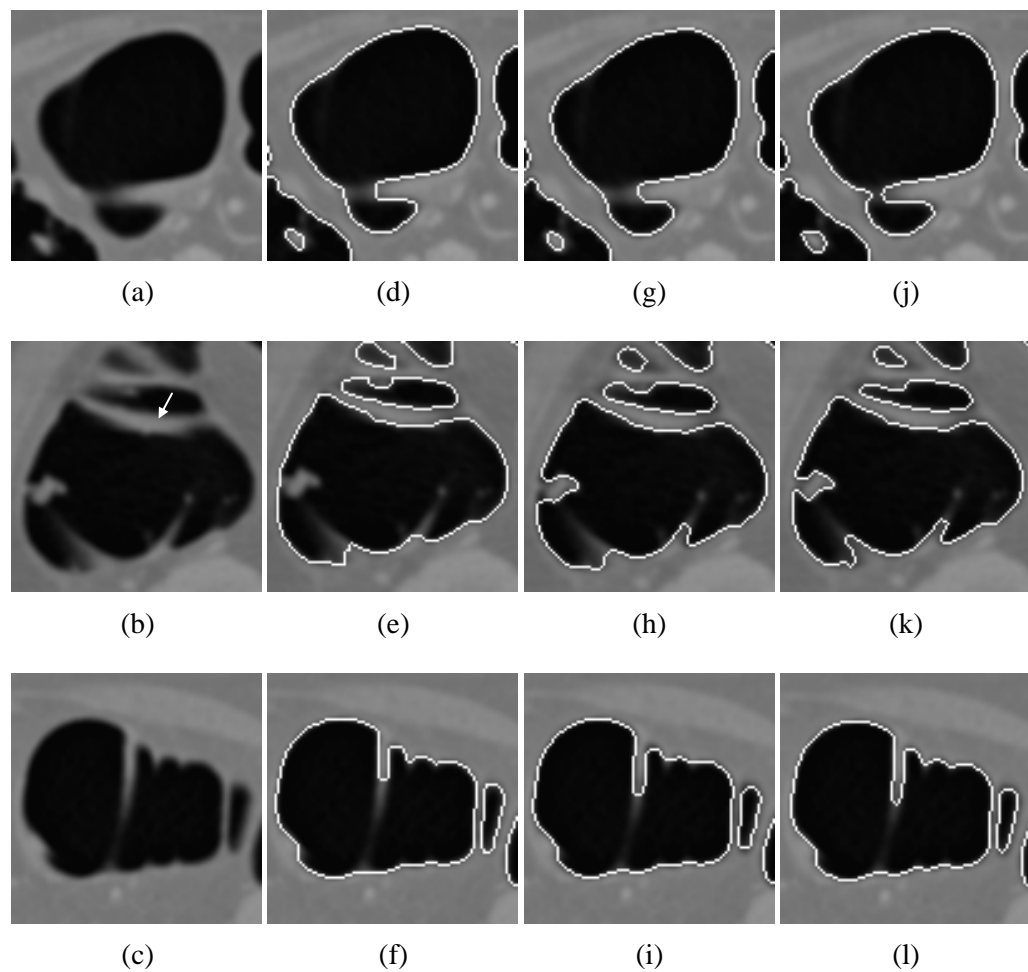
Figure 4.10 (a)–(c) Original image (d)–(f) Watershed algorithm
(g)–(i) Level set method (j)–(l) Proposed EGVF
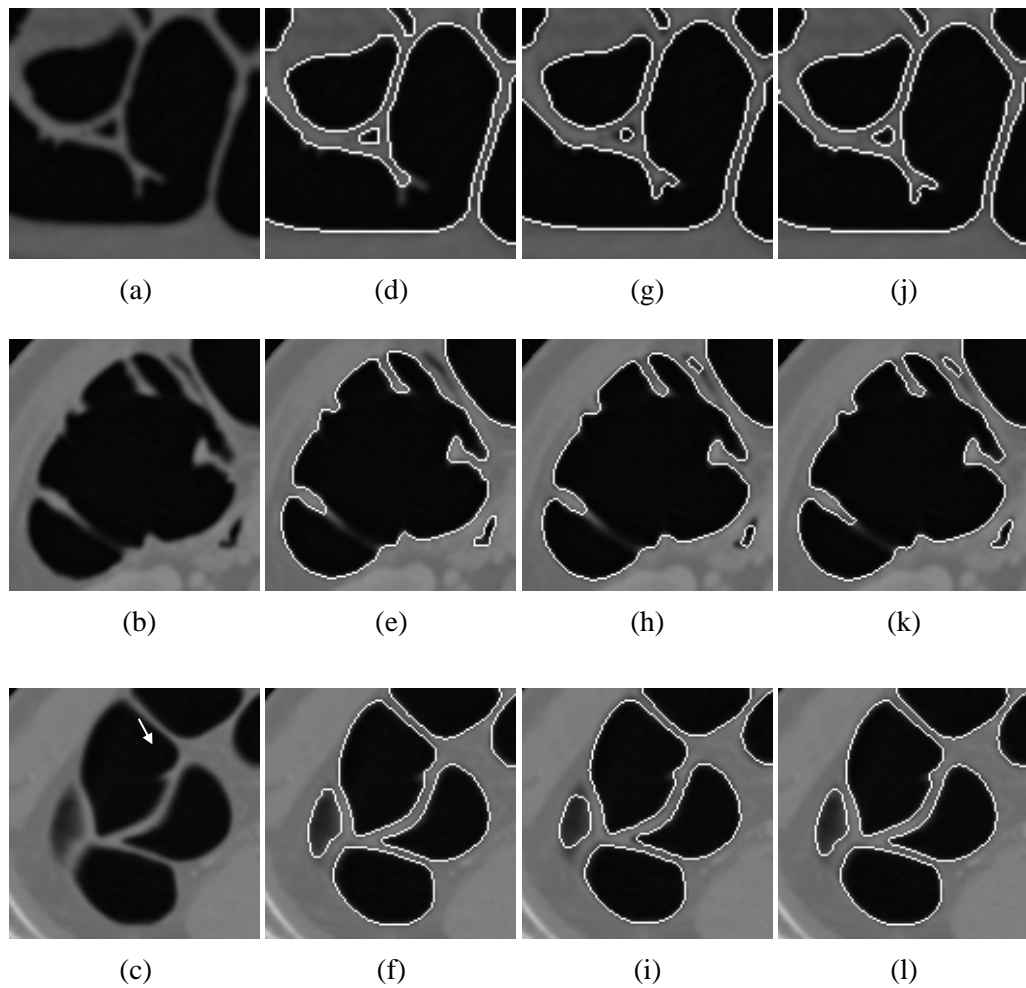
Figure 4.11 (a)–(c) Original image (d)–(f) Watershed algorithm
(g)–(i) Level set method (j)–(l) Proposed EGVF

From Figure 4.10 and Figure 4.11, the results of watershed algorithm show its capability on detection obvious colon wall and the descending shaded intensity, however it sometimes produces sharpened edges and miss on the small thin layers with low intensity. Similarly, the results of level set method shows its capability on detection explicitly colon wall with smoothen curve and also can detect small thin layer with low intensity. Nevertheless, it cannot move to the real shape on descending contrast intensity. While, the proposed method represented in better results on colon wall detection. The small thin layer with low intensity were almost detected. Additionally, it also can ascertain colon lumen on diminishing contrast intensity.

Consequently, the proposed method produced better contour with more capture range, more extraction capability and can converge to boundaries of various shapes of colon wall.

(a)

(b)

(c)
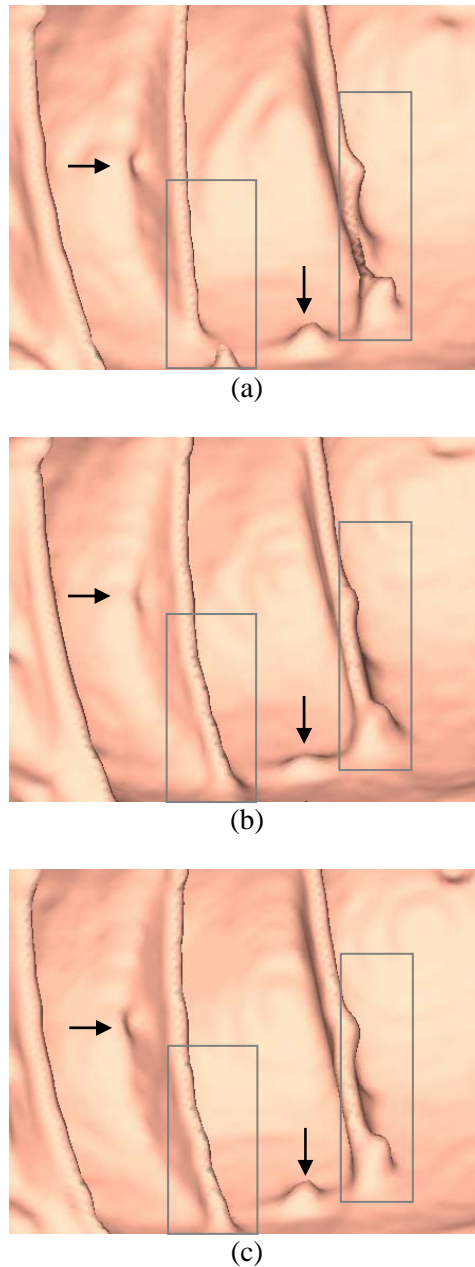
Figure 4.12 3D inner view of colon wall detection by
(a) Watershed algorithm (b) Level set method (c) Proposed EGVF

The other way to represent the results in the special cases where colon lumen have small protrusion layer or have descending shaded in intensity, the example comparison results of the special cases are illustrated in 3D inner view of colon wall, as shown in Figure 4.12. From Figure 4.12, it shows that each technique gives the results in different ways, the areas where the square boxes located are the areas that have thin layer with low shaded intensity and the area where the arrows point are small protrusion layer.

(a)

(b)

(c)
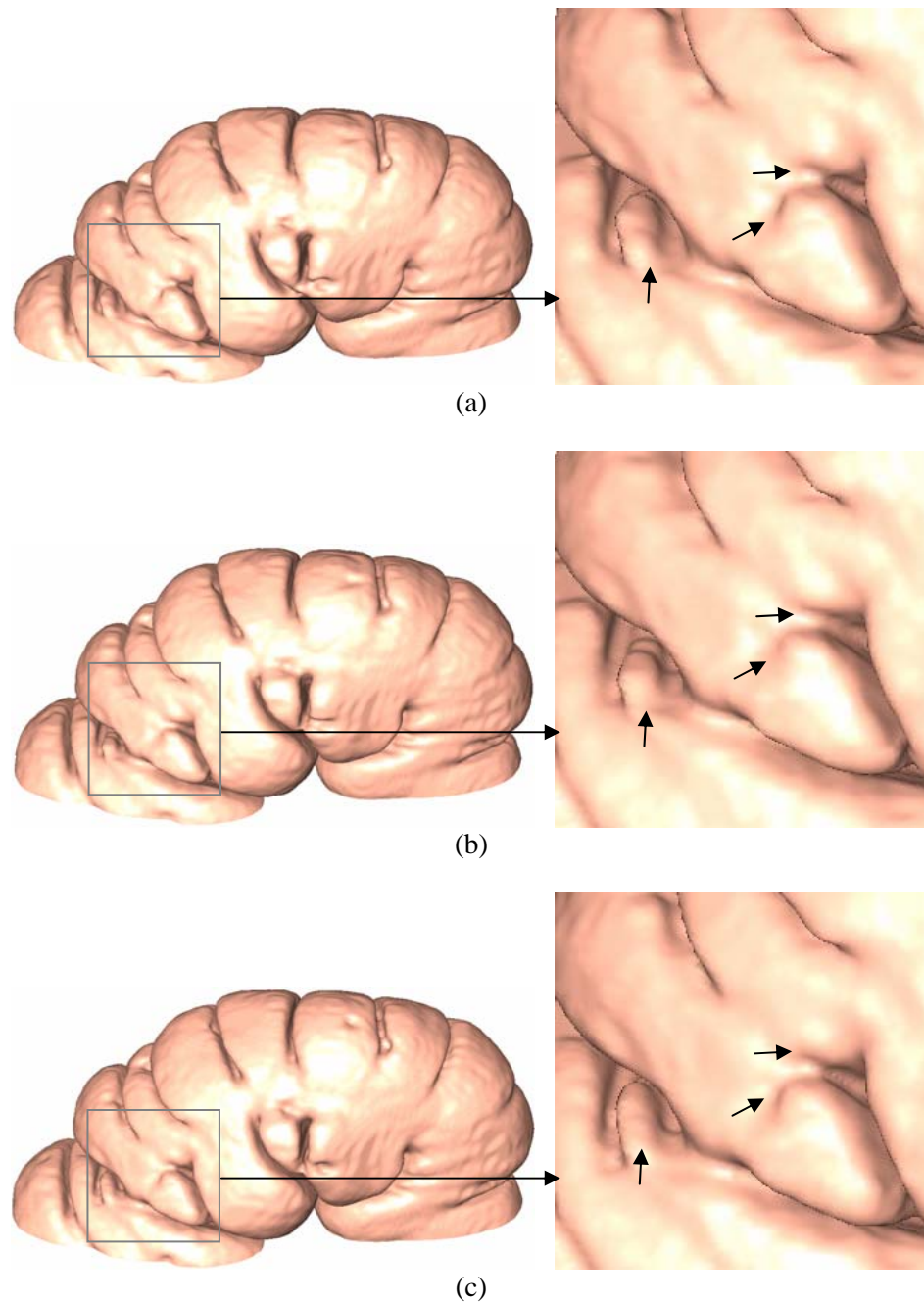
Figure 4.13 3D external view of colon wall detection by
(a) Watershed algorithm (b) Level set method (c) Proposed EGVF

The example comparison results on 3D external view of colon wall from all techniques are shown in Figure 4.13. The results show that each technique gives different results. The area where the square box located is zoomed and is shown on the right side of an image. The areas where the arrows point are the areas of concave boundary with descending shaded intensity.

To represent all results in the special conditions, the segments of colon in these cases were selected from both radiologists. The comparative assessment scores on quality of colon wall detection on these cases of each dataset from both radiologists for all techniques are shown in Table 4.6

Table 4.6 Assessment scores comparison on quality of colon wall detection
in special cases

		Radiologist 1			Radiologist 2		
		Watershed	Level set	Proposed	Watershed	Level set	Proposed
Dataset 1	Mean	8.78	8.62	9.35	9.70	9.72	9.93
(257 segments)	S.D.	1.46	0.88	0.84	1.00	0.59	0.30
Dataset 2	Mean	9.20	9.26	9.74	9.09	9.05	9.83
(199 segments)	S.D.	1.18	0.87	0.48	1.41	0.86	0.54
Dataset 3	Mean	8.09	8.92	9.42	8.26	9.08	9.52
(118 segments)	S.D.	1.80	0.95	0.83	2.09	0.94	0.78
Dataset 4	Mean	7.33	8.73	9.02	8.27	9.53	9.92
(83 segments)	S.D.	2.59	1.14	1.05	2.95	0.77	0.36
Dataset 5	Mean	7.01	8.25	9.05	8.82	9.49	9.80
(209 segments)	S.D.	2.73	1.35	1.21	2.10	0.94	0.81
Dataset 6	Mean	7.30	9.04	9.30	8.21	9.36	9.73
(132 segments)	S.D.	2.60	1.01	0.86	2.72	1.01	0.74
Dataset 7	Mean	8.85	9.04	9.41	9.61	9.47	9.97
(157 segments)	S.D.	1.64	1.33	1.21	0.76	0.54	0.18
Dataset 8	Mean	8.63	9.02	9.28	9.26	9.66	9.91
(179 segments)	S.D.	1.63	0.71	0.70	1.61	0.64	0.37
Total mean		8.25	8.84	9.34	9.03	9.44	9.84

For simple comparison, the assessment scores on quality of colon wall detection with special cases in each dataset from both radiologists are represented by line graph in Figure 4.14 and Figure 4.15, respectively. The assessment scores on quality of colon wall detection with special cases in each dataset from both radiologists presented that the proposed colon wall detection method achieves the highest scores.
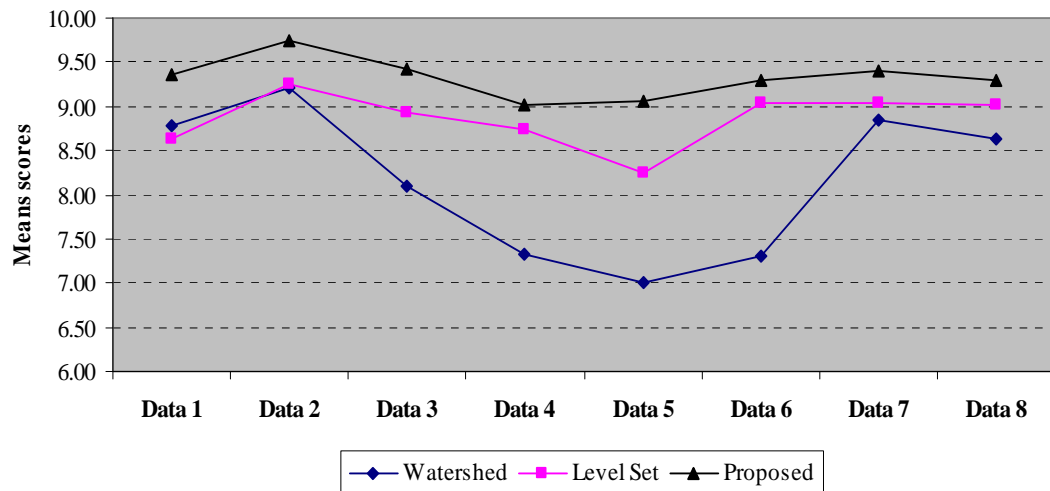
Figure 4.14 Assessment scores on quality of colon wall detection on special cases from radiologist 1
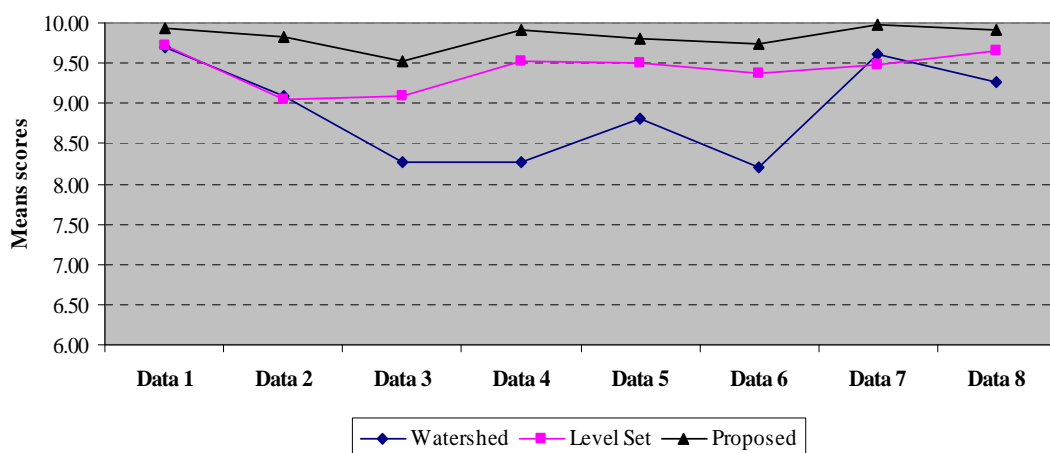
Figure 4.15 Assessment scores on quality of colon wall detection on special cases from radiologist 2

From Table 4.6, the total mean of assessment scores on quality of colon wall detection on special cases from both radiologists evaluation on the proposed method are 9.34 and 9.84, respectively. While, the total mean of assessment scores on quality of colon wall detection on special cases from both radiologists evaluation on watershed algorithm are 8.25 and 9.03, respectively. The total mean of assessment scores on quality of colon wall detection on special cases from both radiologists evaluation on level set method are 8.84 and 9.44, respectively. The results revealed that the proposed method gives better results on colon wall detection than other existing methods such as watershed algorithm and level set method, despite of the special cases.

In order to compare whether the mean assessment score on quality of colon wall detection in existing methods and proposed method are significantly difference in all datasets, paired t-test and p-value are calculated. The significance level (α) is chosen to be 0.05 or equal to 5%.

For examination that the mean assessment score on quality of colon wall detection in each pair of existing methods and proposed method are equal or not equal, the null hypothesis (H_0) and the alternative hypothesis (H_1) are defined as follows

H_0 : There is no difference in mean assessment scores on quality of colon wall detection between two comparative methods ($\mu_1 = \mu_2$).

H_1: There is difference in mean assessment scores on quality of colon wall detection between two comparative methods ($\mu_1 \neq \mu_2$).

where μ_1 is the mean assessment scores on quality of colon wall detection on the first comparative method and μ_2 is the mean assessment scores on quality of colon wall detection on second comparative method.

The comparison results of mean difference examination by paired t-test and p-value of mean assessment scores on quality of colon wall detection between each pair of existing methods and proposed method in all datasets from both radiologists are shown in Table 4.7.

From Table 4.7, t-value is positive if the mean value of the first comparative method is larger than the mean value of the second comparative method and t-value is negative if mean value of the first comparative method is smaller than the mean value of the second comparative method.

Table 4.7 Mean difference examination by paired t-test and p-value of mean assessment scores on quality of colon wall detection

	Paired test		Radiologist 1		Radiologist 2	
			t-value	p-value	t-value	p-value
Dataset 1	Watershed - Level set		2.0397	0.0416	-0.3845	0.7007
(1,352 segments)	Watershed - Proposed		-7.0526	2.79428E-12	-4.0852	4.6623E-05
	Level set - Proposed		-11.8430	7.40729E-31	-6.6524	4.17755E-11
Dataset 2	Watershed - Level set		-1.1048	0.2694	0.4204	0.6743
(1637 segments)	Watershed - Proposed		-6.8478	1.05761E-11	-7.2558	6.13944E-13
	Level set - Proposed		-8.9149	1.27306E-18	-10.7305	5.24857E-26
Dataset 3	Watershed - Level set		-5.4096	8.00695E-08	-4.6481	3.82615E-06
(945 segments)	Watershed - Proposed		-6.8620	1.22762E-11	-5.9950	2.89421E-09
	Level set - Proposed		-6.3107	4.26723E-10	-5.9156	4.62015E-09
Dataset 4	Watershed - Level set		-4.3537	1.45279E-05	-3.5628	0.0004
(1,201 segments)	Watershed - Proposed		-5.0515	5.06205E-07	-4.5018	7.39524E-06
	Level set - Proposed		-4.1436	3.6591E-05	-4.6584	3.54159E-06
Dataset 5	Watershed - Level set		-6.4280	1.64007E-10	-5.0856	4.03466E-07
(1,854 segments)	Watershed - Proposed		-9.4709	8.13379E-21	-6.8076	1.3361E-11
	Level set - Proposed		-10.3609	1.71584E-24	-7.6589	3.00184E-14
Dataset 6	Watershed - Level set		-6.7211	2.45255E-11	-5.1505	2.89983E-07
(1,702 segments)	Watershed - Proposed		-7.2449	6.53277E-13	-6.1393	1.02917E-09
	Level set - Proposed		-4.7492	2.21375E-06	-6.0486	1.79302E-09
Dataset 7	Watershed - Level set		-2.6357	0.0085	1.7214	0.0854
(1,729 segments)	Watershed - Proposed		-6.3240	3.23727E-10	-5.4550	5.60535E-08
	Level set - Proposed		-6.0434	1.84447E-09	-8.8021	3.18963E-18
Dataset 8	Watershed - Level set		-3.6931	0.0002	-3.6682	0.0003
(1,661 segments)	Watershed - Proposed		-5.8138	7.31109E-09	-5.5462	3.39195E-08
	Level set - Proposed		-5.8884	4.70901E-09	-6.0515	1.77003E-09
Total	Watershed - Level set		-11.0723	2.33923E-28	-8.5589	1.27683E-17
(12,081 segments)	Watershed - Proposed		-18.7218	4.04036E-77	-15.6312	1.525E-54
	Level set - Proposed		-21.5689	2.8299E-101	-20.3780	8.74128E-91

From Table 4.7, p-value between watershed algorithm and level set method on dataset 1, 3, 4, 5, 6, 7 and 8 from radiologist 1, and dataset 3, 4, 5, 6 and 8 from radiologist 2, are less than 0.05 significant levels and are not defined as member of the critical region. Then, the null hypothesis (H_0) is rejected. Therefore, these results are statistically significantly difference in the mean assessment scores on quality of colon wall detection between watershed algorithm and level set method. However, p-value between watershed algorithm and level set method on datasets 2 from radiologist1 and dataset 1, 2 and 7 from radiologist 2, are more than 0.05 significant levels and are defined as member of the critical region. Then, the null hypothesis (H_0) is accepted. Hence, these results are not statistically significantly difference in the mean assessment scores on quality of colon wall detection between watershed algorithm and level set method.

In additional, p-value between the existing methods such as watershed algorithm and level set method compare to the proposed method in all datasets from both radiologists, are less than 0.05 significant levels and are not defined as member of the critical region. Then, the null hypothesis (H_0) is rejected. Consequently, the results of the mean assessment scores on quality of colon wall detection between existing methods and the proposed method are statistically significantly difference at 5% significance level. In other word, the mean assessment scores on quality of colon wall detection in the proposed method is not equal to the mean assessment scores on quality of colon wall detection in existing methods at 95% confidence level.

Similarly, in order to compare whether the mean assessment scores on quality of colon wall detection in special cases from existing methods and the proposed method is significantly difference, paired t-test and p-value are calculated. The significance level (α) is chosen to be 0.05 or equal to 5%. The null hypothesis (H_0) and the alternative hypothesis (H_1) are assumed as follows

H_0:　　There is no difference in the mean assessment scores on quality of colon wall detection in special cases between two comparative methods ($\mu_1 = \mu_2$).

H_1:　　There is difference in the mean assessment scores on quality of colon wall detection in special cases between two comparative methods ($\mu_1 \neq \mu_2$).

where μ_1 is the mean assessment scores on quality of colon wall detection in special cases on the first comparative method and μ_2 is the mean assessment scores on quality of colon wall detection on second comparative method.

Table 4.8 Mean difference examination by paired t-test and p-value of mean assessment scores on quality of colon wall detection in special cases

|	Paired test		Radiologist 1		Radiologist 2	
			t-value	p-value	t-value	p-value
Dataset 1 (257 segments)	Watershed - Level set		2.0500	0.0414	-0.3840	0.7013
	Watershed - Proposed		-7.6686	3.6269E-13	-4.1906	3.8343E-05
	Level set - Proposed		-15.8340	7.8222E-40	-7.1603	8.5165E-12
Dataset 2 (199 segments)	Watershed - Level set		-1.1053	0.2704	0.4196	0.6752
	Watershed - Proposed		-7.6734	7.4537E-13	-8.2641	2.0009E-14
	Level set - Proposed		-11.0420	2.1330E-22	-15.2732	2.5955E-35
Dataset 3 (118segments)	Watershed - Level set		-6.0917	1.4660E-08	-5.0538	1.6152E-06
	Watershed - Proposed		-8.4770	8.0492E-14	-6.9753	1.9496E-10
	Level set - Proposed		-7.4915	1.4109E-11	-6.8503	3.6457E-10
Dataset 4 (83 segments)	Watershed - Level set		-4.8792	5.1593E-06	-3.8258	0.0003
	Watershed - Proposed		-5.9464	6.4412E-08	-5.0930	2.2096E-06
	Level set - Proposed		-4.5858	1.6049E-05	-5.3261	8.6045E-07
Dataset 5 (209 segments)	Watershed - Level set		-7.0641	2.3884E-11	-5.3788	2.0088E-07
	Watershed - Proposed		-12.0121	1.3619E-25	-7.5800	1.1240E-12
	Level set - Proposed		-14.0173	7.2060E-32	-8.8199	4.6677E-16
Dataset 6 (132 segments)	Watershed - Level set		-8.0975	3.3928E-13	-5.6869	8.0403E-08
	Watershed - Proposed		-9.0743	1.4818E-15	-7.1289	6.1049E-11
	Level set - Proposed		-5.1566	9.0585E-07	-6.9870	1.2794E-10
Dataset 7 (157 segments)	Watershed - Level set		-2.6826	0.0081	1.7313	0.0854
	Watershed - Proposed		-7.1941	2.4732E-11	-5.9790	1.4748E-08
	Level set - Proposed		-6.7866	2.2568E-10	-11.8228	1.9616E-23
Dataset 8 (179segments)	Watershed - Level set		-3.8159	0.0002	-3.7884	0.0002
	Watershed - Proposed		-6.3601	1.6492E-09	-6.0127	1.0096E-08
	Level set - Proposed		-6.4587	9.7518E-10	-6.6769	3.0001E-10
Total (1,334 segments)	Watershed - Level set		-11.5509	1.75443E-29	-8.7730	5.21495E-18
	Watershed - Proposed		-21.3806	1.93617E-87	-17.0794	2.685E-59
	Level set - Proposed		-25.9620	1.3293E-120	-23.9568	9.037E-106

The comparison results of the mean difference examination by paired t-test and p-value of the mean assessment scores on quality of colon wall detection between each pair of existing methods and the proposed method in special cases are shown in Table 4.8.

From Table 4.8, t-value is positive if the mean value of the first comparative method is larger than the mean value of the second comparative method and t-value is negative if the mean value of the first comparative method is smaller than the mean value of the second comparative method. P-value between watershed algorithm and level set method in special cases on dataset 1, 3, 4, 5, 6, 7 and 8 from radiologist 1, and dataset 3, 4, 5, 6 and 8 from radiologist 2, are less than 0.05 significant levels and are not defined as member of the critical region. Then, the null hypothesis (H_0) is rejected. Therefore, these results are statistically significantly difference in the mean assessment scores on quality of colon wall detection in special cases between watershed algorithm and level set method. However, p-value between watershed algorithm and level set method in special cases on datasets 2 from radiologist1 and dataset 1, 2 and 7 from radiologist 2, are more than 0.05 significant levels and are defined as member of the critical region. Then, the null hypothesis (H_0) is accepted. Hence, these results are no statistically significantly difference in the mean assessment scores on quality of colon wall detection in special cases between watershed algorithm and level set method.

Moreover, p-value in special cases between existing methods such as watershed algorithm and level set method compare to the proposed method in all datasets from both radiologists, are less than 0.05 significant levels and are not defined as member of the critical region. Then, the null hypothesis (H_0) is rejected. Consequently, the results of the mean assessment scores on quality of colon wall detection between existing methods and the proposed method in special cases are statistically significantly difference at 5% significance level. In other word, the mean assessment scores in special cases on quality of colon wall detection in the proposed method is not equal to the mean assessment scores on quality of colon wall detection in existing methods at 95% confidence level.

Subsequently, the proposed algorithm for colon segmentation was performed on the results from the previous stage after colon cleansing and colon wall detection. In order to examine the proposed algorithm for colon segmentation, twenty datasets were tested. The results from segmentation were completely built without contiguous of inflated small intestine. The example results of removing small intestine are shown in Figure 4.16. The results show that the method can completely eliminate other organs, especially small intestine from colon.

(a)   (c)

(b)   (d)
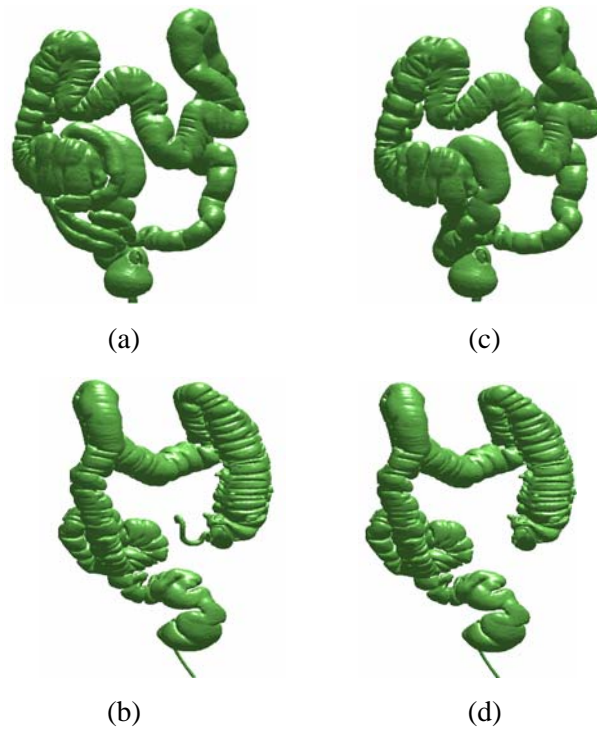
Figure 4.16 (a) (b) Contiguous small intestine and colon (c) (d) Removing small intestine

Finally, the successfully segmented colon was acquired and the surface rendering was performed to reconstruct the 3D model of colon. The results of 3D model of colon are shown in Figure 4.17. More results for all datasets are in Appendix.

Figure 4.17 3D model of colon reconstruction from dataset 1–8

CHAPTER V

DISCUSSION AND CONCLUSION

5.1 Discussion

A hybrid framework for reconstructing 3D colon model from oral contrast-enhanced CT colonography image is presented. The process of framework is composed of three main parts, the first part is colon cleansing, the second part is colon wall detection and the third part is colon segmentation and 3D model reconstruction.

The first part of the proposed framework is colon cleansing process which uses the K-means clustering algorithm to detect and eliminate any retained material of contrast-enhanced material inside the colon lumen. However, applying K-means clustering directly on original data can not correctly classify the regions. Consequently in the proposed method, a sharpened image by Laplacian operator is applied to K-means clustering to highlight the discontinuity intensity level and to improve classified regions. The next process on lung removal, most of traditional methods always apply threshold value to segment lung. Nevertheless, the proposed method uses anatomical lung analysis by blood vessel in lung to distinguish lung from other organs. Afterward, automatic contrast-enhanced material segmentation is employed to separate contrast-enhanced fluid from bone. Subsequently, automatic partial volume effect segmentation is undergone to detect partial volume effect at two transition intensities between air and contrast-enhanced material. This partial volume effect segmentation method is flexible can be applied to different intensities data. Then after that, colon cleansing and mucosa layer reconstruction is performed to remove contrast-enhanced material and partial volume effect, and reconstruct mucosa layer of colon wall to be as realistic as possible. The examination was performed on four datasets of CT images. The results are evaluated by the expert radiologist and they reveal that the accuracy on cleansing is satisfactory, all partial volume effect voxels and the contrast-enhanced material were successfully removed and the inner colon layer after cleansing become realistic. However, in the case that patients did not follow the diet instruction prior to the bowel preparation, datasets contain tiny spot of artifacts which sometimes could not be completely removed. Moreover, when the presence of beam hardening artifact that made the residual materials not completely enhanced was occurred, the colon wall was jagged.

The second part is colon wall segmentation which applies enhanced gradient vector flow (EGVF) to assist on colon lumen detection. Hybrid edge, which combined the edge obtained from Canny and Laplacian of Gaussian detection, is used to construct the enhanced edge map of EGVF. The scale of threshold values which is applied on Canny edge detectors is automatically set by applying the Otsu's method with gradient magnitude and the threshold of Laplacian of Gaussian detector is mechanically set by the mean absolute value of Laplacian of Gaussian. The proposed method was examined on eight datasets of CT images and is compared with the existing colon wall detection methods. The quality of accuracy is evaluated by the two skilled radiologists. The total mean of assessment score on quality of colon wall detection of all datasets from both radiologists are 9.93 and 9.98, respectively. Similarly, the total mean of assessment score on quality of colon wall detection on special cases from both radiologists are 9.34 and 9.84, respectively. The p-value when comparing the mean difference of the mean assessment score on quality of colon wall detection between existing methods such as watershed algorithm and level set method to the proposed method on all datasets and special cases, are less than 0.05. Consequently, these results are statistically significant difference in the mean assessment score on quality of colon wall detection between existing methods and the proposed method at 95% confidence level. The results show that the proposed method performs better on all datasets and even if in special cases.

The third part is colon segmentation method bases on volume analysis and anatomical structures. Twenty datasets are examined and the results show that the 3D colon models are constructed although in the case that the small intestine is inflated with the shape similar to colon.

5.1 Conclusion

In summary, the hybrid framework for reconstructing 3D colon model from oral contrast-enhanced CT colonography image is proposed. The process of framework is composed of three main parts, the first part is colon cleansing, the second part is colon wall detection and the third part is colon segmentation and 3D model reconstruction.

The first part of the proposed framework is colon cleansing process which uses the K-means clustering algorithm to detect and eliminate any retained material of contrast-enhanced fluid (CEF) inside the colon lumen and applied the morphological operations to remove the undesirable partial volume effect. The examination was performed on four datasets of CT

images. The results was evaluated by the expert radiologist and revealed that the accuracy on cleansing was satisfactory, all partial volume effect voxels and the contrast-enhanced material were successfully removed and the inner colon layer after cleansing became realistic.

The second part is colon wall detection. The enhanced gradient vector flow (EGVF) is proposed to assist on colon lumen detection. Hybrid edge which combined the edge from Canny and Laplacian of Gaussian detector is used to construct the enhanced edge map of EGVF. The proposed method was examined on eight datasets of CT images and is compared with existing colon wall detection methods. The quality of accuracy was evaluated by the two skilled radiologists. The total mean of assessment score on quality of colon wall detection of all datasets from both radiologists revealed that the results from the proposed method were satisfy and give better results even if in the special cases.

Finally, the proposed colon segmentation method bases on volume analysis and anatomical structures are applied. Twenty datasets are examined and 3D colon models are constructed.

5.2 Future Work

In future, the development on 3D colon model should display as the virtual camera moving fly through the colon to view inside colon. Moreover, the centerline of colon should be defined for assisting in automatic virtual camera moving. The tool for contribution the internal view of fly through in 3D model of colon should be support on real time rendering. So, this view can simulate the virtual colonoscopy like the optical colonoscopy to automatically examine colon.

References

[1] Jemal, A., Siegel, R., Ward, E., Hao, Y., Xu, J., Murray, T., and Thun, M.J. Cancer statistics, 2008. CA A Cancer Journal for Clinicians 58 (December 2008): 71–96.

[2] Mols, B. Polyps revealed on a virtual colon voyage: Three-dimensional colonoscopy reduces discomfort. Delft Outlook scientific magazine 2003

[3] Heiken, J. P., Peterson, C. M., and Menias, C. O. Virtual colonoscopy for colorectal cancer screening: current status. Cancer Imaging 5 (October 2005): 133–139.

[4] Bielen, D. J., Bosmans, H. T., Wever, L. L., Maes, F., Tejpar, S., Vanbeckevoort, D., and Marchal, G. J. Clinical validation of high-resolution fast spin-echo MR colonography after colon distention with air. Journal of Magnetic Resonance Imaging 22 (September 2005): 400–405.

[5] The National Digestive Diseases Information Clearinghouse (NDDIC). Virtual colonoscopy [Online]. 2008. Available from : http://digestive.niddk.nih.gov/ ddiseases/pubs/virtualcolonoscopy/ [2010, September 9]

[6] Johnson, C. D., and Abraham H. D. CT colonography: the next colon screening examination? Radiology 216 (August 2000): 331–341.

[7] Pickhardt, P. J., and others. Computed tomographic virtual colonoscopy to screen for colorectal neoplasia in asymptomatic adults. The New England Journal of Medicine 349 (December 2003): 2191–2200.

[8] Wyatt, C. L., Ge, Y., and Vining, D. J. Automatic segmentation of the colon for virtual colonoscopy. Computerized Medical Imaging and Graphics 24 (January 2000): 1–9.

[9] Chen, D., Liang, Z., Wax, M., Li, B., and Kaufman, A. A novel approach to extract colon lumen from CT images for virtual colonoscopy. IEEE Transactions on medical imaging 19 (December 2000): 1220–1226.

[10] Lakare, S., Chen, D., Li, L., Kaufman, A., Mark, W., and Liang, Z. Robust colon residue detection using vector-quantization-based classification for virtual colonoscopy. <u>Proceeding of SPIE, Medical Imaging 2003: Physiology and Function Methods, Systems, and Applications</u> (2003): 515–520.

[11] Sato, M., Lakare, S., Wan, M., Kaufman, A., Liang, Z., and Wax, M. An automatic colon segmentation for 3D virtual colonoscopy. <u>IEICE Trans. Information and Systems</u> 1 (January 2001): 201–208.

[12] Lakare, S., Wan, M., Sato, M., and Kaufman, A. 3D Digital Cleansing using Segmentation Rays. <u>The 11th IEEE Visualization 2000 Conference (VIS 2000)</u> (2000): 37–44.

[13] Lakare, S., Chen, D., Li L., Kaufman A., and Liang Z. Electronic colon cleansing using segmentation rays for virtual colonoscopy. <u>Proceeding of SPIE, Medical Imaging - Physiology and Function from Multidimensional Images</u> (2002): 412–418.

[14] Skalski, A., Socha, M., Zieliftski, T., and Duplaga, M. Colon cleansing for virtual colonoscopy using non-linear transfer function and morphological operations. <u>IEEE International Workshop on Imaging Systems and Techniques</u> (2007): 1–5.

[15] Skalski, A., Socha, M., Zieliftski, T. and Duplaga, M. CT data processing and visualization aspects of virtual colonoscopy. <u>The European Association for Signal Processing</u> (2007): 2509–2513.

[16] Bidgoli, H., Ahmadian, A., Akhlaghpor, S., Alam, N. R., and Mahmodabadi, S. Z. An efficient colon segmentation method for oral contrast-enhanced CT colonography. <u>27<u>th</u> Annual Conference of the Engineering Medicine and Biology society</u> (2006): 3429–3432.

[17] Bevilacqua, V., and others. Image Processing Framework for Virtual Colonoscopy. <u>Lecture Notes Computer Sciences</u> 5754 (2009): 965–974.

[18] Sadleir, R., and Whelan, P. Fast colon centerline calculation using optimised 3D topological thinning. <u>Computerized Medical Imaging and Graphics</u> 29 (2005): 251–258.

[19] Lapeer, R. J., Tan, A. C., and Aldridge, R. A combined approach to 3D medical image segmentation using marker-based watersheds and active contours: the active watershed method. <u>Lecture Notes Computer Sciences</u> (2002): 165–168.

[20] Lapeer, R. J., Tan, A. C., and Aldridge, R. Active Watersheds: Combining 3D watershed segmentation and active contours to extract abdominal Organs from MR Images. <u>Lecture Notes Computer Sciences</u> 2488 (2002): 596–603.

[21] Yuchong, J., Jinjie, M., Lixu, G., Berliner, L. and Jaffer, N. Improved diagnosis and navigation for CT colonography. <u>Annual International Conference of the IEEE Engineering Medicine and Biology Society 2005</u> (2005): 5140–5144.

[22] Uitert, R. V., Bitter, I., and Summers, R. M. Detection of colon wall outer boundary and segmentation of the colon wall based on level set methods. <u>28th Annual International Conference of the IEEE Engineering Medicine and Biology Society 2006 (EMBS'06)</u> (2006): 3017–3020.

[23] Hamidpour, Sh. F., Ahmadian, A., Zoroofi, R.A and Bidgoli, J. H. Hybrid segmentation of colon boundary CT images based on geometric deformable model. <u>Signal Processing and Communications, 2007. ICSPC 2007</u> (2007): 967–970.

[24] Chen, D., Fahmi, R., Farag, A.A., Falk, R.L. and Dryden, G. W. Accurate and fast 3D colon segmentation in CT colonography. <u>IEEE International Symposium on Biomedical Imaging: From Nano to Macro, 2009. ISBI 2009</u>. (2009): 108–115.

[25] Kass, M., Witkin, A., and Terzopoulos, D. Snakes: active contour models. <u>International Journal of Computer Vision</u> 1 (November 2007): 321–331.

[26] Xu, C., and Prince, J. L. Gradient vector flow: A new external force for snakes. <u>IEEE Computer Society Conference on Computer Vision and Pattern Recognition</u> (1997): 66–71.

[27] Xu, C. and Prince, J. L. Generalized gradient vector flow external forces for active contours. <u>Signal Processing</u> 71 (December 1998): 131–139.

[28] Xu, C. and Prince, J. L. Snakes, shapes, and gradient vector flow. <u>IEEE Transaction on Image Processing</u> 7 (March 1998): 359–369.

[29] Cheng J. and Foo, S. W. Dynamic directional gradient vector flow for snakes. <u>IEEE Transaction on Image Processing</u> 15 (June 2006): 1563–1571.

[30] Wu, X., Spencer, S. A., Shen, S., Fiveash, J. B., Duan, J. and Brezovich, I. A. Development of an accelerated GVF semi-automatic contouring algorithm for radiotherapy treatment planning Computers Biology and Medicine. <u>Journal Computers Biology and Medicine</u> 39 (July 2009): 650–656.

[31] Seokyoon, C., and Changsoo, K. Automatic initialization active contour model for the segmentation of the chest wall on chest CT. <u>Healthcare informatics research</u> 16 (March 2010): 36–45.

[32] Cvancarova, M., Albregtsen, F., Brabrand, K., and Samset, E. Segmentation of ultrasound images of liver tumors applying snake algorithms and GVF. <u>International Congress Series</u> 1281 (May 2005): 218–223.

[33] Huang, S., Wang, B., and Huang, X. Using GVF snake to segment liver from CT images. <u>The 3rd IEEE-EMBS International Summer School and Symposium on Medical Devices and Biosensors</u> (2009): 3561–3564.

[34] Wu, M. N., Lin, C. C., and Chang, C. C. Brain tumor detection using color-based K-means clustering segmentation. <u>The 3rd International Conference on International Information Hiding and Multimedia Signal Processing</u> (2007): 245–250.

[35] Guillermo, A. N., and Virginia, B. L. A weighted K-means algorithm applied to bratissue classification. <u>Journal of Computer Science & Technology</u> 5 (October 2005): 121–126.

[36] Oprea, A. E., Strungaru, R. and Ungurean, G. M. A self organizing map approach to breast cancer detection. <u>The 30th International Conference of IEEE Engineering Medicine and Biology Society</u> (2008): 3032–3035.

[37] Canny, J. F. A computational approach to edge detection. <u>IEEE Transactions on Pattern Analysis and Machine Intelligence</u> 8 (June 1986): 679–698.

[38] Ramamurthy, B., and Chandran, K. R. CBMIR: Shape-Based Image Retrieval Using Canny Edge Detection and K-Means Clustering Algorithms for Medical Images. <u>International Journal of Engineering Science and Technology</u> 3 (Mar 2011): 1870–1877.

[39] Marr, D., and Hildreth, E. Theory of edge detection. <u>Proceedings of the Royal Society of London. Series B, Biological Sciences</u> 207 (February 1980): 187–217.

[40] Otsu, N. A threshold selection method from gray-level histograms. <u>IEEE Transaction on Systems, Man and Cybernetics</u> 9 (January 1979): 62–66.

[41] Gonzalez, R. C., and Woods, R. E. <u>Digital Image Processing</u>. Massachusetts: Addison-Wesley Publishing Company, 1992.

[42] Basu, M. Gaussian-based edge-detection methods–a survey. <u>IEEE Transactions on Systems, Man and Cybernetics Part C: Applications And Reviews</u> 32 (August 2002): 252–260.

[43] Roushdy, M. Comparative study of edge detection algorithms applying on the grayscale noisy image using morphological filter. <u>International Journal on Graphics, Vision and Image Processing</u> 6 (December 2006): 53–59.

[44] Bennamoun, M., Boashash, B., and Koo, J. Optimal parameters for edge detection. <u>IEEE International Conference on Systems, Man and Cybernetics</u> (1995): 1482–1488.

[45] Wikipedia. Virtual colonoscopy [Online]. 2012. Available from : http://en.wikipedia.org/wiki/Virtual_colonoscopy [2012, January 9]

[46] National Cancer Institute. Virtual colonoscopy [Online]. Available from : http://imaging.cancer.gov/patientsandproviders/cancerimaging/virtualcolonoscopy [2012, January 9]

[47] The Radiology Information Resource for Patients. CT colonoscopy [Online]. Available from : http://www.radiologyinfo.org/en/info.cfm?pg=ct_coloy [2012, January 9]

[48] Louis S. Colonoscopy [Online]. 2007. Available from : http://www.gastroenterology.au/procedure-colonoscopy.php [2012, January 9]

[49] Health Hype. Colonoscopy – Preparation, Procedure, Pictures, Risks, Cost [Online]. Available from : http://www.healthhype.com/colonoscopy-preparation-procedure-pictures-risks-cost.html [2012, January 9]

[50] American Cancer Society. <u>Colorectal Cancer</u> [Online]. 2012. Available from : http://www. cancer.org/Cancer/ColonandRectumCancer/DetailedGuide/colorectal-cancer-detection [2012, January 25]

[51] Somkantha, K. <u>A novel edge detection for ill-defined edges noisy images</u>. Doctoral dissertation, Department of Electrical Engineering Chiangmai University, 2010.

[52] Senthilkumaran, N. and Rajesh2, R. Edge detection techniques for image segmentation –a survey of soft computing. <u>International Journal of Recent Trends in Engineering</u> 1 (May 2009): 250–254.

[53] Ramamurthy, B. and Chandran, K.R. CBMIR: Shape-based image retrieval using canny edge detection and K-means clustering algorithms for medical Images. <u>International Journal of Engineering Science and Technology</u> 3 (Mar 2011): 1870–1877.

[54] Juneja, M. and Sandhu, P. S. Performance evaluation of edge detection techniques for images spatial domain. <u>International Journal of Computer Theory and Engineering</u> 1 (December 2009): 1793–8201.

[55] Haralick, R. and Shapiro, L. <u>Computer and Robot Vision</u>. 1, Massachusetts: Addison-Wesley Publishing, 2002

[56] Davies, E. R. <u>Machine Vision Theory, Algorithms, Practicalities 3rd Edition</u>. USA: Morgan Kauffmann Publications, 2005.

[57] Sonka, M, and Hlavac, V., and Byle, B. <u>Image Processing, Analysis, and Machine Vision 3rd Edition</u>. Thomson Learning Publishing, 2007.

[58] Xu, C. and Prince, J. L. <u>Gradient Vector Vlow Deformable Model, Handbook of Medical Imaging</u>. Academic Place, 2000.

[59] Xu, C. and Prince, J. L. Global optimality of gradient vector flow. <u>Proceeding of 34th Annual Conference on Information Sciences and Systems</u> (2000).

[60] Promkumtan p. and Kantapanit K. X-ray Film Analysis for Periapical Lesion Detection Using Gradient Vector Flow Deformable Model. <u>9th Tri-University International Joint Seminar & Symposium 2002</u> (2002): 6–10.

[61] Promkumtan p. and Kantapanit K. Application of Gradient Vector Flow Active Contour Model for Preriapical Lesion Detection on X-ray Film. 25th Electrical Engineering Conference (EECON-25) (2002): 96–99.

[62] Prince, J. L. Statistical snake: active region model. Doctoral dissertation, Department of Electrical and Computer Engineering University of Sheffield, 1996.

[63] Chen, Q., Yang, X., and Petriu, E. Watershed segmentation for binary images with different distance transforms. The 3th IEEE International Workshop on Haptic, Audio and Visual Environments and their Applications (2004): 111-116.

[64] Baccar, M., Gee, L. A., Gonzalez, R. C., and Abidi, M. A. Segmentation of Range Images via Data Fusion and Morphological Watersheds," Pattern Recognition. Pattern Recognition 29 (October 1996): 1673–1687.

[65] Nguyen, H. T., Worring, M., and Boomgard, R. V. D. Watersnakes: energy-driven watershed segmentation. IEEE Transactions on Pattern Analysis and Machine Intelligence 25 (March 2003): 330–342.

[66] Jayadevappa, D., Kumar, S. S., and Murty, D. S. A Hybrid Segmentation Model based on Watershed and Gradient Vector Flow for the Detection of BraTumor. International Journal of Signal Processing, Image Processing and Pattern Recognition 2 (September 2009): 29–42.

[67] Osher S., Sethian A. J. Fronts propagating with curvature dependent speed: algorithms based on Hamilton-Jacobi formulations. Journal of Computational Physics 79 (1988): 12–49.

[68] Caselles V., Kimmel R., and Sapiro G. Geodesic active contours. International Journal of Computer Vision 22 (1997): 61–79.

[69] Li C. and Xu, C., Gui C. and Fox D. M. Level Set Evolution Without Re-initialization: A New Variational Proceedings of the 2005 IEEE Computer Society Conference on Computer Vision and Pattern Recognition (CVPR'05) (2005). 430–436.

[70] William E. Lorensen, Harvey E. Cline. Marching Cubes: A high resolution 3D surface construction algorithm. International Conference on Computer Graphics and Interactive Techniques 21 (1987):163–169.
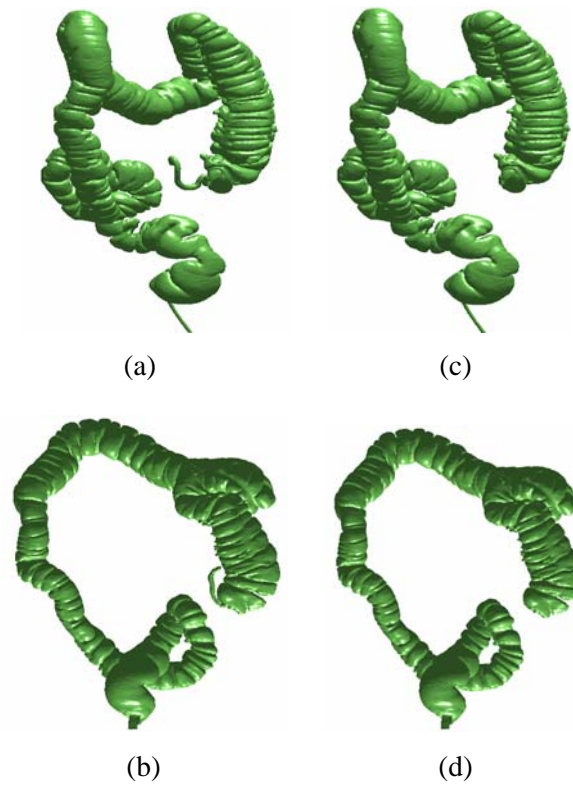
Appendix

Appendix A: Example Results of Colon Cleansing

The example results from the removing contiguous intestine with colon are illustrated in Figure A.1 and Figure A.2.
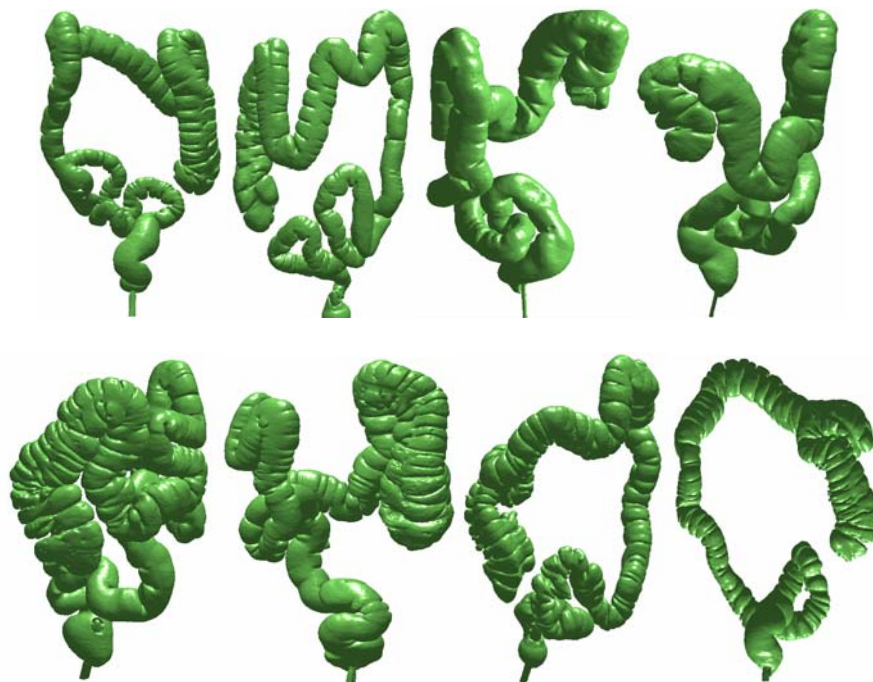

(a)   (d)

(b)   (e)

(c)   (f)
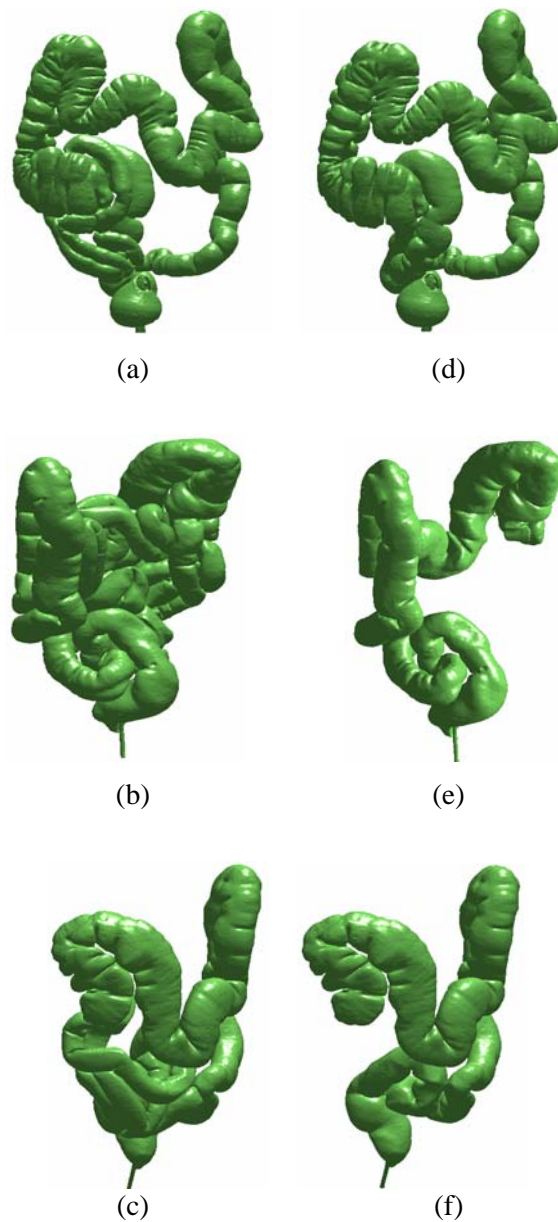
Figure A.1 (a)–(c) Contiguous intestine and colon (d)–(f) After removing intestine

(a)   (c)

(b)   (d)

Figure A.2 (a)–(b) Contiguous intestine and colon (c)–(d) After removing intestine

The results from 20 datasets for examination in colon segmentation and reconstruction are illustrated in Figure A.3 and Figure A.4.

Figure A.3 Colon reconstruction from dataset 1–8

Figure A.4 Colon reconstruction from dataset 9–20

Biography

Name: Miss Pataraporn Promkumtan

Date of Birth: 27th August, 1977.

Educations:

- Ph.D., Program Computer Science, Department of Mathematics, Faculty of Science, Chulalongkorn University, Thailand, (June 2007 – May 2012).
- M.Eng. Program Electrical Engineering, Faculty of Engineering, Chiangmai University, Thailand, (June 2000 – March 2002).
- B.Eng. Program Electrical Engineering, Faculty of Engineering, Chiangmai University, Thailand, (June 1996 – March 1999).

Publication papers:

- Promkumtan P., Vajragupta L., Chaopathomkul B., Cooharojananone N. and Lipikorn R.. Colon Cleansing Method for Oral Contrast-Enhanced CT Colonography using K-means Clustering and Morphological Operations. IEEE 4th International Symposium on Biomedical Engineering (2009).
- Promkumtan p. and Kantapanit K. X-ray Film Analysis for Periapical Lesion Detection Using Gradient Vector Flow Deformable Model. 9th Tri-University International Joint Seminar & Symposium 2002 (2002): 6–10.
- Promkumtan p. and Kantapanit K. Application of Gradient Vector Flow Active Contour Model for Preriapical Lesion Detection on X-ray Film. 25th Electrical Engineering Conference (EECON-25) (1995): 96–99.

Work:

- Lecturer, Computer Program, Department of Mathematics, Faculty of Science and Technology, Chiangmai Rajabhat University

Scholarship:

- Internship scholarship from National Institute of Informatics (NII), Japan. (August 2010 – March 2011).